Impact of renewable energies to European energy systems under historical and future climate conditions

Inaugural-Dissertation

zur

Erlangung des Doktorgrades

der Mathematisch-Naturwissenschaftlichen Fakultät

der Universität zu Köln

vorgelegt von

Philipp Henckes

aus Köln

Köln, 2019

Berichterstatter:
Prof. Dr. Susanne Crewell
PD Dr. Hendrik Elbern

Tag der Mündlichen Prüfung:
07.06.2019

An meinen Vater, mit dem ich diese letzten Tage meines Studiums und viele andere Moment gerne geteilt hätte.

Contents

Zusammenfassung

Die Entwicklung des Erdklimas dürfte eine der größten Bedrohungen für Mensch und Natur im 21. Jahrhundert sein, mit kaum vorhersehbaren und im Zweifel auch irreversiblen Folgen für zukünftige Generationen. Daher erscheint es unerlässlich, dass weltweit versucht wird, die sich abzeichnenden Herausforderungen mit allen verfügbaren Mitteln anzugehen. Erhebliche Veränderungen sind daher nötig, insbesondere im Bereich des Ressourcenmanagements. Der Übergang von fossilen zu erneuerbaren Energien kann dabei eine wichtige Rolle spielen, einen Beitrag zum Klimaschutz durch drastische CO_2 Reduzierungen zu leisten. Ein Schlüssel ist hierbei, die charakteristischen Eigenschaften der variablen erneuerbaren Energien (VRE) unter gegenwärtigen und zukünftigen kilmatischen Bedingungen besser zu verstehen, um einen neuen Weg in Richtung CO_2-freie Energiesysteme und eine insgesamt nachhaltigere Welt einschlagen zu können.

Das damit einhergehende Forschungsfeld ist hochgradig komplex und interdisziplinär. *Energy Transition and Climate Change*, ein Projekt der Universität zu Köln, zielt beispielsweise darauf ab, einen interdisziplinären Rahmen für die Durchführung verschiedenster Forschungsarbeiten in diesem Bereich zu schaffen, aktuelle Fragen zu beantworten und Neue zu erarbeiten. Die vorliegende Arbeit, als Teil dieses Projekts, profitiert insbesondere vom Wissensaustausch zwischen dem Fachbereich der Meteorologie und der Wirtschaft. Im Rahmen des Projekts ergeben sich drei Hauptstudien, die sowohl der Dissertation, als auch Teilen von Publikationen dienen.

Studie I zielt darauf ab, die Lücke bezüglich verfügbaren, zuverlässigen und umfassenden Windenergie-Datensätzen zu schließen, die für sich anschließende Modellierungen des Energiesystems von Bedeutung sind. Hierfür wird ein neuer Langzeitdatensatz simuliert, der Zeitreihen aller europäischen Windkraftanlagen beinhaltet. Als Grundlage dient hierbei eine hochauflösende Reanalyse (COSMO-REA6) des Deutschen Wetterdienstes. Hierdurch soll zur Verbesserung und Vertiefung des aktuellen Wissensstands bzgl. der einzigartigen VRE-Merkmale beigetragen und deren mögliche Rolle für Europäische Energiesysteme besser verstanden werden. Die Analyse der neuen Daten zeigt für Europa und Deutschland eine starke Variabilität der jährlichen Windenergieproduktion, sowie der Auftretenswahrscheinlichkeit von Extremsituationen. Darüber hinaus deuten die Ergebnisse auf hohe Potentiale

von Ausgleichseffekten innerhalb Europas und insbesondere Deutschland hin. Dies unterstreicht das vielversprechende Potenzial von VRE, um bei der Realisierung einer Europäischen Energiewende zu helfen.

Reanalyseprodukte, wie beispielsweise COSMO-REA6, werden häufig als meteorologische Grundlage für sich anschließende Energiesystemstudien genutzt, bei denen hohe Anteile an VRE Technologien eine Rolle spielen. Da Reanalysen zum Teil erhebliche Fehlerbereiche aufweisen, kommen Fragen nach deren Auswirkungen auf Energiesystem-Modelle auf. Studie II zeigt, dass sowohl die Energieumwandlungs-, als auch Energiesystem-Modelle sehr sensitiv auf Anfangsfehler in den meteorologischen Eingangsdaten reagieren. Das gilt insbesondere bei hohen Anteilen an VRE. In diesem Zusammenhang, können starke Auswirkungen auf die generelle Zusammensetzung des deutschen Stromsystems, sowie Allokationseffekte von VRE-Kapazitäten beobachtet werden. Eine solche Fehleranalyse ist neu im Bereich der Energiesystem-Modellierung.

Schließlich untersucht Studie III die Auswirkungen des Klimawandels auf ein vereinfachtes Europäisches Stromsystem, unter strengen Dekarbonisierungszielen, zum Ende des 21. Jahrhunderts. Dabei liegt der Fokus auf Effekten in Bezug auf VRE-Technologien. Hierfür werden Simulationen durchgeführt und verglichen, die auf historischen und zukünftigen Klimabedingungen basieren. Datengrundlage bilden hier Auszüge aus dem EURO-CORDEX Projekt. Die Simulationen zeigen, dass sich das Gesamtsystem zum Einen an den Klimawandel durch ausgeprägte Verschiebungen der Anteile innerhalb der VRE-Technologien anpasst. Zum Anderen können erhebliche lokale räumliche Verschiebungen von VRE-Kapazitäten beobachtet werden, die das System umsetzt, um die Nachfrage bei gleichzeitiger Erfüllung des CO_2-Ziels zu erfüllen. Die Ergebnisse zeigen weiterhin, dass, obwohl die europäischen VRE-Potenziale und ihre Variabilität im Klimawandel-Szenario zunimmt, keine wesentlichen Veränderungen im sonstigen Gesamtsystem (Systemkosten, Verhältnis zwischen VRE und Nicht-VRE Kapazitäten, Strompreis) stattfinden. Diese Anpassungsstrategie verdeutlicht die Notwendigkeit ausreichender Investitionen in Netzkapazitäten, die Dringlichkeit eines gemeinsamen und gemeinschaftlichen Europäischen Ansatzes als auch entsprechende notwendige Maßnahmen in diesem Bereich umzusetzen.

Abstract

The development of the Earth's climate is expected to be one of the greatest threats to mankind and nature in the 21st century, with hardly predictable and perhaps irreversible consequences for future generations. Hence, it appears essential that societies worldwide try to tackle the emerging challenges with all possible means and need to undergo substantial changes, in particular, for resource management. Energy transition from fossil-based to renewable energies may play a major role contributing to climate change mitigation via drastic CO_2 reductions. Here, a key is to better understand the variable renewable energies' (VRE) characteristics for present and future conditions, in order to strike a new path towards CO_2-free energy systems and a more sustainable world.

The emerging corresponding research field is highly complex and interdisciplinary. The *Energy Transition and Climate Change* project, hosted by the *University of Cologne*, aims to establish an interdisciplinary framework to tackle various research questions as well as to raise new ones. The present thesis is embedded in the project and benefits in particular from the exchange of knowledge between meteorology and economics. Three main studies are related to the project and are subject to this thesis, as well as in parts to publications.

Study I aims to reduce the gap of available, reliable and comprehensive wind power data sets for follow-up investigations by generating a novel long-term European wind power time series based on a high resolution reanalysis by the *German Weather Service* (*COSMO-REA6*). Hereby, the improvement of a comprehensive understanding of the unique VRE power characteristics and their potential role for energy systems in Europe is supported. Analyzing this data base reveals strong variations in annual wind productions as well as of frequencies of extreme situations in Europe and Germany. In addition, results show high potentials of balancing effects within Europe and in particular for Germany, emphasizing the promising potential of VRE to help realizing the energy transition.

Reanalyses products, such as COSMO-REA6, are often used as a meteorological basis for subsequent energy system studies including high shares of VRE. Since reanalyses contain considerable biases, the question of their impact to energy system models arises. Study II shows that energy conversion as well as energy system models are highly sensitive to initial errors associated with the meteorological input

data, in particular under high shares of VRE. In this context, impacts on the overall composition of German electricity system as well as allocation effects of VRE capacities are observed. Such an uncertainty evaluation is a novelty in energy system modeling.

Finally, Study III investigates the impact of climate change on a simplified European electricity system under strong decarbonization targets until the end of the 21st century. Here, the focus is on effects with respect to VRE technologies. For this purpose, simulations based on historical and future climate change scenarios, under strong CO_2 emission assumptions, from the *EURO-CORDEX* project are compared. Simulations exhibit, that the system on the one hand adapts to climate change by pronounced shifts within VRE capacities and on the other hand by substantial local allocation adjustments, in order to fulfill the demand side while meeting the decarbonization target. The outcomes further show that, although European VRE potentials decline and their variability increases in the future climate change scenario, no substantial changes in the overall system (costs, ratio between VRE and non-VRE, electricity price) can be observed. This adaption strategy emphasizes the need for sufficient investments in transmission capacities, the urgency of a common and joint European approach and corresponding adequate actions from this day forward.

Chapter 1

Introduction

1.1 Climate change risks & the role of variable renewable energy

Following the Intergovernmental Penal on Climate Change (IPCC, 2014), one of the biggest challenges and threats for mankind in the 21st century appears to be the change in observed and predicted climate conditions. Numerous recent and ongoing research suggests that climate change leads to consequences concerning many aspects of ecosystems as well as socio-economic related questions and may cause irreversible damage (IPCC, 2014; Tobin et al., 2016). Increased risks of climate change impacts, such as species extinction (Pacifici et al., 2015), ecosystem shifts (Pecl et al., 2017), impairment of human health (Watts et al., 2015), sea level rise (Neumann et al., 2015), intensification of extreme weather events (Forzieri et al., 2016), e.g. heat waves (Schär, 2016), droughts (Teuling, 2018) and floods (Madsen et al., 2014), are to some extent relevant on the global but also on the local scale.

The combination of global economic and population growth in the 20th century and beyond are estimated to be the main drivers for the large increase in the atmospheric greenhouse gas (GHG) emissions with respect to pre-industrial decades (IPCC, 2011). This leads to the highest concentrations ever observed, mainly for carbon dioxide (CO_2), methane (CH_4) and nitrous oxide (N_2O) (IPCC, 2014). While effects assigned to population growth remained constant in recent years, the contribution allocated to economic growth experience a strong enhancement. According to the IPCC (2014), it is extremely likely that the increase in anthropogenic GHG emissions represents the dominant cause (more than 50%) of the observed global warming since the mid-20th century (1951-2010). Pervasive supply of energy services has substantially contributed to these historical and present changes in GHG emissions. The IPCC finds that, in particular, fossil fuel combustion accounts for the majority of these anthropogenic changes (IPCC, 2014).

A continuing evolution of current GHG emissions is expected to foster further

global warming in the future, leading to associated perseverative changes for all climate system components with an increased likelihood of severe and irreversible impacts and risks for human systems as well as ecosystems (IPCC, 2014). In consequence, substantial near future changes, such as sustained pronounced reductions of GHG emissions, are necessary in order to limit future climate change and affiliated impacts and risks, as claimed for example by the International Energy Agency (IEA, 2011). For instance, a successful realization of the Paris climate agreement[1], which aims "to strengthen the global response to the threat of climate change by keeping a global temperature rise this century well below 2 degrees Celsius above pre-industrial levels" appears to be a distant prospect, since under current mitigation ambitions annually averaged global temperature is expected to rise by 2.9°C-3.4°C towards the end of the 21st century (in relation to pre-industrial conditions) (IPCC, 2018).

Several recent studies highlight the possibility and various pathways towards fully renewable and sustainable energy systems (Pleßmann et al., 2014; Connolly et al., 2016; Papaefthymiou and Dragoon, 2016), which may potentially contribute to the required adaptions in order to mitigate climate change and its consequences. Hereby, power generation by variable renewable energy (VRE) technologies, such as wind and solar power plants may play a key role for the mitigation solution (Deng et al., 2012; Connolly and Mathiesen, 2014). Additionally, Bloomberg (2018) mentions that cost-optimal electricity systems are increasingly based on VRE generation technologies, triggered by recent cost reductions of VRE power plants as well as enhanced awareness and regulation of environment related aspects.

VRE based power generation is highly flexible and exhibits pronounced variability on multiple spatio-temporal scales due to the highly variable nature of the associated resources, being near surface wind speed and solar radiation (Perez et al., 2016; Ueckerdt et al., 2015; Monforti et al., 2016; Staffell and Pfenninger, 2016). Therefore, with rising shares of VRE power supply, the dependency of power production on weather and climate related aspects increases significantly. Enhanced variability of large parts of the power supply side sharpen the challenge concerning security of supply and system reliability (Lund et al., 2015; Peter and Wagner, 2018). Hence, it appears crucial to understand VRE characteristics on short to long-term scales in order to estimate their potential contribution to an energy transition triggered by policies regarding decarbonization targets. Furthermore, on one hand climate change is a major motivation for large VRE expansions, on the other hand it may influence and alter energy yields from these renewable sources to a

[1] At COP 21 in Paris (12 December 2015), the Paris climate agreement emerged within the international environmental agreement *United Nations Framework Convention on Climate Change (UNFCCC)*, https://unfccc.int

significant extent in the future. The conservation of the future energy systems' capability implies an adequate adaptation to changing conditions and, therefore, requires a sophisticated analysis of climate change related effects on these systems (Peter, 2019).

1.2 Contributions within this thesis

The following Sections contain an overview and a detailed introduction to the studies carried out in the scope of this thesis. They aim to contribute to existing research by investigating VRE characteristics under historical and future climate conditions in Europe.

Study I

This study is related to the publication in *ENERGY* in 2018 with the title *"The benefit of long-term high resolution wind data for electricity system analysis"* (Henckes et al., 2018).

As mentioned before, renewable energies such as wind and photovoltaics (PV) are recently gaining major significance for energy systems world-wide. For example, Europe's wind capacity increased from 41 GW (6% share) in 2005 to 154 GW (16.7% share) in 2016 (WindEurope, 2017). To understand and anticipate future energy systems, the VRE contribution and inherent unique characteristics, e.g. short- and long-term variability, have increasing importance. For instance, regarding the reliability of energy systems distinct low or high VRE power supply situations play an important role. Low VRE generation cases trigger the need for conventional plants, compensating the missing capacity for a stable demand satisfaction. In contrast, very high VRE supply might lead to increased pressure on the electricity grid, forcing transmission system operators (TSOs) to regulate the grid load by powering down certain suppliers. Both cases contribute to additional cost and planning uncertainties for all market participants (Hirth et al., 2015; Wu et al., 2015). A better understanding of the VRE characteristics could reduce these cost and uncertainties to a significant extent. Since wind and solar radiation are spatially highly variable, it is crucial to derive high resolution data for accurate follow-up analyses such as electricity dispatch and investment models, transmission grid expansion or security of supply analyses.

At least two major challenges arise. First, while wind and PV employment experience rapid expansions, the availability of historical VRE production data for

analyses and predictions are insufficient. Necessary empirical long-term observations of VRE production for large numbers of installed capacities are scarce. Data for individual production sites might be publicly available. However, time series for a high share of the wind and especially PV fleets in an entire country like Germany or even the European Union are unfortunately missing for such analyses and research. Therefore, simulations of VRE time series are required incorporating long-term and high resolution meteorological input with current and expected future wind and PV plant fleets. However, this in turn leads to the second issue. Historical meteorological observations of wind speed and solar radiation are lacking either high spatio-temporal resolution, the long-term scale or sparse spatial coverage (Staffell and Pfenninger, 2016; Henckes et al., 2018; Cannon et al., 2015). Performing simulations at locations matching exactly with operation sites even complicates the data supply, since observation and production sites usually would not coincide.

A variety of recent studies are applying wind input data from different reanalysis products to tackle these issues (Gunturu and Schlosser, 2012; Cosseron et al., 2013; Hallgren et al., 2014; Ritter and Deckert, 2017; Staffell and Pfenninger, 2016). They are systematic approaches to generate long-term data sets on a homogeneous grid for climate research by combining assimilation schemes for historical observations with atmospheric circulation models. However, most studies focus only on single countries, reveal comparably low resolutions or lack an advanced level of details, in particular, concerning the energy conversion process. Staffell and Pfenninger (2016) for instance use the Modern-Era Retrospective Analysis (MERRA) by the National Aeronautics and Space Administration (NASA) to model long-term wind power time series in Europe. Besides a sufficiently high temporal resolution (hourly) for VRE related aspects, the MERRA reanalysis has a comparably coarse spatial grid of approximately 50 km in Europe, since sub-grid scale effects might be important to local wind and solar conditions (Liléo et al., 2000; Carvalho et al., 2014).

The work carried out in the scope of this thesis contributes by developing a novel energy conversion model and its application to a unique state-of-the-art reanalysis, bringing along a high spatio-temporal resolution and a long time horizon of 20 years. In combination with a location specific European wind park data set, a high resolved long-term wind power time series is generated on a high level of details. The resulting database allows to further address the following questions in Study I:

- How is the European wind power characterized? Is it possible to determine a representative wind power year for further investigations?
- How pronounced is the potential of balancing effects related to wind power in Europe and on a national scale in Germany?

Study II

This study is subject to the article "Uncertainty Estimation of Investment Models under High Shares of Renewables using Reanalysis Data" by Henckes et al. (2019) submitted to *ENERGY* in April 2019 and will closely follow this work.

As outlined previously, to tackle the issue of the insufficient availability of reliable long-term VRE power production data, many studies are making use of reanalysis products serving as the meteorological basis for VRE representation in energy system modeling (Andresen et al., 2015; Bett and Thornton, 2016; Ritter and Deckert, 2017). Besides the advantages of reanalyses, questions about effects of their potential errors on modeling outcomes arise.

As it has been observed in many studies (Bollmeyer et al., 2015; Kaiser-Weiss et al., 2015; Staffell and Pfenninger, 2016; Rose and Apt, 2015) and confirmed by this study (Section 3.1.2), reanalysis products show significant uncertainties (e.g. biased) to different extents, depending on the estimated quantity. Staffell and Pfenninger (2016) for instance highlight the urgency for wind power production studies to consider calibration with respect to reanalysis biases. However, when it comes to energy system modeling, these errors are usually omitted (Peter and Wagner, 2018; Huber et al., 2015; Dolter and Rivers, 2018) and, hence, their potential impact to model results is not considered. The topic gains even more importance for future energy systems, since VRE expansion and shares are expected to strongly increase. In general, the matter of uncertainties in a sense of error estimation in this field of research appears to leave room for several further investigations and improvements.

Therefore, the approach of this study has the objective to give first insights on potential uncertainties introduced by reanalysis errors and their impact on the affiliated model chain. The approach follows the idea of focusing on the overall range of potential errors rather than quantifying uncertainties of actual real case scenarios. The analyses related to Study II attempts to answer on three main questions:

- What are potential error sources associated with VRE power modeling?
- What are the sensitivities of the applied power conversion models (wind and PV) with respect to these estimated errors? What are the most dominant parameters?
- What are the impacts of these uncertainties on future energy system simulation results regarding the dominant parameters?

Study III

This branch within the framework of this thesis has the objective to comprise the developed methods in order to simulate projections of future energy markets in Europe under high shares of renewable energies. As recent economic and political developments world-wide and, in particular, in Europe reveal, contributions of renewable energies to the total energy mix will play a central role (e.g. Connolly et al., 2016). With expansion of VRE technologies, however, uncertainties for the energy system increase due to the variable nature of wind and PV energy (Boyle, 2009; Beaudin et al., 2010; Bessa et al., 2014). In consequence, this leads to stronger challenges regarding energy system related aspects, for instance, security of supply. At the same time, global climate is expected to go through significant changes in the future, as described earlier. Since these changes might vary essentially between continents or single countries (e.g. IPCC, 2014), some regions could experience strong implications to their potentials of wind and solar related energy generation. As such, the world-wide wind energy potential is expected not to change significantly on average, but climate projections indicate an overall decrease for Europe (e.g. Tobin et al., 2016). In addition, the variability on different time scales is also expected to change, affecting, for instance, the need for conventional backup capacities. With respect to these assumptions, the following question emerges: what is the potential impact of local climate change to the European energy markets?

The topic combines complex processes from various research fields. Therefore the aim of this study is to keep track on the overarching goal to combine meteorological and economical aspects without getting lost in details and to keep the entire framework as simple as possible in order to focus on the impact of climate change to VRE sources. For instance, various studies examine the impact of climate change on wind or PV energy sources in detail only for single European countries (e.g. Najac, 2014; Nolan et al., 2012; Cradden et al., 2017) or even for the entire European continent (e.g. Reyers et al., 2016; Tobin et al., 2016; Moemken et al., 2018), but would not investigate the subsequent implications for the local energy markets. This has been done by some recent studies, applying future projections from global climate models to energy system modeling (e.g. Tobin et al., 2018; Peter, 2019). However, they concentrate on the economical point of view and try to implement as many details of the entirety of the energy system as possible, while meteorological details are slightly neglected.

This study, in contrast, aims to give first insights on the potential impact of climate change on Europe with a focus on VRE sources as well as the affiliated electricity sector. Here, the main objective is to analyze potential future changes with respect to each step of the necessary model chain in detail – from changes in

wind speeds and solar radiation over their impacts on European VRE potentials to final changes in the European energy system. For this purpose, the modeling approach is kept as simple as possible. By intentionally omitting certain processes and details, the resulting signals are further isolated, so that cause and effect can be related more easily. For instance, climate change might also affect other aspects of the energy systems as pointed out by (e.g. Peter, 2019), such as cooling water availability for thermoelectric power plants (Tobin et al., 2018), hydro power potentials (Schlott et al., 2018) or electricity demand (Wenz et al., 2017).

The overall approach of Study III is to compare future European energy systems under both, present-day climate and future changing climate conditions. For this purpose, VRE time series for both climate conditions are generated by applying the developed energy conversion model to outcomes of global climate model simulations. By the development and application of a clustering scheme, as well as an energy system model, the impacts of climate change on the European electricity system towards the end of the century are examined.

Structure

Research and analyses within this thesis are closely related to the *Energy Transition and Climate Change (ET-CC)* project[2], being part of the Institutional Strategy of the University of Cologne funded by the *Excellence Initiative*. Since the subject of renewable energies with respect to energy transition triggered by future climate changes and their impact on energy markets requires cooperation of various different research fields and disciplines, the ET-CC project aims to provide an interdisciplinary framework, which contributes to relevant ongoing research. Hereby, the objective is not only to work on open research questions, but also to understand the connection between the various participating disciplines and, from this, to address emerging questions concerning renewable energies, energy transition and climate change which can only be answered in close collaboration between, for example, meteorology, economics and informatics. For that matter, the project brings together expertise from various institutions, such as the *Institute for Geophysics and Meteorology (IGM)*[3] and the *Institute of Energy Economics (EWI)*[4]. With the outlined studies, this thesis tries to contribute to the projects interdisciplinary research by three major topics:

- Study I: What are the present main characteristics of wind power in Europe and Germany?

[2] http://et-cc.uni-koeln.de/project.html
[3] http://www.geomet.uni-koeln.de/home/
[4] http://www.ewi.uni-koeln.de/

- Study II: What is the impact of VRE uncertainties on outcomes of energy system models?
- Study III: What are the climate change impacts on European energy markets by the end of the 21st century under high shares of VRE?.

All three investigations share and apply parts of tools and methods developed and described in Chapter 2. Chapter 3 outlines the combination and application of these tools and methods as well as the necessary input data sets used for the respective study. This is followed by Chapter 4, describing the respective results for Studies I-III. Chapter 5 concludes with a discussion of the emerging results and provides an outlook.

Chapter 2

Theory

2.1 Renewable Energy Output Model

In the scope of this thesis, the Renewable Energy Output Model (REOM) is developed: A tool which creates historical and future VRE power production data sets for given wind speed and radiation data and installed plant capacities in a certain domain. Applying the model to high resolution input data sets such as meteorological reanalysis fileds yields spatially and temporally accurate VRE generation time series. Section 3.1.2 discusses reanalysis data sets in detail. REOM is highly flexible at any stage of transition from input resource quantity, i.e. wind speed and solar radiation, to the actual power generation output by a certain power plant fleet. For instance, it is possible to switch between different interpolation schemes or to choose the level of details considered for the calculations. Another key feature of the model is the ability to handle any level of spatial and temporal resolution. The following Sections 2.1.1-2.1.2 depict the model Equations, structure and different settings as well as all crucial details of REOM.

2.1.1 Energy conversion

The REOM model core incorporates one wind and one PV model to derive the conversion from the environmental quantity to electrical power supply of a given plant facility. These are processed for every plant and time step contained in the simulation.

Wind model

Following Henckes et al. (2018), the power output P_{out} of a single wind turbine at a known location for given instantaneous wind speeds at hub height v_{hub} is derived

by the Equation 2.1, also called power curve:

$$P_{out} = \begin{cases} 0, & v_{hub} < v_{in}, \\ \frac{1}{2}\pi R^2 c_p \rho_{hub} \cdot v_{hub}^3, & v_{in} \leq v_{hub} < v_r, \\ C_{plant}, & v_r \leq v_{hub} < v_{out}, \\ 0, & v_{hub} \geq v_{out}. \end{cases} \tag{2.1}$$

On the meteorological side, the power output depends on the wind speed v_{hub} and air density ρ_{hub} at hub height of the rotor. The rotor diameter R, efficiency c_p, capacity C_{plant}, cut-in wind speed v_{in}, cut-out wind speed v_{out} as well as rated wind speed v_r are determined by the specific turbine type. Equation 2.1 shows that a wind turbine produces energy as long as wind speeds at turbine hub height v_{hub} range between the cut-in and cut-out point. With wind speeds higher than the rated speed v_r this is accomplished at a maximum rate – the capacity of the turbine. Between cut-in and rated speed the power production is mainly proportional to the cubic wind speed at hub height. Below v_{in} the unit would not produce any power due to the mechanical inertia of the turbine. Also, it stops for wind speeds higher than v_{out} due to technical limitations and security issues.

Due to the cubic dependency of the power output to the wind speed at hub height in Equation (2.1), it is crucial to have highly accurate wind input data. The wind input data is obtained on a consistent grid defined by the meteorological input data set. As the grid points on the horizontal and vertical level usually do not coincide with the wind park position and hub height, three steps are necessary to get the wind speed at the specific turbine spot. First of all, the absolute values at each grid point need to be calculated from the horizontal components vx and vy of a gridded wind field by

$$v_{i,j,k} = \sqrt{vx_{i,j,k}^2 + vy_{i,j,k}^2} \qquad \begin{matrix} i = 1, ..., m \\ j = 1, ..., n \\ k = 1, ..., p \end{matrix} \tag{2.2}$$

where i, j and k are the grid points in x, y and z-direction. As a second step the absolute wind speeds are horizontally interpolated from adjacent grid points to the exact specific turbine or wind park location. Different interpolation schemes are offered in REOM. Beside a bilinear interpolation, the inverse distance weighting method (IDW) is featured. For the studies designed in Sections 3.1-3.3 the latter is applied – accounting for the exact distance of the known grid point values to the unknown wind park location values, using distance weights. The interpolated wind

speed v at point P is given by

$$v(p) = \begin{cases} \frac{\sum_{i=1}^{N} w(p_i) \cdot v(p_i)}{\sum_{i=1}^{N} w(p_i)} & , d(p, p_i) \neq 0 \\ v(p_i) & , d(p, p_i) = 0 \end{cases} \tag{2.3}$$

with

$$d(p, p_i) = \sqrt{(p_x - p_{x,i})^2 + (p_y - p_{y,i})^2}$$

being the distance between the interpolation point p and the gridded sampling points p_i. The corresponding weight is expressed by

$$w = d(p, p_i)^{-\zeta}$$

where ζ, the power parameter, is set to 2.

Finally the horizontally interpolated wind speeds need to be vertically interpolated, respectively extrapolated to the adjacent hub height. This can be obtained in various ways. The two most common approaches apply the logarithmic wind profile or the Hellmann exponential law (power law) to extrapolate near surface (e.g. 2 m or 10 m) wind speeds to the desired height (Andresen et al., 2015; Hueging et al., 2012; Reyers et al., 2016; Tobin et al., 2014). The vertical wind profile may only in some cases follow a logarithmic profile depending, for instance, on the atmospheric stability conditions. A resulting disadvantage is therefore the inherent inability to reproduce the vertical wind profile at any time and time scale due to different prevailing atmospheric stability conditions (Stull, 1988; Kaimal and Finnigan, 1994; Motta et al., 2005). Extending the logarithmic profile by stability correction terms would be a possible solution to this problem (Stull, 1988; Manwell et al., 2009; Rose and Apt, 2015). However, in addition to the wind fields, several other variables would be necessary to account for atmospheric stability, increasing the model complexity significantly (Stull, 1988). The second approach, the power law, is widely used for engineering and wind energy applications due to its mathematical simplicity: the ratio between the wind speed v_{hub} at hub height and v_{ref} at a reference height near the surface are equal to the ratio of these heights raised to the power of the Hellmann exponent α:

$$v_{hub} = v_{ref} \cdot \left(\frac{z_{hub}}{z_{ref}} \right)^{\alpha} \tag{2.4}$$

According to Emeis and Turk (2007), Equation 2.4 offers a nearly perfect fit to the corrected logarithmic wind profile under stable conditions for certain surface roughness conditions and a good approximation under neutral and unstable conditions

in the limit of very smooth surfaces. REOM features both extrapolation schemes, bringing along the advantage of moderate input data requirements (e.g. only one level of 2-dimensional wind speeds necessary). As a third option, REOM offers the possibility to use a vertical interpolation between different wind speeds at different model layers obtained from the input data set. For this purpose, wind speeds of the first vertical levels are taken as sampling points for a 3rd order fit, which is used for an interpolation from the closest level to the actual hub height. Certainly, in order to apply the latter scheme the meteorological input data set needs to contain vertical resolved wind speed data.

PV model

Following Quaschning (2011) the ideal power output of a PV module $P_{out,ideal}$ can be estimated by the product of the module's area A_{mod}, efficiency η and the global solar radiation on a tilted plane G_{tot}^{tilt}:

$$P_{out,ideal} = A_{mod} \cdot \eta \cdot G_{tot}^{tilt}. \tag{2.5}$$

Due to various effects of energy loss, the power yield of a PV module is actually lower in reality as depicted in Equation 2.5. Amongst others, Quaschning (2011) mentions the following effects contributing to the power loss:

- efficiency decline due to module warming and part load operation,
- reflection losses,
- change of efficiency due to spectral effects,
- soiling and snow,
- shading,
- conduction and diode losses.

Thus the so called performance ratio of a PV module P_r is implemented to yield the real power output $P_{out,real}$:

$$P_{out,real} = P_r \cdot P_{out,ideal}. \tag{2.6}$$

Multiplication of the module area by the efficiency η_{STC} of the module at Standard Test Conditions (STC) and the global solar radiation G_{STC}^{tilt} yields the theoretical capacity of the module C:

$$C = A_{mod} \cdot \eta_{STC} \cdot G_{STC}^{tilt}$$

Equations 2.5 and 2.6 can then be rearranged to

$$P_{out,real} = P_r \cdot \left[C \cdot \frac{\eta}{\eta_{STC}} \cdot \frac{G_{tot}^{tilt}}{G_{STC}^{tilt}} \right] \tag{2.7}$$

The efficiency η depends on the module's actual temperature T_{mod} and the temperature at Standard Test Conditions T_{STC} (Mack et al., 2013):

$$\eta = \eta_{STC} \cdot \left[1 - \beta \left(T_{mod} - T_{STC} \right) \right] \tag{2.8}$$

where β is the temperature coefficient in units of $°C^{-1}$. In Equation 2.8 it describes the loss in efficiency, and hence power loss, the module is facing per °C increase in temperature. T_{mod} is a function of the global solar radiation on the tilted plane and the ambient air temperature T_{2m} and given by:

$$T_{mod} = T_{2m} + c_T \cdot \frac{G_{tot}^{tilt}}{G_{STC}^{tilt}} \tag{2.9}$$

The proportionality factor c_T is a constant temperature and depends on the specific location of the PV module – ranging from 22°C for complete elevation free spots to 55°C for facade integrated non-ventilated solutions (Quaschning, 2011). It can be seen as the temperature surplus the module faces compared to the STC case (Equation 2.9). Actually c_T depends on the ambient wind speed accounting for a cooling of the module by the wind. For simplicity and the fact that the local situation and specific module characteristics are often unknown in large PV facility data sets, the same c_T is set for all data set members.

Finally, Equation 2.7 requires the feed-in of the global solar radiation G_{tot}^{tilt} on the tilted plane, which is defined by the sum of the two solar radiation components, direct G_{dir}^{tilt} and diffuse G_{dif}^{tilt}, as well as a part reflected by the surface G_{ref}^{tilt} (Quaschning, 2011).

$$G_{tot}^{tilt} = G_{dir}^{tilt} + G_{dif}^{tilt} + G_{ref}^{tilt} \tag{2.10}$$

First, the direct radiation on the tilted plane in Equation 2.10 can be calculated given the direct solar horizontal radiation G_{dir}^{hor}, an estimate of the solar incident angle on the tilted plane Θ_{tilt} as well as the actual sun's zenith angle γ_s:

$$G_{dir}^{tilt} = G_{dir}^{hor} \cdot \frac{\cos \Theta_{tilt}}{\sin \gamma_s} \tag{2.11}$$

The incident angle on the tilted plane can be estimated by using the sun's zenith γ_s and azimuth angle α_s as well as the module's tilt angle γ_m and azimuth angle

α_m:

$$\Theta_{tilt} = \arccos\Big(-\cos\gamma_s \sin\gamma_m \cos\left(\alpha_s - \alpha_m\right) + \sin\gamma_s \cos\gamma_m \Big)$$

Second, the estimation of the diffuse fraction on a tilted plane in Equation 2.10 is more complex than for the direct part. According to Quaschning (2011) an anisotropic approach reveals significantly increased accuracy in contrast to the rather simple isotropic ones. They take into account that the radiation density might vary substantially with different cardinal directions, in particular for clear-sky cases. In Chapter 3, two different anisotropic schemes are applied and compared – one approach by Klucher (1979) and one by Perez et al. (1986). For the Klucher model (KM), the diffuse solar radiation on a tilted plane is derived by:

$$G_{dif}^{tilt} = G_{dif}^{hor} \cdot \frac{1}{2}\Big(1 + \cos\gamma_m\Big)\Big(1 + F\sin^3\frac{\gamma_m}{2}\Big)\Big(1 + F\cos^2\Theta_{tilt}\cos^3\gamma_s\Big) \tag{2.12}$$

with

$$F = 1 - \left(\frac{G_{dif}^{hor}}{G_{tot}^{hor}}\right)^2.$$

The more accurate but also more computationally expensive approach compared to Equation 2.12, is the Perez model (PM). First of all, the clear-sky index ϵ and the lightness index Δ are derived:

$$\epsilon = \left(\frac{G_{dif}^{hor} + G_{dir}^{hor}\sin^{-1}\gamma_s}{G_{dif}^{hor}} + \kappa\cdot\Theta_{hor}^3\right)\left(1 + \kappa\cdot\Theta_{hor}^3\right)^{-1} \tag{2.13}$$

$$\Delta = \frac{G_{dif}^{hor}}{\sin\gamma_s \cdot E_0} \tag{2.14}$$

with the constant $\kappa = 1.041$, the incident angle on the horizontal plane Θ_{hor} and the solar constant E_0. By using Equations 2.13 and 2.14, both, the lightness index for the horizon and for the sun's near ambience, can be calculated:

$$\begin{aligned} F_1 &= F_{11}(\epsilon) + F_{12}(\epsilon)\cdot\Delta + F_{13}(\epsilon)\cdot\Theta_{hor} \\ F_2 &= F_{21}(\epsilon) + F_{22}(\epsilon)\cdot\Delta + F_{23}(\epsilon)\cdot\Theta_{hor} \end{aligned} \tag{2.15}$$

The constants F_{11}-F_{23} in Equations 2.15 are assembled in the Appendix, Table C.1. Here, Perez et al. (1986) distinguish between eight different clear-sky classes. Finally, the indices F_1 and F_2 as well as

$$\begin{aligned} a &= \max\left(0; \cos\Theta_{tilt}\right) \\ b &= \max\left(0.087; \sin\gamma_s\right) \end{aligned}$$

yield the diffuse solar radiation on the tilted plane:

$$G_{dif}^{tilt} = G_{dif}^{hor} \cdot \left[\frac{1}{2}(1+\cos\gamma_m)(1-F_1) + \frac{a}{b}\cdot F_1 + \sin\gamma_m \cdot F_2\right] \tag{2.16}$$

Since analyses in Chapter 3 show that the differences between the schemes of KM and PM are neglectable concerning long-term energy production simulations and by comparing their complexity, only the KM is implemented in REOM and used for upcoming simulations.

Third, for the reflected solar radiation on the tilted plane G_{ref}^{tilt} in Equation 2.10, an isotropic approach is sufficiently accurate:

$$G_{ref}^{tilt} = G_{tot}^{hor} \cdot \alpha_{sfc} \cdot \frac{1}{2}\Big(1-\cos\gamma_m\Big). \tag{2.17}$$

The surface albedo α_{sfc} is defined as the ratio of reflected radiation to the received radiation by the surface. Therefore, it's dimensionless value is determined by the surface type and characteristics and ranges between 0.05 for certain forests and up to 0.9 for fresh snow covers. If the surface type, and hence albedo, in the vicinity of the PV module is unknown a value of 0.2 is commonly set over land.

Many available meteorological data sets only supply the total solar radiation on a horizontal plane G_{tot}^{hor}. However, to derive the total solar radiation on a tilted plane required in Equation 2.7, it is necessary to differentiate into direct and diffuse radiation parts (see Equations 2.11, 2.12 & 2.16). This can be accomplished using statistical relations (Quaschning, 2011). Using hourly values of G_{tot}^{hor} and the solar constant E_0 as well as the sun's zenith angle γ_s, the factor k_T in Equation 2.18 can be derived by

$$k_T = \frac{G_{tot}^{hor}}{E_0 \cdot \sin\gamma_s}.$$

The diffuse and direct fractions are then estimated applying Equations 2.18 and 2.19:

$$G_{dif}^{hor} = \begin{cases} G_{tot}^{hor} \cdot \Big(1.020 - 0.254\cdot k_T + 0.0123\cdot\sin\gamma_s\Big), & k_T \le 0.3 \\ G_{tot}^{hor} \cdot \Big(1.400 - 1.749\cdot k_T + 0.177\cdot\sin\gamma_s\Big), & 0.3 < k_T < 0.78 \\ G_{tot}^{hor} \cdot \Big(0.486\cdot k_T - 0.182\cdot\sin\gamma_s\Big), & k_T \ge 0.78 \end{cases} \tag{2.18}$$

$$G_{dir}^{hor} = G_{tot}^{hor} - G_{dif}^{hor} \tag{2.19}$$

To obtain radiation time series at all operation sites, the values incorporated in the meteorological data set need to be interpolated from the underlying grid to the specific locations. This is processed equivalent to the previously discussed wind

model.

2.1.2 Model structure

As illustrated in Figure 2.1, REOM consists of five main modules, namely *CAPS*, *GEO*, *FIELDS*, *INTP* and *ENERGY*. A central configuration file controls which modules to run as well as all input and simulation settings. The former three modules gather and assimilate input data and settings, in *INTP* variables are interpolated and extrapolated, and *ENERGY* builds the actual REOM core processing the energy conversion.

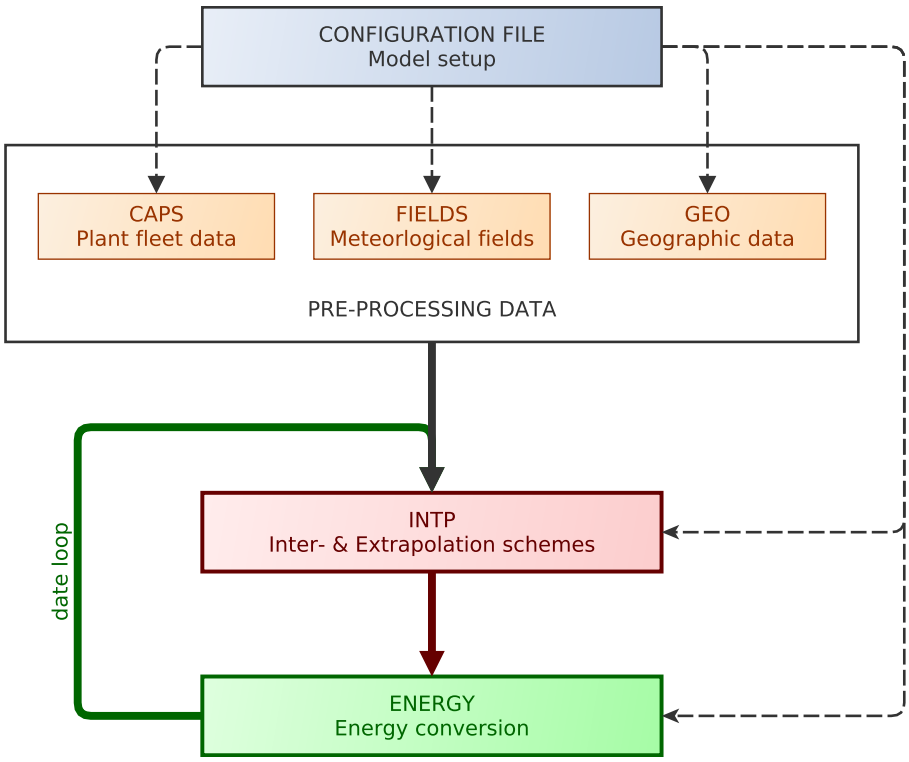

FIGURE 2.1: Schematic illustration of the REOM model.

CAPS

This module prepares all necessary information for the VRE plant fleets as outlined in Section 2.1.1. These include site coordinates, altitudes and locations (onshore/offshore), commission dates (date when a plant started to produce power) and total capacity as well as the manufacturer and plant type. In addition, specific turbine characteristics like rotor hub height and diameter, cut-in, cut-out and rated wind speed are assembled in case of wind parks. Whereas in case of PV plants, plane tilt and azimuth angle are set as well as the module's specific temperature factor, performance ratio, efficiency and temperature at Standard Test Conditions

(STC). For all plant specific characteristics, it is possible to determine whether an existing data base or constant values are processed. Furthermore, REOM provides different handling options for missing data, i.e. whether to take average values or predefined constants. As part of the country loop, *CAPS* provides information and characteristics of every individual VRE operation site for all countries set in the configuration file.

GEO

In *GEO* the domain, geographical and meteorological 2-D fields are imported and processed for every country. For instance, the meteorological grid is coupled to the boundaries of participating countries to reduce all following input fields to the required domain. Surface altitude, albedo and the vertical coordinate are also read from the meteorological data set.

FIELDS

The next step is to read and prepare all the meteorological 2-D and or 3-D fields of all required variables. These include the wind speed, surface temperature and solar radiation. Depending on the chosen meteorological data set and vertical extrapolation scheme, the wind components of either only the first or the first five vertical levels is read. Using Equation 2.2 yields the wind speed time series. In case of radiation, the input data set determines whether the global horizontal solar radiation on the horizontal plane is processed or the two components separately, being direct and diffuse radiation. The configuration file determines the time horizon for which REOM simulates the energy output. Hence, all variables are extracted for the defined time period and spatial domain (including all countries).

INTP

For both, the wind and solar radiation resource *INTP* interpolates the variables horizontally from the meteorological grid to all operational sites using the interpolation scheme according to the configuration file. In case of wind, a vertical extrapolation scheme is applied afterwards yielding the wind speed at required hub heights.

Depending on the availability of the solar radiation quantities in the meteorological data set, Equations 2.12 and 2.11 might be applied to separate the radiation fractions from the global solar radiation. Since radiation is so far referred to a horizontal plane, the KM is used for the conversion to a tilted plane. This is followed by derivations of the reflected part applying Equation 2.17 (incorporating the surface albedo) and finally the global solar radiation on the tilted plane via Equation 2.10.

ENERGY

This module is the main core of REOM since the conversion from the meteorological resource to power output by a power plant is processed. For wind, the power curve relation (Equation 2.1) is applied, whereas Equations 2.7-2.9 are used to model PV modules.

REOM offers the option to run a simulation in "live" or "fixed" mode (set in the configuration file). The former means that the actual commission dates are taken into account – for all time steps prior to the commission date of a plant the power output is set to zero. In contrast, when the model runs in "fixed" mode, a reference date is predefined in the configuration file by the user. In this case, only outputs of plants which started prior to that reference date are taken into account. Therefore, in "fixed" mode the plant fleet is the same for any given time step in the simulation. This is very useful when different time steps or periods are compared, e.g. if the question is whether 1995 was a rather good or bad VRE year compared to other years: Since in 1995 there were almost no wind parks or PV plants installed in the European Union (EU) compared to, e.g. 2014, the "live" mode would not be able to generate comparable years.

Finally, the outcome of a full REOM simulation contains VRE (wind and PV) output time series for each operation site in the pre-defined spatial domain and for the entire time period. Both, the maximum spatial and temporal resolution is determined by the meteorological input data set, but might be decreased by the user. REOM writes output files on a daily, monthly or yearly basis and for each country separately. The model is implemented in *MATLAB*[1] and is able to run in MATLAB's parallel mode (country loop).

As a very last step, the power production time series is converted to a time series of so called capacity factors (CF). This quantity is obtained by normalizing the total sum of power production P of an operation site at all time steps t with its capacity value C multiplied by the respective considered time period Δt:

$$CF = \frac{\sum_t P_t}{C \cdot \Delta t}.$$

The capacity factor is unitless (mostly given in %) and can be interpreted as a measure of the efficiency and capacity utilization of a power plant. Hence it is a very useful parameter for comparisons of different plants as well as different power production technologies. Typically, investigations deal with yearly production values, which gives rise to another quantity of interest – the so called full load hours

[1] MATLAB is developed by MathWorks. In the first place it is a numerical computing environment and programming language. www.mathworks.com

(FLH). The FLH value of an operation site estimates how many hours the facility theoretically has to be operated at full capacity to gain the same annual power yield: the capacity factor is simply multiplied by 8760 h to obtain the FLH of an operation site. In conclusion, both parameters supply the same information.

2.2 Clustering algorithm

To model an energy market system for one entire year, the system of Equations (e.g. see Section 2.3) is fed with time series of wind and PV energy as well as demand – for example, with an hourly resolution that would lead to three times 8760 of data points. Investment models often even simulate time periods of several years or decades, increasing the amount of data and hence set of Equations dramatically. Applied to these kinds of systems, even a very simplified investment model would need high amounts of computational costs. Therefore, in many cases it is crucial to reduce the dimensions of the model (set of Equations). This can be accomplished by decreasing the spatial and or temporal resolution of the VRE input data. For instance, the resolution within a day can be reduced to 3, 6 or even 12h. Regarding the spatial dimension, an option would be to decrease the number of horizontal grid points taken into account. However, in many cases these solutions might not be effective enough. In addition, in most of the studies, wind and PV time series are even accumulated for an entire country (e.g. Gils et al., 2017; Dominković et al., 2016; Cebulla et al., 2017). This might have a great impact on the computational costs but at the same time significant uncertainties might be introduced concerning VRE profiles due to the coarse accumulation step.

Hence the objective is to reduce the complexity of the system and at the same time not to loose too much information regarding important characteristics contained in the original input data. One way to tackle these problems is the application of cluster algorithms (Merrick, 2016). Such an algorithm tries to find a set of unique clusters (characteristic subsets) inside the complete data set, containing data points or time series (e.g. days) as similar as possible. In other words, the complete data set is divided into groups with members of similar characteristics. As a next step, one representative data point or time series needs to be derived from each cluster. For instance, this can be the average of a cluster or one specific cluster member.

In the scope of this thesis, cluster methods are developed for either, the spatial and temporal scale as well as a combination of these. Figure 2.2 illustrates the implemented method depicted in detail in the following. The spatial clustering is supplied by a VRE time series with certain locations and for a defined time period.

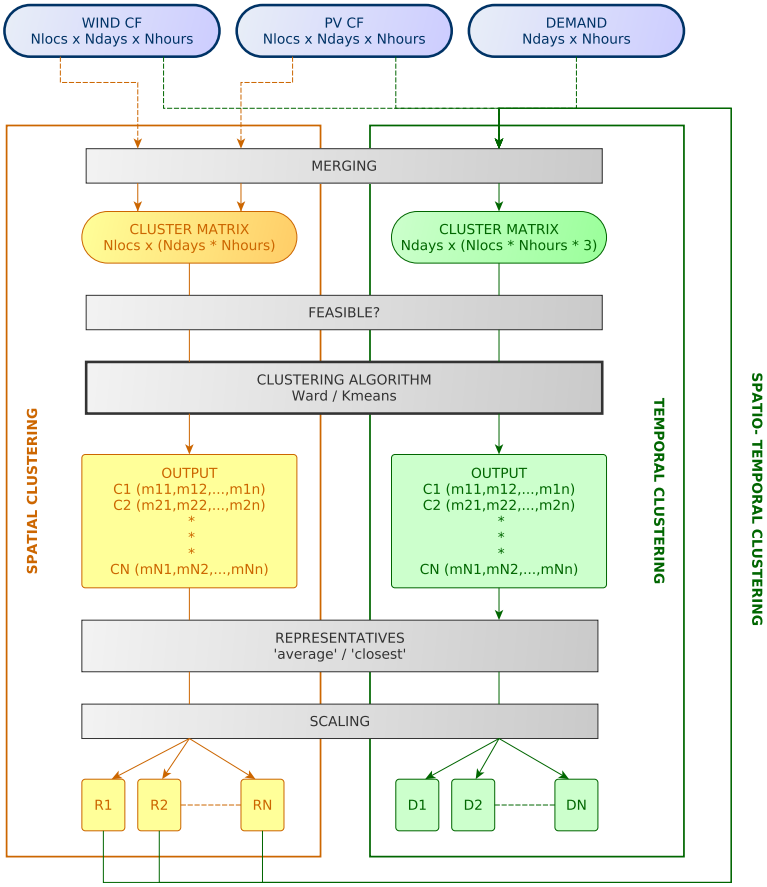

FIGURE 2.2: Schematic illustration of the clustering method and its pathways.

As an output of REOM, a VRE matrix would usually have the dimensions:

$$N_{locations} \times N_{days} \times N_{hours}.$$

To process the algorithm, it needs to be reshaped so that the locations are still represented by the rows (cluster dimension) and the time steps by the columns:

$$N_{locations} \times \left(N_{days} \cdot N_{hours}\right).$$

The output of the clustering algorithm will be characteristic and unique groups or clusters of locations which are similar to each other, i.e. a set of representative regions. Note that the spatial clustering is applied separately for different VRE sources – leading to potential differences in the regional partitioning concerning wind and PV energy.

Concerning temporal clustering, the wind and PV as well as the energy demand time series need to be merged in a first step as the characteristics of each time step are depending on all three quantities in energy system modeling. Similar to the

spatial case, a reshape of the clustering matrix is necessary. In order to generate typical characteristical days (from now on called typedays), the day-dimension is object to the clustering algorithm. Therefore, this time rows represent days, leading to the following matrix:

$$N_{days} \times \Big(N_{locations} \cdot N_{hours} \cdot 3 \Big).$$

Note that the number of 3 appears due to the three time series merged in the beginning. As a last step, the output matrix needs to be separated again yielding diurnal time series for wind, PV and demand respectively. In other words, the temporal clustering generates distinct typedays containing diurnal profiles of all three quantities.

The clustering routine is developed in MATLAB and provides, as indicated in Figure 2.2, three pathways:

i. temporal clustering only $\longrightarrow$ full location grid & typedays,

ii. spatial clustering only $\longrightarrow$ region cluster & entire time series,

iii. spatial & temporal clustering $\longrightarrow$ region cluster & typedays.

For the latter, the output of the spatial clustering step is serving as an input for the temporal clustering. In all cases, the actual algorithm can be selected between *ward* and *k-means* (MATLAB functions *"ward"* and *"k-means"*). They are set to use the Euclidean distance as a measure and, in case of *k-means*, a maximum of 100 iterations is chosen. Both schemes provide the possibility to pre-define the actual number of clusters (i.e. typedays or regions). Therefore, the clustering routine offers two options – using either fixed cluster numbers or identifying the optimal cluster numbers (only valid for spatial clustering). The latter is implemented by evaluating the silhouette scores while iterating the number of clusters (MATLAB function *"eval"*). The higher the score, the closer to the optimal number of clusters.

As mentioned before, the developed routine provides two ways of extracting a representative R of each cluster c, namely "average" and "closest". The former takes the mean of N cluster members M:

$$R_c = \frac{1}{N_c} \cdot \sum_{i=1}^{N_c} M_i, \qquad \text{for } c = 1, ..., N_{cluster}.$$

whereas for the second way the most similar cluster member M to the cluster mean μ is determined by an estimation of the minimum of the standard deviation:

$$R_c = \min\left(\sqrt{\sum_{j=1}^{N_c}\frac{(M_j-\mu_c)^2}{N_c}}\right), \qquad \text{for } c = 1, ..., N_{cluster}$$

An advantage of the latter is that it keeps the inherent variability of the time series, in contrast to a damping due to the averaging process.

Furthermore, the routine checks for the feasibility of the system – is a sample size too small, the entire sample is considered as one cluster. This becomes essential for the spatial clustering, since certain smaller domains (in combination with the spatial resolution) contain only a few grid points. For instance, a country like Luxembourg and a horizontal resolution of 44 km (as in Section 3.3) provides only two sample points for the routine. Hence the clustering looses its classical meaning. In this example, only one region is assigned to Luxembourg consisting of all grid points in the country. The feasibility is given when

$$\begin{aligned} \text{k-means:} \quad & \frac{sample\ size}{N_{cluster}} > 2 \quad \text{and} \\ \text{ward:} \quad & sample\ size \geq 2 \end{aligned}$$

.

Comparing the characteristics of a set of clusters with its original data set sometimes shows significant deviations, even for the mean of the quantity. Obviously this can be a problem, e.g. concerning the overall level of energy production of a VRE quantity in a specific region or country. Therefore, after all a scaling process is implemented in the end of the clustering routine to ensure that the production levels are at a similar magnitude in the set of cluster representatives CF_{clust} and the original data CF_{orig}. This is accomplished by a comparison of mean values in both data sets yielding a factor f

$$f = \frac{\text{mean}(CF_{orig})}{\text{mean}(CF_{clust})}.$$

which is then used to scale the cluster representatives:

$$\begin{aligned} CF'_{clust} &= CF_{clust} \cdot f, \\ CF'_{clust}(CF'_{clust} > 1) &= 1. \end{aligned}$$

The scaling might generate capacity factors greater than 1, a 100% capacity utilization, which is obviously impossible and therefore corrected. The scaling is iterated until the factor is converging to 1 within a pre-defined precision range p_r (e.g. $p = 0.001$):

$$1 - p_r < f < 1 + p_r.$$

The final output of the clustering routine is a set of cluster representatives (either regions, typedays or a combination of both) with the aim to capture the main characteristics of the original data set while realistically representing the overall level of energy production rates as well as demand levels. To be able to reconstruct the original data set or parts of it, the output is complemented by the occurrence frequencies of each cluster. For instance, to generate one year of VRE production and demand from a typeday data set, the respective occurrence frequency needs to be applied to each typeday and the result multiplied by the number of days, in this case 365.

2.3 Renewable Power System Model

Given a system of various power generating technologies, each with different characteristics such as fuel costs, efficiency or carbon dioxide (CO_2) emissions, and a determined power demand: what would be the favorable composition of capacity assets to be able to serve the demand at minimum costs for every time step in a certain period of time? This question implies that a sort of optimization is necessary to solve the problem, i.e. a minimization of costs under certain assumptions and constraints. Numerous optimization models were developed to tackle similar problems – some more complex than others, depending on the exact objective and research question.

Such an optimization model is developed to approach the specific problems of this thesis. From now on, this model is called Renewable Power System model (RPSM). Compared to other investment models used for energy system studies, the RPSM is in most parts a rather simple model since it lacks some characteristics of a realistic reproduction of the energy market system. For instance, the RPSM only considers the electricity sector of the energy system, ignoring that energy in the form of heat might play a major role as well. Also the electricity net within a country as well as storage and diversified plant technologies are neglected. However, the energy system model is kept to a lower complexity on purpose to be able to isolate crucial processes for an easier interpretation of the outcomes.

2.3.1 Model Equations

The RPSM core contains a linear programming model, which minimizes the overall costs of the energy system for a certain domain and time period. It is considered a perfect foresight model – the optimization scheme knows all relevant information as well as future processes and developments are anticipated. For example, the model might decide to invest in a certain asset in the beginning of the time period due to the knowledge of future needs.

The main Equation – in linear optimization also called objective function – in the RPSM, which needs to be minimized, is the total sum of all costs C in the system arising from all regions R, technologies T and time steps (years) Y:

$$min \quad C = \sum_{r \in R} \sum_{t \in T} \sum_{y \in Y} \left(C^{inv}_{r,t,y} + C^{fix}_{r,t,y} + C^{var}_{r,t,y} \right) \tag{2.20}$$

where

$$C^{inv}_{r,t,y} = P^{add}_{r,t,y} \cdot c^{inv}_{t,y}, \tag{2.21}$$

$$C^{fix}_{r,t,y} = P^{exi}_{r,t,y} \cdot c^{fix}_{t,y} \cdot dt_y, \tag{2.22}$$

$$C^{var}_{r,t,y} = \sum_{d \in D} \sum_{h \in H} G_{r,t,y,d,h} \cdot c^{var}_{t,y} \cdot f_d \cdot dt_y \cdot \tau \cdot 365. \tag{2.23}$$

The investment costs C^{inv} are determined by the product of the technology specific investment costs c^{inv} and the total amount of capacities added to the system P^{add} (Equation 2.21). Similarly, fixed costs for operation and maintenance (FOM) C^{fix} of the assets are derived by multiplying the existing installed capacities of a technology at a time step by its specific FOM costs c^{fix} (Equation 2.22). Since FOM costs are usually given per year, the amount of years between two simulation time steps need to be considered here ($dt_y = Y(y) - Y(y-1)$). In contrast, the so called variable costs C^{var} are the total sum of generation costs composed of the power generation G of a technology and the associated fuel costs c^{var} (Equation 2.23). In the first place, this product is calculated for all time steps (for more details on time steps see Section 2.3.2), however in case of applying typedays (see Section 2.2) an upscaling towards an entire year of production is derived with the typeday occurrence frequencies during a year f_d, the amount of days in a year and the hourly resolution τ.

All regional installed existing capacities P^{exi} of each technology and time step consist of the installed capacities from the last time step $y-1$, which can be complemented by additional capacities P^{add} or subtractive capacities P^{sub} by the

model:

$$P^{exi}_{r,t,y} = P^{exi}_{r,t,y-1} + P^{add}_{r,t,y} + P^{sub}_{r,t,y}. \tag{2.24}$$

For the first time step, in Equation 2.24, P^{exi} at $y-1$ is defined by the exogenous predefined existing assets $P^{exi,exo}$. In most European countries, the river-runoff potential is either exceeded or rather small. Therefore the initial existing capacities of that technology are taken as its threshold for the whole simulation period:

$$P^{exi}_{r,runoff,y} \leq P^{exi,exo}_{r,runoff}. \tag{2.25}$$

The total European power production from biomass is limited by its available resource amounts. This is imposed by the sum of exogenous biomass capacity bounds and the exogenous predefined existing biomass capacities $P^{exi,exo}$ for the entire model domain (e.g. EU) serving as an upper bound:

$$P^{exi}_{r,biomass,y} \leq \sum_{r \in R} \sum_{y \in Y} P^{bnd}_{r,biomass} + P^{exi,exo}_{r,biomass,y}. \tag{2.26}$$

Looking at wind and solar energy capacities another constraint is considered to be important – large-scale expansion of wind and PV parks require non-negligible amounts of land and/or sea area. Equation 2.27 shows the implementation in RPSM:

$$P^{exi}_{r,tres,y} \leq P^{poss}_{r,tres}. \tag{2.27}$$

The maximal possible installed capacity P^{poss} of each VRE technology serves as an upper bound to the respective existing capacities at each time step and region. Section 2.4 illustrates how the potential available areas are estimated.

Additional capacity investments P^{add} can be either exogenous (pre-determined, $P^{inv,exo}$) or endogenous (model decision, P^{inv}) induced. However, expanding fleets endogenously is prohibited for the first model year (depending on model setup):

$$P^{add}_{r,t,y} = \begin{cases} P^{inv,exo}_{r,t,y}, & y = Y(1), \\ P^{inv}_{r,t,y} + P^{inv,exo}_{r,t,y}, & y > Y(1). \end{cases} \tag{2.28}$$

In addition, the model has the option to account for possible phase-outs of certain technologies, such as for nuclear and coal. This for instance, should find consideration in Germany, where politics recently decided a nuclear phase-out and coal is currently subject to debates and negotiations. In these particular cases, P^{add} is set to zero for participating regions and any given time step.

In future scenarios where VRE technologies are expected to gain more and more significance in the European energy mix, e.g. due to policy making, the invest model

would tend to build excessive VRE capacities. However, recent years have shown that fabrication capacities of VRE plants have their limitations. Hence, in order to consider more realistic extensions of VRE fleets, these technologies are subject to investment bounds $P^{add,bnd}$, defined per year as depicted in Equation 2.29:

$$P^{add}_{r,tres,y} \leq P^{add,bnd}_{r,tres,y}. \tag{2.29}$$

Equation 2.30 represents all subtracted capacities P^{sub} in each technology and time step. The first term represents exogenous predefined subtractions $P^{sub,exo}$. The second term stands for endogenous subtractions induced by lifetime limitations for each technology. It is calculated using invested P^{add} in earlier time steps in combination with the respective lifetime λ_t:

$$P^{sub}_{r,t,y} = \begin{cases} P^{sub,exo}_{r,t,y}, & y - \lambda_t \leq Y(1), \\ P^{sub,exo}_{r,t,y} + P^{add}_{r,t,y-\lambda_t}, & y - \lambda_t > Y(1). \end{cases} \tag{2.30}$$

Equation 2.20 is object to several further constraints determining the behavior of the system. The most important condition is the energy balance constraint – the total electricity demand L needs to be satisfied by the overall sum of power generation G of all technologies and the import and/or export F of a region at any given time step. That leads to

$$L_{r,d,h,y} \leq \sum_{t \in T} G_{r,t,y,d,h} - \sum_{r' \in R'} F_{r,r',y,d,h} + \sum_{r \in R} F_{r',r,y,d,h} \cdot \eta^{ntc} \tag{2.31}$$

The power generation G is defined by the product of existing capacities of a technology and its respective generation profiles g:

$$G_{r,t,y,d,h} \leq P^{exi}_{r,t,y} \cdot g_{r,t,y,d,h}. \tag{2.32}$$

Furthermore, Equations 2.31 and 2.32 are complemented by the fact that the maximum possible total electricity generation in the system is restricted by its availability or capacity value cv and needs to exceed the yearly peak demand $L^{YP}_{r,y}$, expressed in Equation 2.33:

$$L^{YP}_{r,y} \leq \sum_{t \in T} P^{exi}_{r,t,y} \cdot cv_t. \tag{2.33}$$

The energy transmission or trade F between one region $r \in R$ to another region $r' \in R'$ in Equation 2.31 is bounded by the net transfer capacities P^{ntc}:

$$F_{r,r',y,d,h} \leq P^{ntc}_{r,r',y}. \tag{2.34}$$

Transportation of power is linked to a certain energy loss – represented by the multiplication with the net transfer capacity efficiency η^{ntc}.

Emissions, in particular CO_2, recently gained more and more significance for energy market systems, since they play a major role for climate change discussions and policy making. To account for CO_2 policies, an emission cap E^{cap} per year and region is introduced with Equation 2.35. It constrains the total sum of all conventional (CO_2 emitting) power generations in one entire year multiplied by the technology specific CO_2 emission factor ε (Equation 2.36). Since these factors are usually provided in tons of CO_2 per thermal MWh_{th}, the net efficiency (unit MWh_{el}/MWh_{th}) of a technology η needs to be applied.

$$E_{r,y} \leq E^{cap}_{r,y}, \tag{2.35}$$

$$E_{r,y} = \sum_{tcon \in T} \sum_{d \in D} \sum_{h \in H} \frac{G_{r,tcon,y,d,h}}{\eta_{tcon}} \cdot \varepsilon_{tcon} \cdot f_d \cdot \tau \cdot 365. \tag{2.36}$$

That concludes the system of equations contained in RPSM. In the following, details concerning model resolution and the *Greenfield* mode are explained.

2.3.2 Spatio-temporal resolution

The RPSM contains several levels of temporal resolution. First of all, the investment simulation time step is in the order of years to decades. That means the model can adjust the installed capacities only for these points in time. For instance, as a result Equation 2.21 is calculated at the coarsest resolution level. In contrast, energy generation and demand are object to a finer resolution, namely intra-annual (e.g. daily or monthly) and intra-daily (e.g. hourly or 6-hourly). Thus, Equation 2.31 is, for example given for days and hours and the variable costs need to be accumulated from hourly values to the time period between two simulation time steps (e.g. year or decade). All resolutions can be pre-set in the RPSM, although the intra-annual and intra-daily resolution is restricted by the input data sets.

When it comes to economical energy system modeling on a transnational scale, the spatial resolution is market based. Since each of the countries in the European Union has its own energy market, the spatial resolution is subject to the number of considered countries. For simplicity and computational reasons, all Equations are solved on this coarse segmentation. That infers that, besides the conventional plants, also the VRE facilities can only be built based on one respective generation profile. In order to account for more distinct generation profiles, different sub-technologies are often implemented (e.g. by the EWI), e.g. the model can invest in

several different wind park types (Fürsch et al., 2013; Knaut et al., 2016). Most of the times, these sub-technologies are applied to one to three country-based average wind time series (Fürsch et al., 2013; Knaut et al., 2016). In some studies by the EWI, for instance, at least two different VRE regions per country are implemented in order to account for the different wind climatology (e.g. Jägemann et al., 2013). Yet, the averaged profiles for these regions are based on a weak data fundament (only 10 years of wind and solar data). However, this is certainly a rather gross approach regarding the spatio-temporal variability of wind and solar radiation, in particular concerning the recently fast increasing shares of VRE supply. Another problem with this approach is that the model output would not contain any information about the location of capacity allocation and related area availability questions within a country. Therefore the objective in RPSM is to implement various distinct VRE generation profiles, which cover the main characteristics for the spatio-temporal scales with a sufficient data basis to be more accurate and realistic.

In order to tackle these challenges, an improved spatial resolution concerning VRE generation profiles is implemented in RPSM. The basis builds the horizontal resolution of the CF input data from REOM, which is required to origin from sufficiently sized data basis. For each location in the CF profile data set, a new "sub-technology" is introduced to the model. By this, the RPSM is able to decide where to build new VRE facilities (based on various profiles) and is constrained by area availability (via area potentials). For instance, a 48 km grid in Germany results in about 150 wind and PV locations. At each grid point, information about the diurnal CF time series and the available area is supplied to the model. Now the RPSM can decide to extend the wind and or PV plant fleets at the best respective spot for a cost optimal solution as long as there is space.

2.3.3 Greenfield mode

As an additional option, the RPSM can be run in *Greenfield* mode. Basically, it means that the model is initiated without any existing installed capacity or exogenous planned expansion strategies. Instead, only the model itself decides endogenously which technologies to invest into and to what extent, for any given time step, including the beginning of the simulation period (initial conditions). Applying this mode might be useful depending on the objective and research question corresponding to the simulation. For instance, in case of simulations of end-of-century scenarios, this approach can be reasonable as existing present-day capacities would not affect the development until the point of interest. These capacities would be already removed by the mid-century. Therefore, it is crucial to determine whether a point of interest in time is affected or not by the systems "memory".

But what precisely is modulated in the RPSM with *Greenfield* enabled? There are some aspects adjusted concerning the input as well as the model Equations. Since exogenously pre-defined installed capacities are omitted, $P_{r,t,y}^{exi,exo}$ and $P_{r,t,y}^{sub,exo}$ are set to 0 (affects Equations 2.24, 2.30, 2.25 and 2.26). Capacity expansion strategies are represented by Equation 2.28. In *Greenfield* mode, it simplifies to

$$P_{r,t,y}^{add} = P_{r,t,y}^{inv}.$$

In addition the VRE extension bounds in Equation 2.29 are disabled since the model must be able to expand the VRE technologies immediately within one simulation time step.

2.4 Area potentials

As depicted in Section 2.3.1, the available area for VRE expansion needs to be taken into account as an additional constraint. In Equation 2.27 the maximum possible installable VRE capacity P^{poss} works as an upper bound and depends on the available area for constructions. The following Section illustrates the methodology to obtain these areas, comprising several basic steps.

2.4.1 Spatial tessellation

Meteorological fields are given on spatially equally spaced grid points in a certain domain. Since the RPSM is able to invest in VRE capacities on each of these points, it is necessary to consider their potential area for VRE plants. One approach is to partition the entire domain into areas associated to the grid points. By this, the surroundings of each grid point are considered, accumulated and hence concentrated in that point. In the RPSM, countries are treated separately concerning their energy production and hence also their VRE capacity expansions. Therefore political borders need to be implemented. The first step is, hence, to clip the meteorological grid to shapes of the political borders. The geographic information system software *ArcGIS* is able to solve this and is also used for the following tasks.

In a second step the partitioning is processed, which can be accomplished by spatial tessellation of the entire domain in combination with the underlying grid. In *ArcGIS* the tessellation is realized by using *Thiessen Polygons* (also called *Voronoi Diagram* or *Dirichlet Tessellation*). This results in equally expanded areas associated with the grid points. However, due to the clipped borders, some of the polygons located close to the edge are smaller than others located on the inside of a country. These polygons are adjusted to the exact shape of the adjacent border. Yet, at this

point of the method, different area values are obtained. Figure 2.3 illustrates the resulting tessellation and polygons at this step of the process. Note that countries as well as on- and offshore regions within a country are treated separately.

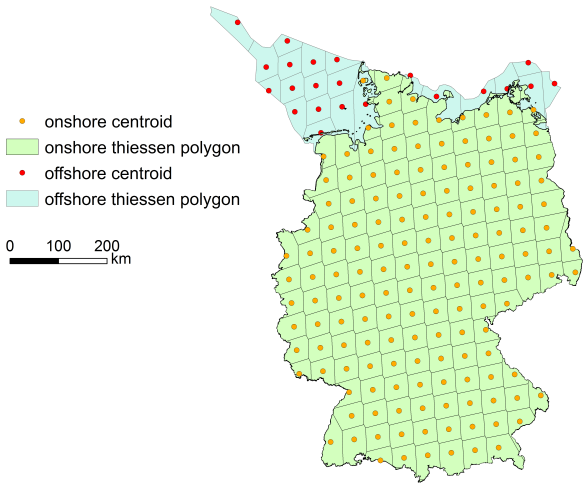

FIGURE 2.3: Offshore and onshore poylgons as a results of the spatial tessellation for Germany. Dots are onshore (orange) and offshore (red) centroids.

2.4.2 Area restrictions

So far only the extent of a country and the grid characteristics are considered. However, the potential areas for VRE capacity expansion are restricted for various reasons, e.g. different land uses, buildings, nature reserves and technical limitations such as hill slopes. McKenna et al. (2015) face similar challenges when analyzing the cost potential of VRE in the EU. They apply a successive procedure to account for these restrictions. The applied method in this work follows their approach.

First of all, the total potential European area is reduced stepwise by subtracting unsuitable land use types. For this purpose, the *Corine Land Cover 2000 (CLC2000) Version 16* provided by the European Environmental Agency (EEA), is used as a basis. The data set contains 44 different land use types with a horizontal resolution of 100 km covering the European domain. The exclusion criteria – the criteria which land use type would not contribute to the area potentials – and offset distances are applied following the German Federal Ministry of Environment, Nature Conservation & Nuclear Safety (BMU). Note that the criteria are not changed by country, but kept to the German guidance for simplicity. In Table C.2 in the Appendix both the CLC2000 land use categories by the EEA as well as the corresponding distances to plants from the BMU are assembled (McKenna et al., 2015).

Secondly, additional area restrictions due to protected areas and technical limitations are considered evaluating *NATURA 2000*, the *National Designated Areas (CDDA)* and the *Shuttle Radar Topography Mission (SRTM)* deliver information about protected areas. NATURA 2000 is a continuous network of protected areas which has the objective to secure natural reserves in the EU. Via the CDDA data set, the EEA delivers "individual nationally Designated Areas and corresponding Protected Site spatial features in EEA member and collaborating countries". The SRTM is operated by the NASA and taken as a source for hill slope data. Here, the applied criterion discards areas with hill slopes exceeding 20°. As an example, Figure 2.4 shows the onshore and offshore area restrictions in Germany when combining step one and two.

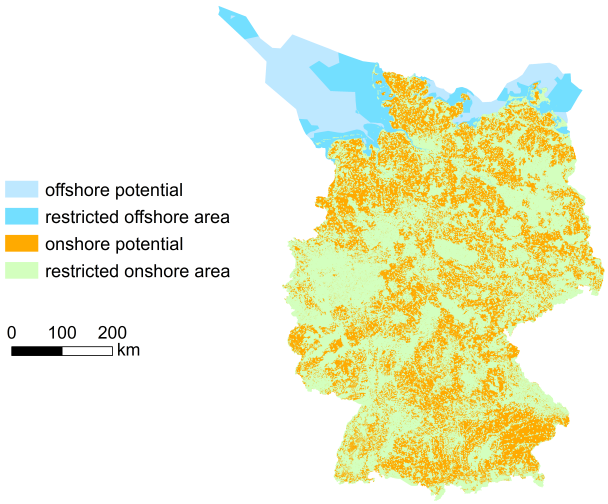

FIGURE 2.4: Resulting offshore and onshore area restrictions in Germany.

In contrast to McKenna et al. (2015), transport infrastructure (e.g. via *Open Street Map*[2]) as well as suitability factors are not considered due to simplicity and computational reasons. Note that the estimated areas are taken for wind and PV sites seperately. For the applications examined in this work the available areas for VRE expansion need to be implemented on a rather coarse level of details. Therefore, the depicted approach seems sufficient and reasonable.

2.4.3 Area conversion: area power densities

Certainly, the resulting area potentials in Section 2.4.2 might lack further restrictions due to other aspects not considered here. Therefore, the sum of area potentials at grid points P in a country is compared to area potential values for that country

[2]www.openstreetmap.de

from literature ($A^{lit}_{r,tres}$). That yields a factor which can be applied to further reduce the available areas for VRE expansion ($A_{r,tres}$) in the country:

$$A'_{r,tres} = A_{r,tres} \cdot \frac{A^{lit}_{r,tres}}{\sum_{p=1}^{NP} A_{r,tres}|_p} \tag{2.37}$$

with NP the number of grid points in a country. Sources for the total area values of European countries are McKenna et al. (2015) for onshore wind, EEA (2009) and WindEurope (2017) for offshore wind and Schmidt et al. (2016) for PV. Note that for the latter, potential areas for roof PV and base PV are accumulated. After this last step, realistic area potentials for any grid point and VRE technology in a certain country are obtained – or in other words: the estimated area potentials show realistic total amounts on a country basis and are horizontally resolved at the same time.

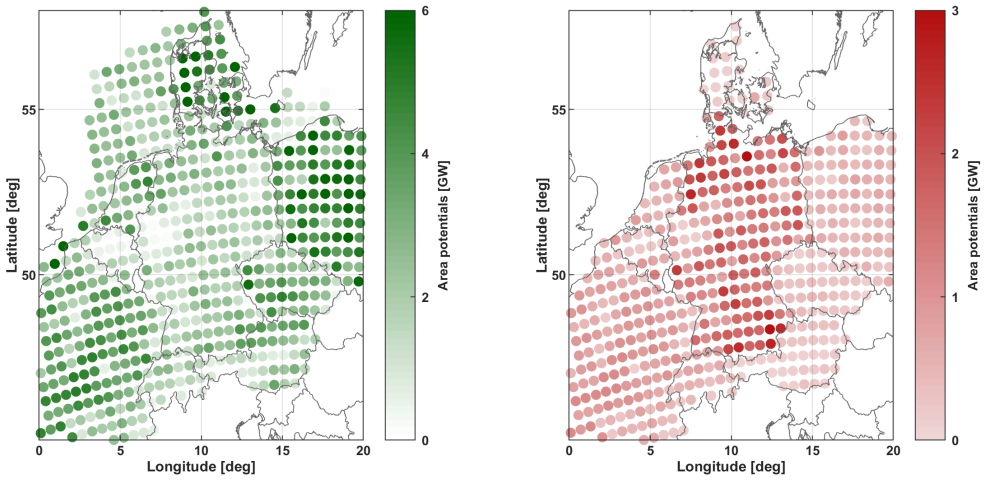

(A) (B)

FIGURE 2.5: Area potentials[GW] on a 44x44 km grid in Germany and neighboring countries, for wind energy (A) and PV energy (B).

In RPSM the area potentials are implemented regarding maximal possible expansion potential for VRE capacities with respect to an area corresponding to a certain grid point (see Equation 2.27). Thus, area potentials in km^2 resulting from Section 2.4.2 need to be converted to area potentials in GW. For this purpose so called area power density factors ρ^{area}_{tres} are introduced and applied to the area potentials yielded from Equation 2.37:

$$P^{poss}_{r,tres} = A'_{r,tres} \cdot \rho^{area}_{tres} \tag{2.38}$$

The area power density in Equation 2.38 is technology specific – values are set following EEA (2009) to 8 MW km^{-2} for onshore and 12 MW km^{-2} for offshore wind sites. In case of PV, ρ_{tres}^{area} is set to 25 MW km^{-2} (Ong et al., 2013). Figure 2.5 shows an example for obtained area potentials in Germany and neighboring countries on a 48x48 km grid. Note that for offshore areas only territorial waters belonging to the respective countries are considered.

Chapter 3

Application & data

This Chapter presents the application of developed methods (depicted in Chapter 2) and data sets to investigate various research questions in the scope of this thesis. They can be precised to three principal parts related to the Studies I-III. First, Section 3.1 explains the generation process of a long-term wind power data set to analyse wind power characteristics in Europe with a focus on Germany (Study I). Second, Section 3.2 outlines the methodology used to estimate uncertainties in energy market models when applying long-term VRE time series as created in Section 3.1 (Study II). Third, to investigate the impact of climate change on future European energy markets, a combination of all developed methods and tools is required. The emerging model chain and input data is examined in detail in Section 3.3 (Study III). Results and analyses to each of these topics are discussed in an identical structure in Chapter 4.

3.1 Generation of a long-term wind power data set

The following Section is related to Study I. As outlined in Section 1, to understand future energy systems it is essential to recognize the unique characteristics of wind power production. Due to the lack of sufficient historical data sets concerning high resolution long-term wind power time series in Europe, such a data set is generated by model simulations. For this purpose, the novel VRE power model REOM is applied to the combination of a unique high resolution reanalysis product (Section 3.1.2) with a location specific European wind park portfolio (Section 3.1.1). The generation process and applied data sets to obtain a realistic historical time series for Europe as well as further analysis are described in the following. Results can be found in Section 4.1. Note: this part is associated with the publication in *ENERGY* in 2018 with the title *"The benefit of long-term high resolution wind data for electricity system analysis"* (Henckes et al., 2018).

3.1.1 Wind park data

The conversion from energy contained in wind speed to power output by a wind turbine is represented by its power curve. Equation 2.1 shows the requirement of two data sets: On the one hand, the rotor diameter R, efficiency c_p, capacity C, cut-in wind speed v_{in}, cut-out wind speed v_{out} as well as rated wind speed v_r need to be covered by a European wind park data set. On the other hand, the meteorological side requires the wind speed v_{hub} and air density ρ_{hub} at hub height of the rotor.

Besides the parameters in Equation 2.1, the park data set needs to provide two additional information. First, the exact location (coordinates) is necessary to assign the wind park's operation site to adjacent grid points of the underlying meteorological grid. Second, to simulate a consistent time series of power production by a wind park, its commission date (date when a park started operation) is required. In order to yield realistic estimates of wind power production in Europe the actual installed operation sites need to be supplied to REOM. Here, an extract of the database from *The Wind Power* is used (The Wind Power, 2016)[1]. It is a worldwide data set for installed wind turbines and parks including about 1050 different turbine types and more than 18600 wind park sites in Europe.

TABLE 3.1: Wind park specific parameter availability for all wind parks in Europe. The database *The Wind Power* serves as the basis.

Parameter	Availability [%]	Default value
Location	100	-
Commission date	100	-
Number of turbines	100	-
Hub height	60.6	80 m
Rotor diameter	37.5	70 m
Cut-in	66.8	3.5 ms^{-1}
Cut-out	66.8	26 ms^{-1}
Rated speed	66.8	12 ms^{-1}

In order to be able to compare different years of weather and hence wind power production, the European wind power park fleet at the end of 2014 is used as the basis for the long-term wind power production simulations. The *CAPS* module in REOM (Section 2.1.2) is responsible for a pre-filtering of the wind parks due to gaps in the data set. Facilities with either missing location, production status or commission date information are dismissed. This results in 15400 European

[1] Last updated in April 2016

parks contributing to an overall installed capacity of 119.85 GW by the end of 2014. However, some parameters are still lacking to different extent. For instance, for more than half of all parks in Europe the rotor diameter is unknown and for roughly 40% the exact hub height is lacking. In these cases default values are set. Table 3.1 comprises the parameter availability for all remaining operation sites in Europe and Figure D.1 shows their distributions. This is important to be aware of when using the data for analysis, and it leaves room for improvements.

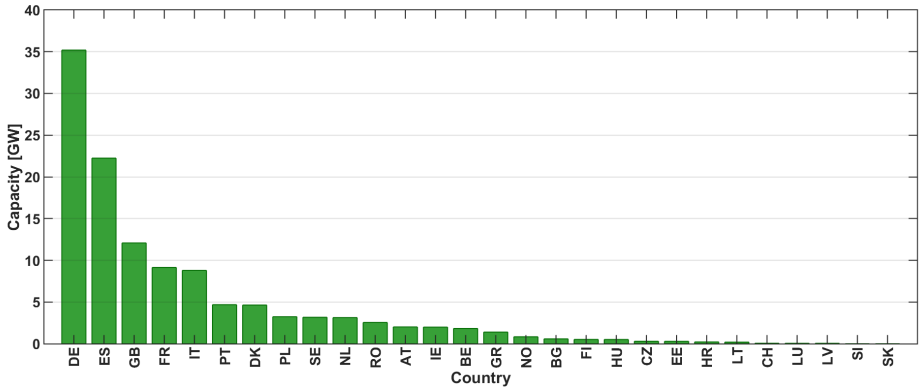

FIGURE 3.1: Country-wise accumulated installed wind power capacities [GW] in European countries by the end of 2014. The database *The Wind Power* serves as the basis. Parks with either missing location or commission date are excluded. Source: Henckes et al. (2018).

Figure 3.1 shows that the installed wind power capacities accumulated by European countries is largest for Germany (35.19 GW), followed by Spain (22.24 GW) and Great Britain (12.08 GW). The facilities' spatial distribution can be examined in Figure 3.2. Since the wind resource is most abundant in coastal regions by trend, capacities are concentrated at the North Sea (Germany, France, Britain) and the Atlantic (Spain, Portugal). One of the biggest wind parks worldwide is found in the North Sea. Since April 2013 the British offshore site *London Array* supplies 630 MW capacity with 175 turbines. Nevertheless, in certain countries like Germany and Spain a significant amount of operation sites is located inside the country. With 347.5 MW the largest onshore wind park in the data set is located in Romania.

Histograms of the turbine specific parameters of the data base are depicted in Figure D.1 and their statistics summarized in Table 3.2. It is evident that a typical European wind turbine (status at the end of 2014) is about 80 m high with a rotor diameter of 72 m. Most likely the non-linear range of the power curve is located between 3 ms^{-1} and 12 ms^{-1} and the turbine can operate until 26 ms^{-1}.

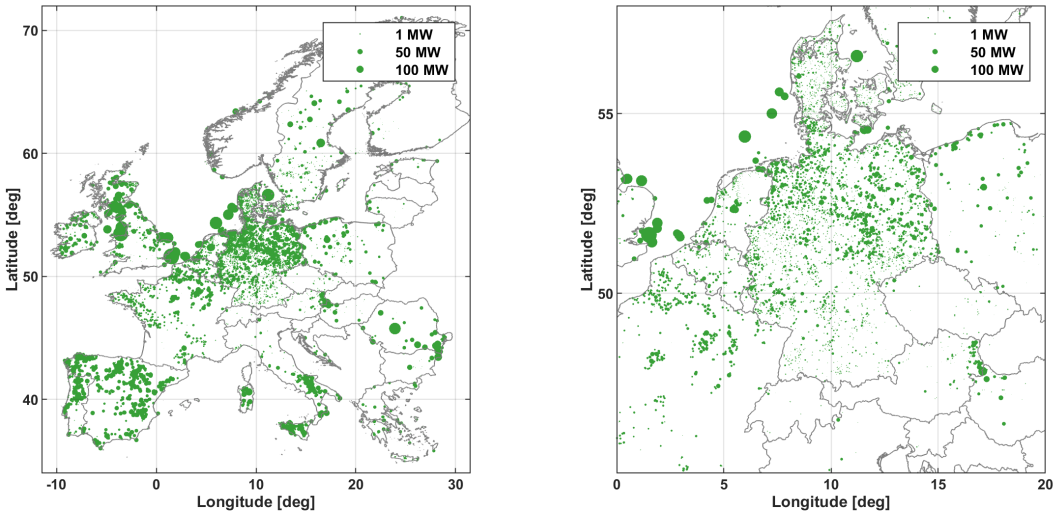

(A) (B)

FIGURE 3.2: Spatial distribution of installed wind power capacities by the end of 2014 for Europe (A) and Germany incl. neighbors (B). Larger circles represent higher capacities. The database *The Wind Power* serves as the basis. Parks with either missing location or commission date are excluded.

3.1.2 Wind speed data

Following Section 2.1 a meteorological data set is necessary to derive wind speeds v_{hub} and air density ρ_{hub} at hub height and thus the power output of a wind turbine. To calculate the wind power productions with high accuracy for a whole region, country or continent, it is crucial to precisely know the wind speeds at the specific wind park locations. Therefore a long-term data set is required which covers a large domain and at the same time features high spatio-temporal resolution. However, historical meteorological observations are not always sufficiently spatially distributed and available for long time spans. Recently, a promising solution is frequently used to tackle this challenge: taking advantage of regional or global reanalysis products, providing long-term and homogeneously distributed meteorological data. Reanalysis is a systematic approach to generate long-term data sets on a defined homogeneous grid for climate research applications by combining data assimilation schemes for historical observations with a certain atmospheric circulation model.

As pointed out in Section 1, recently a vast number of studies are applying various reanalysis data sets modelling wind power generation in different regions and time periods. Most of the available reanalysis data sets have a coarse horizontal resolution (Staffell and Pfenninger, 2016), such as the widely used *European Centre for*

TABLE 3.2: Statistics of wind turbine specific parameters. The database *The Wind Power* serves as the basis. Parks with either missing location or commission date are excluded.

Parameter	Unit	Minimum	Maximum	Mean	Median
Hub height	[m]	16	160	75.03	80.00
Rotor diameter	[m]	10	164	66.70	71.87
Turbine capacity	[MW]	0.0048	12	1.36	1.20
Cut-in	[ms^{-1}]	2	5	3.33	3.27
Cut-out	[ms^{-1}]	15	34	26.33	26.56
Rated speed	[ms^{-1}]	9.6	15	12.17	12.22

Medium-Range Weather Forecasts (ECMWF) reanalysis (ERA-Interim) with about 80 km in Europe, due to their global coverage and computational limits. This might be a problem, in particular for mountainous regions, where the model is not able to reproduce the underlying terrain and adequately capture wind speed variations (Kaiser-Weiss et al., 2015). In order to reduce these inaccuracies, the high resolution reanalysis data set from the *Consortium for Small-scale Modeling (COSMO)* by the *Hans-Ertel-Zentrum for Weather Research (HerZ)* and the *German Weather Service (DWD)* is used, providing 20 years (1995-2014) of hourly wind speed data in Europe on a 0.055° (approximately 6 km in mid-latitudes) horizontal grid spacing with 40 different vertical layers. Certainly, reanalysis is a promising approach meeting the expenses of long time periods, large domains and high resolution. For further details on the reanalysis model and data set see Bollmeyer et al. (2015). The COSMO reanalysis product is from now on referred to as *COSMO-REA6*.

As mentioned in Henckes et al. (2018), there are a few studies dealing with the performance of the COSMO reanalysis product. For instance, Kaiser-Weiss et al. (2015) compare statistical properties of wind speeds observed at 210 meteorological stations across Germany with near-surface fields of COSMO-REA6, ERA-Interim and *ECMWF's reanalysis of the 20th century (ERA-20C)* for recent years. For 96% of stations, they find monthly correlations (r) to be greater than or equal to 0.8 (80% with $r \geq 0.9$) for COSMO-REA6, in contrast to 82% (47%) for ERA-20C and 89% (66%) for ERA-Interim. They state that the improved correlation of COSMO-REA6 is "valid for daily, monthly and seasonal scale" and add that regional reanalysis "improves monthly correlations [...] in areas with more complex topography".

In order to further assess the wind speed quality, Henckes et al. (2018) evaluate COSMO-REA6 (6 km grid), contrasting frequently used reanalysis products,

namely ERA-Interim (80 km grid) and NASA's *MERRA Version 2 (MERRA-2)* (50 km grid), by comparing them to observations. For this purpose, measurements from *Surface Synoptical Observations (SYNOP)* provided by the German Weather Service (DWD) with a temporal resolution of 10 minutes (averages) are employed. Note that when comparing with SYNOP stations, it is crucial to take only independent observations into considerations. Hence, SYNOP stations lower than 100 m above sea surface are omitted, since these observations are used for the COSMO assimilation procedure yet. The observations are compared to the nearest grid point of the respective reanalysis. As observations are compared to 10 m wind data from reanalysis, only observations with measurement height between 8 and 12 m are taken into account. The DWD provides a spatial representativeness value for every SYNOP observation site. To avoid comparisons with observations influenced by local obstacles, only sites with representative values greater than 500 m are considered.

Finally, 59 different SYNOP stations remain. Table 3.3 shows the bias, standard deviation and Pearson correlation coefficient of COSMO-REA6, MERRA-2 and ERA-Interim compared to SYNOP observations. Considered are hourly values from 2014. It turns out that COSMO-REA6 represents the mean absolute wind speeds best with a slight underestimation of -0.14 ms^{-1}. The other two reanalysis slightly overestimate the wind speeds. Besides the smallest systematic error, COSMO-REA6 shows the lowest standard deviation and highest linear correlation coefficient. In conclusion, COSMO-REA6 performs best in representing absolute values of wind speed observations. In addition, as part of the evaluation, Henckes et al. (2018) state that COSMO-REA6 also outperforms both reanalyses concerning processes on all significant scales.

TABLE 3.3: Bias, standard deviation (STD) and Pearson correlation coefficient (R) of COSMO-REA6, MERRA-2 and ERA-Interim compared to 59 SYNOP observation sites in Germany for 2014. Source: Henckes et al. (2018).

	Bias [ms^{-1}]	STD [ms^{-1}]	R
COSMO-REA6	-0.14	1.44	0.74
MERRA	0.53	1.76	0.67
ERA-I	0.17	1.65	0.67

3.1.3 Energy conversion simulations

Two different simulations need to be executed by REOM – one yielding the long-term time series for further investigations and one using real existing power generations for evaluation purposes.

In order to evaluate the model performance, simulation results by REOM should be compared to wind energy output observations for a sufficiently long time period and number of locations. Such model results are expected to represent the real wind energy productions in the EU at a sufficient quality for any given time step. Therefore, the actual installed capacities need to be supplied to REOM for the evaluation time period considered. However as mentioned before, publicly available comprehensive data for VRE energy production are scarce. In particular, acquiring production time series with operation site resolution covering the EU or Germany is not possible. Since the validation of a model is essential, comparisons to two widely accepted benchmarks are made. As shown in Section 4.1, these benchmark data sets for evaluation purposes, one hourly-based by the *European Energy Exchange platform (EEX)* and one monthly-based by the *European Network of Transmission System Operators for Electricity (ENTSO-E)*, comprise time series of 5 years (2010-2014). Hence, the evaluation run is set up in "Live mode" to simulate hourly wind power output from 2010 until 2014 for installed wind park sites in the EU (complemented by Norway and Switzerland).

First, gridded wind speeds are obtained from COSMO-REA6 (Equation 2.2) followed by a horizontal interpolation using the IDW scheme (Equation 2.3). Then, for an accurate vertical extrapolation the level-based scheme of REOM is applied, taking advantage of the vertical resolution of COSMO-REA6. Air density is kept constant since analyses hypothesize that differences are negligible investigating large time periods and domains (see Section 4.2). Furthermore this approach reduces data and computational efforts.

For the actual objective – generation of a high resolution long-term wind power data set for Europe – the entire reanalysis time period from 1995 until the end of 2014 is simulated. All settings are adopted from the evaluation run, except for commission date processing. Here, REOM is executed in "Fixed mode", meaning that the European wind park fleet is kept constant for every single time step. In this case, the portfolio by the 31.12.2014 is applied (see Section 3.1.1). With this approach, 20 years of hourly wind power production for each of the 15400 European operation sites is obtained. Due to the "Fixed mode", all years are inter-comparable: incorporating the same capacities while wind years appear with different and unique characteristics.

3.1.4 Bias correction

After applying REOM to the reanalysis and operation site data set, long-term time series on a location specific basis are derived for European countries. Staffell and Pfenninger (2016) point out that it is highly important to pay attention to inherent biases of the underlying reanalysis data set. For similar previous studies of wind power production using reanalysis products, they state "the need for calibration, or bias correction, to bring simulated capacity factors in line with reality" as a key factor. It appears that reanalysis products are able to adequately simulate the temporal patterns, but lack accuracy capturing the total level and spatial variation of wind power output regarding large regions (e.g. Europe). For instance, Staffell and Pfenninger (2016) find significant variations concerning bias correction factors for different European countries, showing the site dependency of such corrections. However, for many investigations in this research field, this overall power production is highly relevant, in particular on a country basis. Therefore, the following simple and promising bias correction method is adopted from Staffell and Pfenninger (2016) using the bias of the simulated wind power output instead of directly taking reanalysis wind speeds. This assumes that the main bias contribution to power output originates from wind speeds rather than the applied conversion method.

In Equation 3.1, the bias of wind power output is expressed by a comparison of observed to simulated capacity factors. Since facility-based observations of wind power output for the entire European domain are not available, the calibration is applied on a country basis. Note that in consequence all capacity factor values within a country experience the same bias correction factor. The systematic error (bias) ϵ_{bias} for a country is given by

$$\epsilon_{bias} = \frac{CF_{obs}}{CF_{sim}} \tag{3.1}$$

with CF_{obs} being the observed and CF_{sim} the simulated capacity factors. A two-parameter calibration scheme is used to obtain corrected wind speeds v' from original reanalysis values v:

$$v' = \alpha_{bias}(\epsilon_{bias}) \cdot v + \beta_{bias}. \tag{3.2}$$

For each country the factor α_{bias} in Equation 3.2, which depends on the observed CF bias, is estimated using the linear relation:

$$\alpha_{bias}(\epsilon_{bias}) = 0.6\epsilon_{bias} + 0.2$$

The linear offset β_{bias} is obtained by an iterative search, defining a final threshold

value for ϵ_{bias}. When an adequate β_{bias} is found for each country, the final wind speeds and energy outputs can be calculated.

In order to correct the modelled time series by the country specific capacity factor bias, the wind power production database from ENTSO-E is used as a basis. This database contains observed monthly wind power capacity factors between 2010 and 2014 for all European countries. Although the spatio-temporal resolution of this benchmark is rather coarse, it seems appropriate concerning the objective of realistic total power productions on a country basis.

In line with findings by Staffell and Pfenninger (2016), estimated bias factors show significant regional fluctuations – from 0.74 in Slovenia to 2.3 in Romania. Through iterative search, linear offsets (β_{bias}) between -0.78 ms^{-1} in Romania and 2.2 ms^{-1} in Austria are derived. These findings underline the importance and requirement of applying a country based correction. Finally, these calibration factors are applied to outcomes from the simulations depicted in the previous Section – yielding bias corrected wind power production time series for all European wind power parks for both, the 5-year evaluation and 20-year long-term run.

3.2 Towards uncertainty estimations for energy system models

As outlined in the Introduction (Study II), many studies are making use of reanalysis products, which are expected to introduce certain uncertainties to the energy system modeling. These uncertainties are mostly neglected though. Therefore, the upcoming approach has the objective to give first insights on potential uncertainties introduced by reanalysis errors and their impact on the affiliated model chain. The approach follows the idea of focusing on the overall range of potential errors rather than quantifying uncertainties of actual real case scenarios. The following Sections outline the whole model chain related to this branch of the thesis, which is applied to tackle the problem, including methodological details of the estimation of input uncertainties. Results of the analysis can be found in Section 4.2. Note that this research is object to the article "Uncertainty Estimation of Investment Models under High Shares of Renewables using Reanalysis Data" by Henckes et al. (2019) submitted to *ENERGY* in April 2019 and will closely follow this work.

3.2.1 Model chain

In Figure 3.3 the components of the entire model chain are illustrated. In order to cover the whole range of potential uncertainties, three simulation scenarios are

developed: one unperturbed and two maximally perturbed model runs. In contrast to the *unperturbed control run (CON)*, the time series from the COSMO reanalysis are perturbed by subtracting estimated errors for the *negative scenario (NEG)* and adding errors for the *positive case (POS)*. Details of the error estimation of COSMO-REA6 quantities, their potential impact and application are discussed in the upcoming Section 3.2.2. Thereafter, three major modeling steps are necessary to simulate the energy system featuring high shares of VRE generation, namely the conversion of wind and solar energy by REOM, the reduction of computational complexity via clustering and the investment modeling by RPSM.

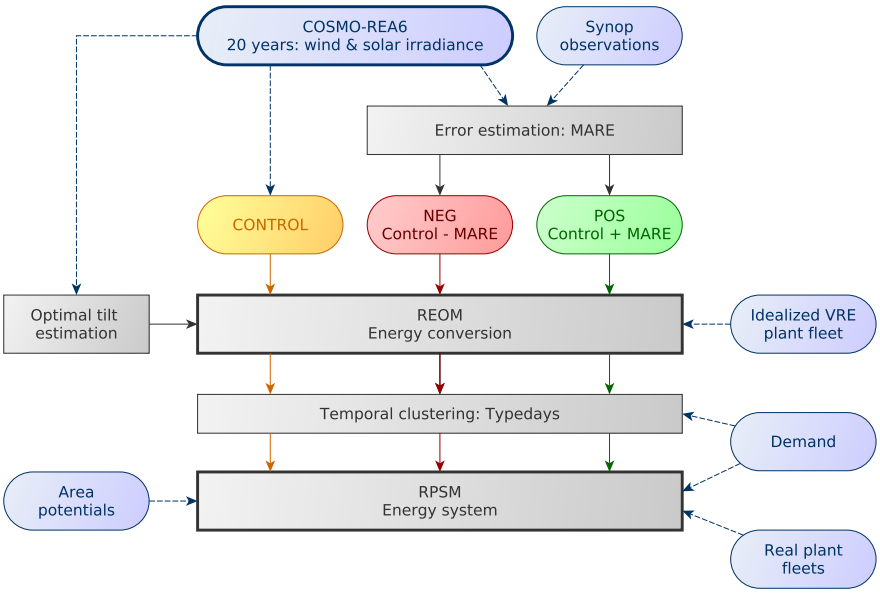

FIGURE 3.3: Schematic illustration of the model chain to estimate the impact of VRE input uncertainties to energy system modeling. Source Henckes et al. (2019).

In order to obtain long-term wind and PV power output time series from wind speed and solar radiation input data, REOM is applied again to COSMO-REA6 in a first step. Except for some adjustments (details following), the generation setup and process of the VRE data set is similar to Section 3.1. This time however, the underlying VRE operation sites are not taken from an actual real plant database but idealized plant facilities: at each grid point of the model, one pre-defined unit of capacity is theoretically installed. The modern state-of-the-art 4.2 MW *Enercon E-126 EP4* wind turbine is taken for onshore grid points. For offshore operations, the *Vestas V164* with 8 MW is set. Table 3.4 summarizes the respective essential turbine characteristics. In contrast to Section 3.1 where only wind power is processed, the simulation is extended by PV power estimations. Similar to wind power, each grid point contains one PV plant with a capacity of 1 MW. For every

TABLE 3.4: Onshore and offshore turbine characteristics used for idealized VRE plants. Source: Henckes et al. (2019).

Characteristic	Unit	Onshore	Offshore
Turbine type		Enercon E-126 EP4	Vestas V164
Capacity	[MW]	4.2	8
Hub height	[m]	135	114
Rotor diameter	[m]	127	164
Cut-in	[ms^{-1}]	3	4
Rated speed	[ms^{-1}]	14	13
Cut-out	[ms^{-1}]	25	25

module, the standard test conditions are defined as $\eta_{STC} = 0.14$, $T_{STC} = 22°C$ and P_r is set to 0.7. Furthermore, the tilt (γ_m) and azimuth angle (α_m) need to be known (c.f. Equation 2.11). Since no objective specifications are available for either of these parameters, they are fixed. The azimuth angle is set to 0° (southerly) for all facilities, assuming a perfect orientation of the PV module at any operation site. To go along with this approach regarding the tilt angle, Henckes et al. (2019) determined an optimal tilt angle (in terms of power production) for each location on the COSMO-REA6 grid. The procedure is explained in detail in Appendix Section A.

In the scope of this investigation, it appears reasonable to focus the analysis on a single country, reducing the complexity of the problem. Since Germany plays a major role concerning VRE expansion in Europe, it is selected as the simulation domain. In addition, constraining computational costs at the stage of the upcoming error estimation (Section 4.2.1), only surface wind speeds are used for simulations and hence the power law (Equation 2.4) is applied as REOM's extrapolation scheme. Finally, REOM generates 20 years (1995-2014) of potential hourly wind power and PV capacity factor time series on a 6 km x 6 km grid in Germany. The data set can be seen as horizontal homogeneous distributions of CF potential profiles.

The second modeling step is to apply the clustering algorithm to the obtained CF data set. The aim is to create a CF data set in Germany with a horizontal resolution which is still manageable by the energy system model in terms of computational costs. In order to be able to compare the perturbed simulations to the control run as well as spatial distributions of investments, the grid is at least kept to a multiple of the COMSO-REA6 grid, i.e. 48 km x 48 km. This resolution leads to 151 wind onshore and PV operation sites and 22 wind offshore locations.

Regarding a reduction of the temporal dimension, the clustering routine following Section 2.2 is applied. For this purpose the 20 years of hourly CF with 48 km resolution in Germany and 5 years (2010-2014) of hourly ENTSO-E German load (demand) data are subject to the clustering algorithm. In order to enlarge the data basis for the algorithm, each of the 20 years is paired with each demand year, yielding a total of 100 years of combined CF and demand patterns. Here the *k-means* scheme is applied to generate 20 typedays containing characteristic daily profiles of wind and PV capacity factors (on a 48 km grid) and demand, respectively. The clustering output is complemented by an occurrence probability (frequency) for each of the 20 typedays.

Third, the RPSM investment model is applied to simulate the resulting cost-optimal development of the energy system until 2050. While the analysis concentrates on the time period from 2014 until 2050, simulations are extended to 2070, due to potential boundary effects at the end of the time frame. This ensures consistent results and investment decision making by the model over the whole requested time horizon. For instance, the model may tend to avoid investments associated with long-living technologies at time steps when their lifetimes exceed the time horizon, leaving unemployed but fully paid generation potential. The model time step is set to 10 years which appears to be sufficient for the examined problem. Certainly, the first time step is 6 years long, since simulations start in 2014. Note, that for the first model step, endogenous investments are prohibited, so that only exogenous expansion strategies are realized.

Incorporating a set of parameters and various constraints, the model is required to satisfy the German electricity demand by electricity generations of available installed capacities at any given point in time (Section 2.3). For the simulations in this context, the following RPSM features are set:

- **CO_2 emission target**: To fulfill Equation 2.35, the German CO_2 emission caps $E^{cap}_{r,y}$ need to be supplied for each model time step. The goal of a 90% reduction by 2050 compared to 1990 (following the German Climate Action Plan 2050[2]) is taken as a basis. For the estimation of the CO_2 emission cap until 2050, estimates of the German CO_2 emissions from the EEA are used. However, simulated yearly total emissions would not automatically show consistent values with the EEA estimates. Thus, simulated emissions for 2014 are obtained before the actual simulation is processed. Afterwards the bias between model and observations is obtained by comparing the values for 2014. Applying the bias to the German EEA value for the reference year

[2]The Climate Action Plan 2050 from 2016 is a climate protection policy document by the German government to tackle climate goals by the EU and the Paris Climate Agreement 2016

1990 and linearly interpolating to 2050 (with 90% reduction) yields the CO_2 emission caps for all time steps.

- **Area potentials**: The maximal possible capacity P^{poss} that can be installed on each specific grid point (Equation 2.27) is constrained by the available area and needs to be estimated following the approach outlined in Section 2.4. Figure D.3 in the Appendix shows the resulting potentials for wind and PV power. Estimated values range between 0.21 to 4.2 GW (0.1 to 4.4 GW) for onshore (offshore) and 0.22 to 3.9 GW for PV capacities. A considerably low potential is observed for North Rhine-Westphalia. In total 320.2 GW (41 GW) are available for German onshore (offshore) wind technologies, whereas PV can be expanded to 250.7 GW.

- **Technology phase-outs**: Due to recent political progressions in Germany, further endogenous investments in nuclear, lignite and coal assets are prohibited. Existing installed capacities of these technologies are dismantled according to their lifetimes.

- **Technology specific bounds**: The constraints for the river-runoff and biomass technologies in Equations 2.25 and 2.26 due to natural restrictions as well as the VRE investment constraint in Equation 2.29 are incorporated.

- **Demand**: No demand differences between model years are assumed. Hence, daily load profiles (typedays) are the same for each model year and by that also the total annual demand does not vary.

- **Initial plant fleets**: Exogenous initial capacities and expansion strategies follow the German *Renewable Energy Sources Act (EEG) 2014*[3] guideline.

- **Dimensions**: Besides the model time step of 10 years, the intra-daily resolution of the 20 typedays in RPSM is reduced to 6h to save computational costs. Concerning the amount of potential VRE investment locations, the simulations in this part comprise of 151 onshore wind and PV and 22 offshore wind operation sites (or in RPSM sense: technologies).

Furthermore, to solve the system of equations depicted in Section 2.3 a set of assumptions is required. These contain for instance technical characteristics of power plants such as technical lifetime, net efficiency, availability, CO_2 emission factors and area power densities as well as costs and EEG targets. In the Appendix,

[3] Capacity values assumed from the *Kraftwerksliste der Bundesnetzagentur* – state of 02.02.2018 (www.bundesnetzagentur.de).

all assumptions and used sources are presented and Tables C.6-C.12 list all the applied parameters.

As illustrated in Figure 3.3, all simulations (i.e. CON, NEG and POS) undertake the previously explained model chain, yet with different VRE inputs. The outputs can then be compared to estimate the range of uncertainties of an investment model induced by meteorological input errors as explained below.

3.2.2 Perturbation of wind and PV power

The upcoming Section depicts the methodology for the error estimation of COSMO-REA6 quantities, their sensitivity to the wind and PV model, and how they are finally applied to generate maximally perturbed VRE power time series.

Potential uncertainty sources

In order to derive maximal perturbed time series of wind and PV power output, the first task is to investigate potential sources for uncertainties in the respective power conversion model. In case of wind power, Equation 2.1 of the wind model in REOM shows that the electricity produced by a wind turbine depends on one hand on technical properties of the turbine (e.g. its capacity, the rotor's hub height etc.). Consequential, the quality of the provided wind park data set determines the effect to the accuracy of the model output. On the other hand, assuming that for all wind assets sufficient technical information is supplied, the air density and, in particular, wind speed time series remain as potential sources for errors. As for wind, the amount of energy produced by a PV panel is constrained by its physical properties and the meteorological parameters, being direct and diffuse horizontal radiation, surface air temperature, ambient wind speed and surface albedo. Following Huld and Amillo (2015) the ambient wind speed has minor importance in this context.

Error estimation

In order to estimate the errors of the potential quantities associated with the meteorological input data set, time series of COSMO-REA6 are compared to measurements in Germany. Using Equation 3.4 and 3.3, the *Mean Absolute Error (MAE)* and *Mean Absolute Relative Error (MARE)* is derived for all quantities, except for surface albedo. For this purpose, measurements from SYNOP by the German Weather Service are used:

- Surface wind speed: Since SYNOP sites located 100 m below sea level are applied to the COSMO assimilation method itself, they can not be seen as

independent. Hence, these stations are excluded from comparisons, so that a set of 59 observation sites remains (Figure 3.4a). Instantaneous reanalysis wind speeds for the time period of 2007-2013 are compared to 10 min averaged site observations assuming the Taylor hypothesis[4]. The IDW interpolation scheme is applied to match the four adjacent COSMO grid points to the respective site.

- Surface pressure & temperature: For these two assimilated parameters, a set of 248 German SYNOP sites is taken to supply hourlytime series between 1995 and 2013.

- Global & direct radiation error: In case of radiation, 118 observational stations are compared to COSMO-REA6 for the time period 2007-2013. They provide hourly values for global and direct radiation on the horizontal plane. By re-arranging Equation 2.18, the diffuse fraction can be estimated from these two quantities. Following the definition of the *World Meteorological Organisation (WMO)* (World Meteorological Organization, 2008), all measurements of the direct radiation below a threshold of 120 Wm^{-2} are expected to be affected by clouds and are therefore omitted.

- Surface albedo: The error of the reflected radiation part is represented by the error in surface albedo values. In contrast to the other parameters, the SYNOP stations would not provide albedo data for comparison. Due to the lack of observations, the approach for the surface albedo is different. The standard deviation of the 20-year COSMO-REA6 albedo time series was derived and taken as an uncertainty estimate instead. This seems to be a reasonable approach to roughly trace out the range of uncertainties for this parameter.

Table 3.5 summarizes the applied observation data sets, while Figure 3.4a shows the distribution of SYNOP sites in Germany used for this analysis. As an error measure for a given COSMO-REA6 parameter k, the MARE is evaluated for N bins using

$$MARE(k)_i = \frac{MAE(k)_i}{mean(k_{sim})_i} \tag{3.3}$$

with the MAE defined as

$$MAE(k)_i = mean(|k_{sim} - k_{obs}|)_i \tag{3.4}$$

[4] An assumption that advection contributed by turbulent circulations themselves is small and that therefore the advection of a field of turbulence past a fixed point can be taken to be entirely due to the mean flow, http://glossary.ametsoc.org

and i the index of the considered bin. It is expressed as the ratio between the MAE of simulated values k_{sim} compared to observed values k_{obs} and the mean of simulated wind speeds. For each parameter the bin size and range is specified, e.g. for wind it is set to $0.1\,\mathrm{ms}^{-1}$ between 0 and $30\,\mathrm{ms}^{-1}$. Results for the error estimation are presented in Section 4.2.1.

TABLE 3.5: Overview of hourly SYNOP observations provided by the DWD, which are used for error estimations of different COSMO-REA6 parameters required for VRE power conversion models. Source: Henckes et al. (2019).

Parameter	Number of sites	Time period
Global & direct radiation	118	2007 - 2013
Surface temperature	248	1995 - 2013
Surface wind speed	59	2007 - 2013
Surface Pressure	248	1995 - 2013

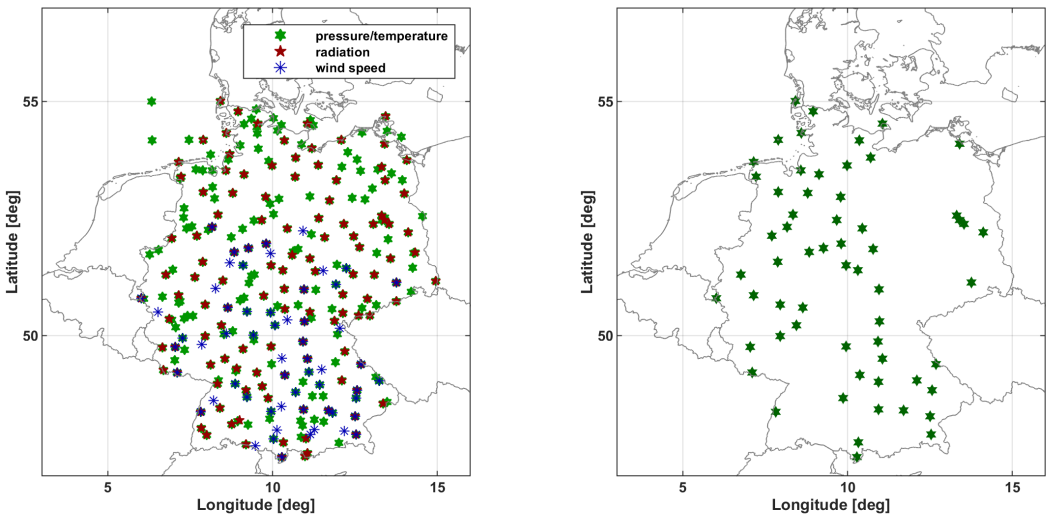

(A) (B)

FIGURE 3.4: Distribution of SYNOP stations by the DWD in Germany used for the error estimation of COSMO-REA6 quantities (A) and for sensitivity study concerning VRE power output models (B). Different colors represent the applications regarding different quantities. Source: Henckes et al. (2019).

Sensitivity study

After deriving error estimates of all important quantities, the question is which of these have major impact (sensitivity) on the conversion models with respect to energy output of a certain power plant.

For the purpose of wind model sensitivities, the *Enercon E-126 EP4* is applied as a reference wind turbine to a set of 19-year time series (1995-2013) from 60 SYNOP stations in Germany (see Figure 3.4b). The 10 m wind speed observations are extrapolated to the rotor hub height via the power law while air density at hub height is estimated from the observed surface pressure in combination with the barometric approximation. Using the power curve, yearly averaged total energy outputs are calculated for each of the observational sites and used as a reference for the sensitivity study. Then, each of the parameters (surface pressure & wind speed) is perturbed by its previously estimated error while the other stays unchanged. Finally, the difference of the total yearly energy generated by the reference and the perturbed case gives insights about the sensitivity of the wind model to the respective parameter.

A similar approach is used for the sensitivity study concerning the PV model: each parameter is disturbed by its uncertainty and the total yearly energy output is compared to the reference. For this analysis, a PV panel with an area of $1\,m^2$, a southerly orientation and an optimal tilt angle (see Appendix A) is assumed. Besides sensitivity estimates for the contributing parameter, the question about the potential impact of the choice of the radiation models, KM and PM, arise. Thus, the study is extended by a sensitivity estimation of the PV model with respect to the applied radiation model by keeping all parameters unchanged but substituting the radiation models.

3.3 Simulations of future European energy markets

This branch within the framework of the thesis (Study III) has the objective to comprise the developed methods in order to simulate projections of future energy markets in Europe under high shares of renewable energies. The following Sections review the necessary model chain applied to implement the simulations, their setup as well as details about the used data sets. A schematic illustration of the sequence of methodologies and components for the modeling procedure are provided in Figure 3.5. The main structure appears very similar to that in Section 3.2, however, several essential details are adjusted and explained here.

The overall idea is to compare historical and future European energy generation patterns in order to investigate the impact of inherent climate change in the

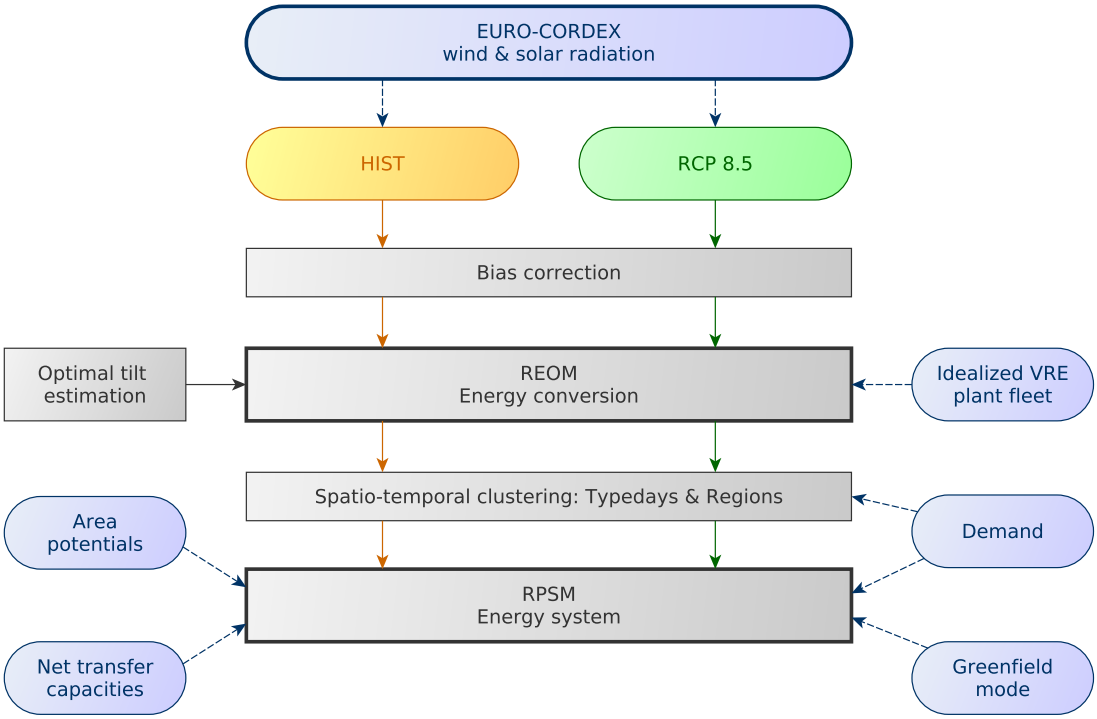

FIGURE 3.5: Schematic illustration of the model chain to simulate future energy system with high VRE shares.

projection scenario. For this purpose, the first modeling step is to simulate two distinct 30-year time series of historical and future European VRE power productions. For that matter, REOM is applied to process the energy conversion of the wind and solar radiation source by wind turbines and PV panels. As for Section 3.2, idealized VRE plant fleets are set up, instead of taking real installed capacities. The dimensions of the resulting historical and future VRE time series are reduced by a spatio-temporal clustering before they serve as the basis for the energy system modeling under high shares of VRE by the RPSM. Investigations of the differences in simulation results are presented in Section 4.3.

3.3.1 Wind and solar radiation time series

In this Section, the meteorological data basis, used for Study II, is presented. Here, a single member of an ensemble of combinations of *global climate models (GCM)* and *regional climate models (RCM)* is taken. The choice as well as its validation is further discussed.

The EURO-CORDEX project

A major difference to the simulation setup in Section 3.3 is the meteorological input data. Here a subset of the *EURO-CORDEX project* is used. The *Coordinated*

Downscaling Experiment (CORDEX) initiative by the *World Climate Research Programme (WCRP)* started in 2009 and aims to provide a coordinated model evaluation framework[5]. An ensemble of regional climate change projections is generated by making use of various downscaling techniques driven by multiple GCM from the *Coupled Model Intercomparison Project Phase 5 (CMIP5)*[6] (Giorgi et al., 2009). Consequently, EURO-CORDEX represents the European branch of the CORDEX project.

The still coarse spatial resolutions of modern GCMs, being usually in the order of 100-300 km, bring along uncertainties due to unresolved sub-grid processes (Viner, 2002; Pan et al., 2001; Knutti and Sedláček, 2013; Weisse and Feser, 2003). For instance, weather phenomena affected by topography and other regional details such as land-sea distribution may be poorly represented. One way to tackle this problem is to apply different downscaling schemes to obtain a higher resolution, e.g. dynamical. For the dynamical approach, a RCM with resolutions typically between 10 and 50 km is forced by a GCM on a much smaller domain to keep the computational costs maintainable. The EURO-CORDEX project provides data for ensembles of various combinations of multiple GCM and RCM, since numerous studies showed the significance of inter-model variability (e.g. Strandberg et al., 2015; Reyers et al., 2016). However, in order to reduce the amount of data and complexity of analyses for the subsequent model chain, it is refrained from applying several GCM/RCM configurations. When using large ensemble data sets, it is common to obtain and apply the ensemble mean (Tebaldi and Knutti, 2007; Semenov and Stratonovitch, 2010). This however would dramatically decrease the variability, in particular, with respect to inter and intra-daily time scales being essential for VRE energy related concerns. Therefore, one set from combinations of two RCM with four GCM is selected by evaluating the differences in climatology and variability compared to a reference simulation.

Considered ensemble members include the *CNRM-CM5*, *EC-EARTH*, *HadGEM2-ES*, *IPSL-CM5A-MR* and *MPI-ESM-LR* as GCMs and the *RCA4* and *CCLM4-8-17* as RCMs. All data sets are publicly available via the EURO-CORDEX project. Table C.3 summarizes all details about model configurations and simulations used in this context while Table C.4 of the Appendix gives further information about the full model name and the corresponding institution. Note that there are no realizations of the IPSL model in combination with the CCLM available. The respective RCM scales each coarse globally coverage GCM down to 0.11° (about 12 km in Europe)

[5] www.euro-cordex.net

[6] The widely known Fifth Assessment Report AR5 from the Intergovernmental Panel on Climate Change (IPCC) is also based on results from the ensemble data set CMIP5.

horizontal resolution on the comparably small European domain (~27°N-72°N and 22°W-45°E).

Choice of model setup

For the purpose of decision making with respect to the adequate model combination within the EURO-CORDEX project, the historical simulations of RCA4 and CCLM4 driven by each GCM are compared to the respective ERA-Interim driven evaluation runs. Results forced by the reanalysis are assumed to serve as a benchmark, since it can be seen as the best guess of atmospheric states at any time step and equally distributed grid points over the large domain of Europe. Taking a reanalysis as a benchmark means comparing two model results, implying that a quantitative evaluation is rather difficult. But the reference choice is still reasonable concerning spatio-temporal variability due to the relative nature of comparisons in the upcoming analysis (Section 4.3).

TABLE 3.6: Root mean square error of residuals between multiple GCM driven historical and ERA-Interim driven evaluation simulations with two RCM, for the mean, standard deviation (STD) and trend of the respective wind speed climatology. Red numbers represent the respective two smallest values.

	Mean [ms^{-1}]	STD [ms^{-1}]	Trend [ms^{-2}] $\times 10^{-6}$
RCA4			
CNRM-CM5	0.33	0.17	2.10
EC-EARTH	0.14	0.07	2.86
HadGEM2-ES	0.23	0.10	3.90
MPI-ESM-LR	0.14	0.10	2.52
IPSL-CM5A-MR	0.25	0.12	3.01
CCLM4-8-17			
CNRM-CM5	0.33	0.17	8.67
EC-EARTH	0.14	0.06	7.40
HadGEM2-ES	0.18	0.08	5.27
MPI-ESM-LR	0.33	0.13	7.53

Since analyses within the scope of this thesis focus more on details concerning wind energy than PV, the evaluation is only undertaken for surface wind speeds.

Additionally, as for example mentioned by Jerez et al. (2015), climate modeling still faces traditional extensive problems regarding solar radiation estimations.

Table 3.6 summarizes the differences of spatio-temporally averaged mean, standard deviation and trend values of 3-hourly surface wind speeds for all model configurations and the ERA-Interim driven setups. Red numbers indicate the two smallest values for each metric. In addition, the mean, standard deviation and trend as well as horizontal distributions of the residuals (GCM minus ERA-Interim) are depicted for all simulations in the Appendix, Figures D.9-D.11. It is evident that the model chain of EC-EARTH forcing RCA4 appears to be most similar to results from the ERA-Interim driven RCA4 evaluation run. The configuration is found to be under the two best candidates for the mean and standard deviation. Also the spatial patterns are reproduced comparably well. The CCLM-ECEARTH and RCA4-MPI combination also appear to be reasonable options. However, in contrast to RCA4-ECEARTH, the other two realizations show larger differences in offshore areas, in particular for the North Sea around Britain (c.f. Appendix, Figure D.11d), the German coast and the Baltic Sea (c.f. Appendix, Figure D.10j). Haas and Pinto (2012), Born et al. (2012), Haas et al. (2014), and Reyers et al. (2016) also observed this behavior. Since these regions play a key role concerning European wind power production, the decision in favor of the RCA4-ECEARTH realization is made.

Validation of model setup

According to Strandberg et al. (2015) RCA4 is generally able to replicate the ERA-Interim large scale circulation and shows good performance. Although they note problems of the downscaled GCM simulations with representation of the large scale circulation, there is no evidence of an impact to surface wind speeds (Moemken et al., 2018; Kjellström et al., 2005; Nolan et al., 2012; Tobin et al., 2016).

Results of the historical simulation by RCA4-ECEARTH are further evaluated with respect to RCA4-ERAI in Figure 3.6. Significance is quantified via t-Tests (95% confidence level). Spatial patterns of the wind speed climatology are captured quite promising, in particular, in regions with high importance for wind power relations, such as onshore areas in Germany, France, Spain and Britain as well as offshore regions in the North and Baltic Sea (Figure 3.6b). In contrast, significant overestimation can be observed at the Finish coast, the coast of Portugal and in the North-West of Britain of about 0.6 ms^{-1} (8%). The latter two are of minor importance, since prevalent water depths exceed the technical limitations of modern offshore wind park facilities. Furthermore, the simulation exhibits some considerable biases in the Northern Adria (up to -0.7 ms^{-1}, 12%) and the Greek coast (up to -0.43 ms^{-1}, 6%). In general, the model tends to underestimate the magnitude of

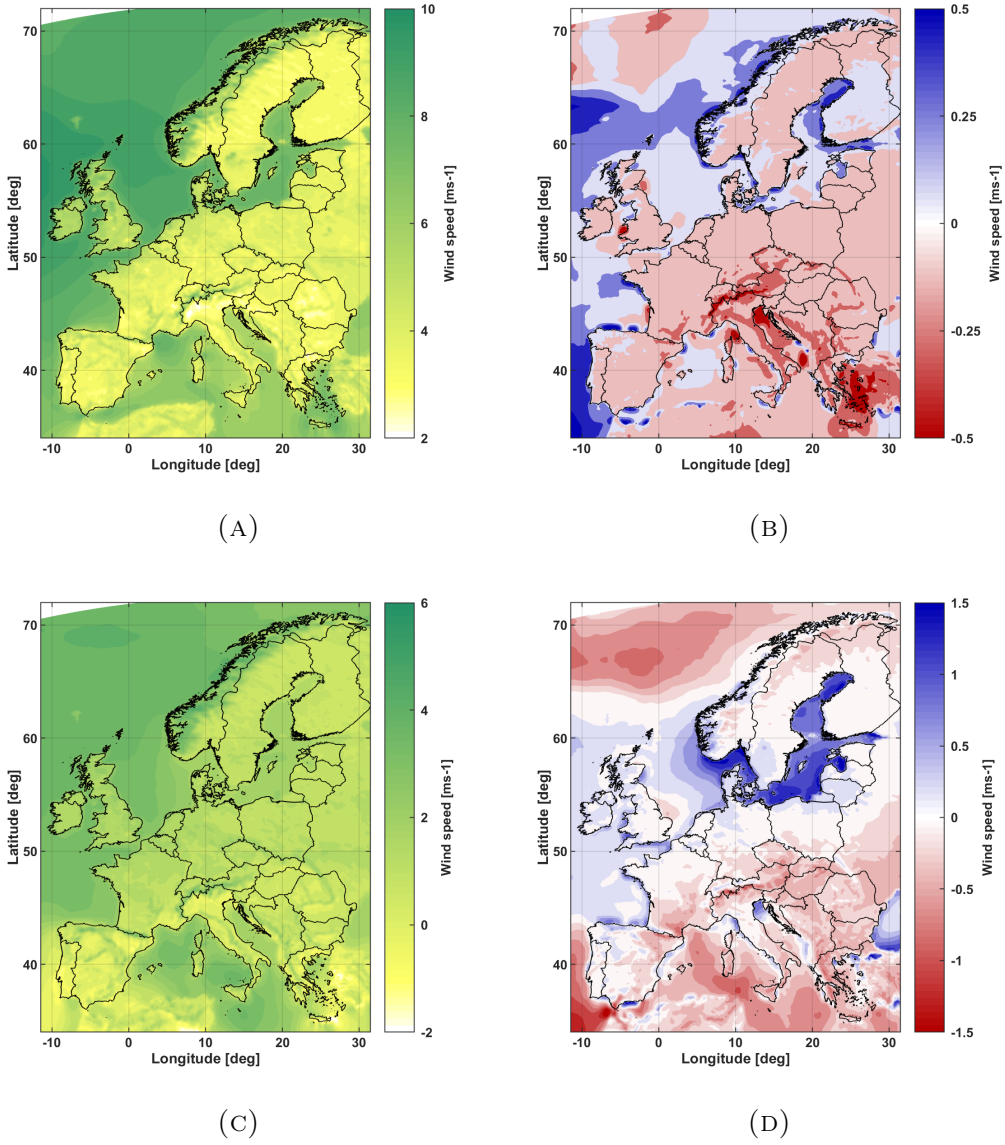

FIGURE 3.6: Climatology of mean surface wind speed from RCA4 driven by ERA-Interim (A) and the residual to RCA4 with EC-EARTH (B). Further, intra-annual variability (winter minus summer) for RCA4 driven by ERA-Interim (C) and the residual to RCA4 with EC-EARTH (D). Residuals are defined as RCA4/EC-EARTH minus RCA4/ERA-Interim).

surface wind speeds over land, for instance in vast parts of northern Germany the difference is found to be below 1% and below 2% for the southern more mountainous regions. This is in line with findings by Kjellström et al. (2005) and Nolan et al. (2012) concerning the previous *RCA3* model version.

Besides the climatological mean, the intra-annual variability is of major importance. Here, it is determined by the difference of winter (December-February) and summer (July-August) climatology of the wind resource. Figure 3.6d highlights

the residual of RCA4-ECEARTH minus RCA4-ERAI, exhibiting substantial biases mainly in the Baltic Sea between 1 and 2 ms^{-1} (up to 60%). This yields a more pronounced difference between winter and summer wind power generation potentials for the respective areas. Vast parts of eastern Europe and the Mediterranean experience slight underestimations for the GCM driven run. In most parts of Europe and the Atlantic however, the simulation shows acceptable performance. The trend in Appendix Figure D.10f shows biases of the same magnitude as the climatology. These magnitudes are negligible though.

Regarding the shortwave downwelling solar radiation at the surface, the spatial distribution of the climatological mean is well reproduced, yet overestimated in most parts of Europe, with decreasing difference for the Mediterranean regions (c.f. Appendix, Figure D.12). For Germany this results in less than 8% deviation to ERA-Interim, probably leading to slightly increased PV potentials. Almost the exact same pattern with a reversed tendency is observed for the intra-annual variability (c.f. Appendix, Figure D.12) decreasing the seasonal differences of up to 20 Wm^{-2} for northeastern Germany. The GCM configuration shows generally a good performance regarding the spatial patterns for the long-term surface temperature mean. Nevertheless, from Figure D.13b it is evident that the simulation significantly underestimates the temperature over the entire domain, with values up to -2.2 K. The difference between winter and summer months is substantially more pronounced, in particular for the Mediterranean (c.f. Appendix, Figure D.13d).

Historical and future simulation

Finally, after deciding in favor of the RCA4-ECEARTH configuration, two data sets are used as input for the subsequent model chain (c.f. Figure 3.5): one historical long-term simulation from 1970 until 1999 and one simulation following a GHG emission scenario with the time horizon of 2070 until 2099. Amongst others, such scenarios are defined in the *Representative Concentration Pathways (RCP)* used for the *Fifth Assessment Report (AR5)* by the IPCC. They are based on assumptions concerning the future greenhouse gas emissions acting as a trigger for different radiative forcing and hence climate changes. Three pathways are available for the present model combination, defined with respect to the radiative forcing in Wm^{-2} (IPCC, 2014):

- RCP 2.6: peaks at 3 Wm^{-2} within the 21st century and declines afterwards;
- RCP 4.5: stabilization after the 21st century at 4.5 Wm^{-2};
- RCP 8.5: increased radiative forcing exceeding 8.5 Wm^{-2} at the end of the 21st century.

In the scope of this thesis, the RCP 8.5 scenario is applied, since recent developments and investigations suggest that the inherent GHG emission scenario appears to have an increased likelihood (Sanford et al., 2014; IPCC, 2014). Present emissions seem to follow or even exceed the assumed GHG trajectory in the most extreme of all scenarios (Sanford et al., 2014). The latest IPCC report AR5 estimates the increase of global mean surface temperature to be likely between 2.6°C and 4.8°C when comparing the periods 1986-2005 and 2081-2100 for the RCP 8.5 scenario.

Both, the historical and projection data sets used from RCA4-ECEARTH (from now referred to as *HIST* and *RCP85*) provide 3-hourly surface wind speeds, surface temperatures and global solar radiation at the surface for the 0.11° gridded EURO-CORDEX domain.

Bias correction

The previously mentioned studies as well as the evaluation of the RCA4-ECEARTH historical simulations with respect to RCA4-ERAI results show essential biases which may affect signals in climate change analyses. In particular this seems to be the case for wind speed applications (Moemken et al., 2018). Therefore, a bias correction is applied to the HIST simulation as well as the RCP85 projection, assuming that the bias patterns for this specific model combination are constant over the whole time horizon until 2100.

For this purpose an probabilistic approach following Haas et al. (2014) and Michelangeli et al. (2009) is adopted (see also Moemken et al., 2018). First, Weibull distributions are fitted to the original time series of the historical RCA4-ECEARTH and evaluation RCA4-ERAI run. The scale (α^{wbl}) and shape (β^{wbl}) parameter are estimated using the cumulative distribution function of wind speeds v (Haas et al., 2014):

$$F(v) = 1 - exp\left(- \left(\frac{v}{\alpha^{wbl}} \right)^{\beta^{wbl}} \right). \tag{3.5}$$

Applying Equation 3.5 to both time series yields two sets of parameters, namely $\alpha^{wbl}_{hist}/\beta^{wbl}_{hist}$ for RCA4-ECEARTH and $\alpha^{wbl}_{eval}/\beta^{wbl}_{eval}$ for RCA4-ERAI. Secondly, by equalizing the Weibull distributions $F_{sim}(v_{sim})$ of the historical (HIST) or projected (RCP85) simulation and $F_{eval}(v_{eval})$ of the evaluation simulation (RCA4-ERAI), a transfer function is determined which yields the bias corrected wind speeds v_{corr} from the estimated sets of parameters (Michelangeli et al., 2009):

$$v_{corr} = F^{-1}_{eval}\Big(F_{sim}(v_{sim})\Big) \quad = \alpha^{wbl}_{eval} \left[- ln\left(1 - \left(1 - exp\left(\frac{v_{sim}}{\alpha^{wbl}_{hist}}\right)^{\beta^{wbl}_{hist}}\right)\right)\right]^{\frac{1}{\beta^{wbl}_{eval}}}. \tag{3.6}$$

The bias correction of Equation 3.6 is applied prior to the energy conversion processing by REOM (c.f. Figure 3.5).

3.3.2 Setup for the energy system modeling

Now, the processing of input data in the subsequent modeling chain and details about the RPSM model setup are explained. In addition, results with respect to area potential estimations for European countries are presented.

Towards VRE time series

In the next step of the modeling chain the HIST and RCP85 time series are object to REOM yielding wind and PV power generation. Unified wind and PV operation facilities are distributed on the underlying meteorological grid. By that VRE time series are assigned to each point in space for 28 European countries including onshore and offshore (only wind) areas. The exact same plant types and REOM setup as presented in Section 3.2.1 are employed, including the application of an optimal tilt angle obtained for the entire European domain.

As for Section 3.2, besides the azimuth angle of equally distributed PV panels (which is again set to 0°), the tilt angle at each grid point of the underlying meteorological data set needs to be supplied. Similarly as depicted in Section A in the Appendix, the optimal angle for each grid point is determined, this time extended to Europe instead of only Germany.

This approach yields the optimal tilt angles for each grid point in Figure 3.7. As expected, a clear North-South pattern can be observed for the whole domain due to the dependency of the direct radiation to the grid points latitude. The inherent difference between magnitudes of latitude and tilt angle of about 10° appears to be the diffuse radiation contribution. The optimum ranges between 30° in Spain and Italy, and 45° in Norway and Sweden. Deviations within regions of the same latitude appear perhaps for two main reasons: first, certainly the optimal angle needs to be adapted for sites with different altitudes, as evident for example in the Alps and Pyrenees. This, however, does not explain variations within the Atlantic for instance. Here, different climatology of cloudiness are expected to be present. More clouds decrease the direct radiation contribution to the power yield by a PV panel and consequently altering its latitudinal dependency.

The dimensions of the resulting 30 years of VRE generation, are then reduced by applying the clustering algorithm. For this purpose, combinations of five ENTSO-E demand years (for each European country), and 30 years of wind and PV capacity factors (yielding a total of 150 source years) are serving as the basis. The affiliated

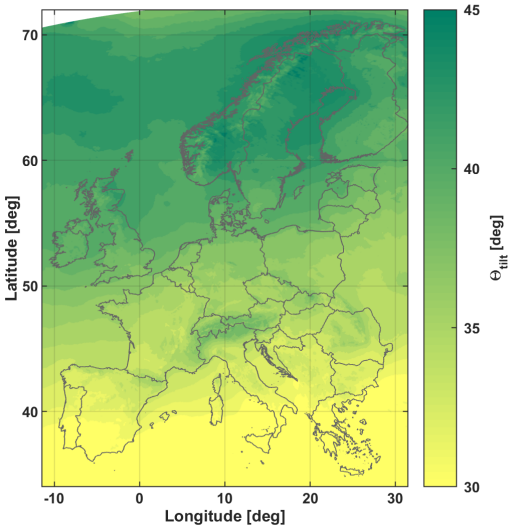

FIGURE 3.7: Optimal tilt angle for southerly oriented PV panels in Europe, determined using Klucher model (KM). COSMO-REA6 radiation data serves as a basis and an uniform albedo of 0.2 is assumed.

output comprises a set of 20 typedays of characteristic demand, wind as well as PV power production patterns with a 3-hourly resolution. The spatial clustering ensures that grid points showing similar characteristic within a country are merged to a maximum of five groups per country for onshore and two for offshore areas. The respective number of clusters per country is determined via the evaluation feature mentioned in Section 2.2.

Figure 3.8 illustrates the spatial distribution and cluster affiliation using the example of Germany (c.f. Appendix, Figure D.7 for Europe). Note that since the outcome of the clustering routine highly depends on the VRE power time series, the spatial patterns and number of clusters for HIST and RCP85 as well as wind and PV may vary to a certain extend within a country. In addition, offshore grid points are omitted for water depths exceeding 250 m, accounting for technology limitations.

For Germany, the offshore wind grid points are clearly separated for the North Sea and Baltic Sea in both simulations, revealing a distinct climatologic differences between both regions with respect to surface winds. Regarding onshore winds, the routine suggests three clusters: North-West, North-East and South. The outcome suggests that there are almost no differences between the periods. Interestingly the algorithm produces very similar patterns for PV, although suggesting to zonally divide the southern region for the future data set.

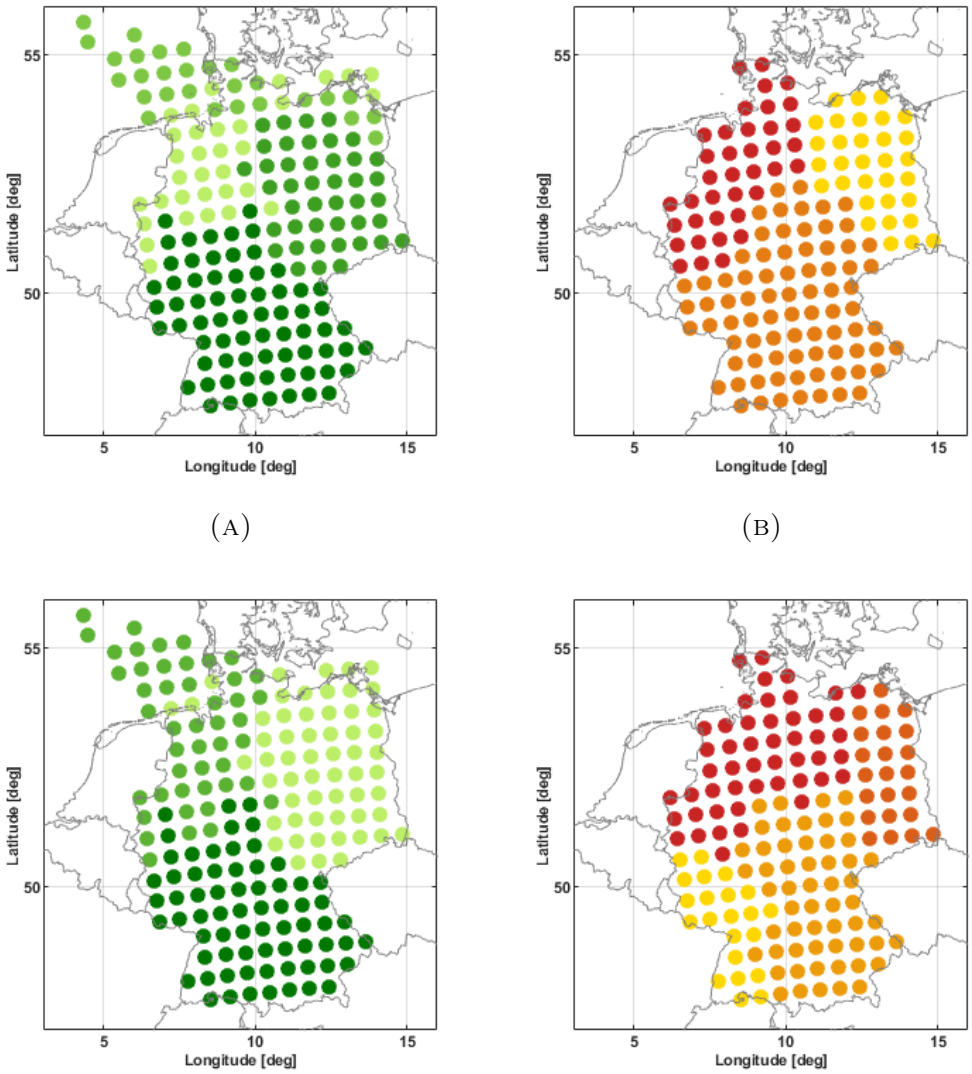

FIGURE 3.8: Spatial distribution of capacity factor cluster in Germany, in (A) for wind and (B) for PV in the HIST simulation and in (C) for wind and (D) for PV in the RCP85. Grid points of the same color within a graph belong to the same cluster.

RPSM framework

The setup for energy system related simulations via RPSM is very similar to Study II (Section 3.2.1), leaving some basic differences for the following assumptions:

- **Greenfield mode**: All exogenous installed capacity parameters are set to zero, since the model starts from scratch developing the necessary power plant composition endogenously within the first time step (see Section 2.3.3). To accomplish this, the fabrication bounding of renewable energies by Equation 2.29 is disabled.

- **CO_2 emission target**: Equation 2.35 is satisfied by CO_2 emission caps for each European country. Consistently with Section 3.2, the emission target of 90% compared to 1990 serves as a guideline and is extracted from the EEA data base for each country. Here however, no calibration of the model is necessary, since initially installed capacities are not existent (*Greenfield mode*). The emission threshold is kept constant for all simulation time steps.

- **Technology phase-outs**: In line with recent developments further investments in nuclear plants is prohibited for: Austria, Belgium, Germany, Italy, Sweden and Switzerland. Regarding coal, the phaseout is extended to the whole set of countries.

- **Net transfer capacities**: In order to account for the incorporation of multiple regions in RPSM and in consequence of inner-continental interactions, the last two terms of the balancing constraint (Equation 2.31) gain relevance regarding the energy import and export by a country. Hence, net transfer capacities acting as trade constraints between countries need to be provided (see Equation 2.34). For this purpose, a data set for 2020 provided by ENTSO-E is applied[7].

- **Dimensions**: The simulation covers the time span of 2100-2180 with a 20 year simulation time step. The focus of subsequent analysis in this part of the thesis lies only on 2100. With the *Greenfield* setup, further time steps would not be necessary. However, the additional 80 years prevent potential boundary effects regarding the lifetimes of the considered technologies. For computational cost reasons, the horizontal resolution is reduced to 48 km (a multiple of the EURO-CORDEX resolution) as well as the intra-daily resolution to 6 hours.

- **Costs & technology specifications**: Values for 2050 from Tables C.6-C.12 in the Appendix are assumed to hold for 2100.

Area potentials

In addition to the previously mentioned assumptions, area potentials for the entire European domain are examined for each grid point and used as VRE expansion constraints. Consistently, values for grid points belonging to a certain spatial cluster are accumulated and the respective mean is assigned for each cluster member. Figure 3.9a presents the resulting potentials in GW for European wind power, Figure D.4 in the Appendix for PV, respectively.

[7] NTC scenario data sets available at https://www.entsoe.eu

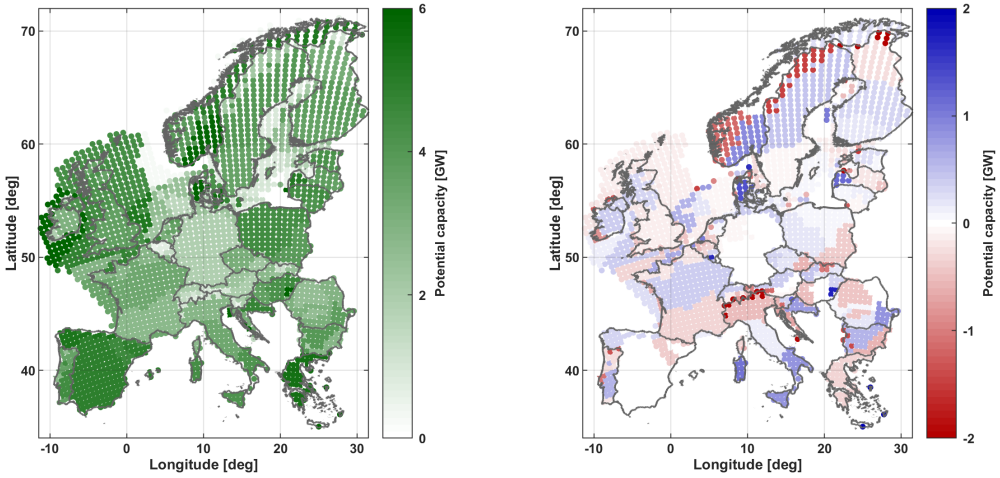

(A) (B)

FIGURE 3.9: Area potentials for European wind power for a method used in RPSM (A) and the residual to an approach by McKenna et al. (2015) (B).

Area potentials regarding onshore wind power reveal values of rather low 1.8-1.9 GW in Germany, 3.6-4.1 GW in Britain and 4.5-5.3 GW in Spain. Offshore potentials range between 1.6 GW (German North Sea) and 15.7 GW (Irish coast). Highest values for PV can be found in Germany with about 1.5 GW per grid point, whereas e.g. Portugal shows potentials of only 0.1 GW per grid point.

In order to evaluate the methodology used to estimate the available areas for VRE expansion (c.f. Section 2.4), results are compared to a more obvious and simple approach in Figure 3.9b: estimations of the total available area of a country from literature (McKenna et al., 2015) are equally distributed to all grid points within that country, still considering the clustered patterns.

Regarding important European wind power regions, differences can be observed, for instance, in France with -0.33 for the South and +0.35 GW for central and northern parts. Local differences are also estimated in the North Sea, Portugal and vast parts of Scandinavia. In case of PV, the comparison exhibits displacements mainly in France, Italy and Germany.

In conclusion, differences between the methods can be observed to a certain extent for several regions in Europe. However, the magnitudes of variations to these of VRE capacities, which would be necessary to tackle the challenge of energy transition, are expected to be very low. In consequence, the choice of method to obtain area potentials seems to be of minor importance for the applications in the scope of the subsequent analysis. Without the spatial clustering, this might not necessarily be the case.

Chapter 4

Results

The upcoming Sections describe and discuss the outcomes emerging from the three studies introduced previously. First, Section 4.1 presents results related to the long-term wind power time series for Europe (Study I). Afterwards, Section 4.2 continues with the estimation of uncertainties in energy system modeling related to reanalysis input data (Study II) and Section 4.3 terminates with the examination of climate change impacts on future energy systems (Study III).

4.1 Twenty years of European wind power

The upcoming Section presents results emerging from Study I. First of all the performance of the wind energy conversion model from REOM is evaluated in Section 4.1.1. This is followed by results from analyses concerning the 20 year time series of European wind power (Section 4.1.2) as well as an investigation regarding potential balancing effects in Europe with a focus on Germany (Section 4.1.3). Note: this part is associated with the publication in *ENERGY* in 2018 with the title *"The benefit of long-term high resolution wind data for electricity system analysis"* (Henckes et al., 2018).

4.1.1 Model evaluation

As discussed in Section 3.1.3 the evaluation of power estimation models is a critical point due to the lack of reliable historical data with sufficiently long time periods while supplying high resolution. Thus, the use of yearly aggregated power production per country is widely spread in the research community as an alternative compromise (Staffell and Pfenninger, 2016; Gonzalez et al., 2016). As a first step, results of the bias corrected control simulation by REOM are compared to the ENTSO-E time series between 2010 and 2014 of monthly wind power generation, accumulated by countries. The analysis comprises only European countries with

sufficient and reliable installed capacities for the considered time span. Table C.5 lists the remaining set of 21 European countries.

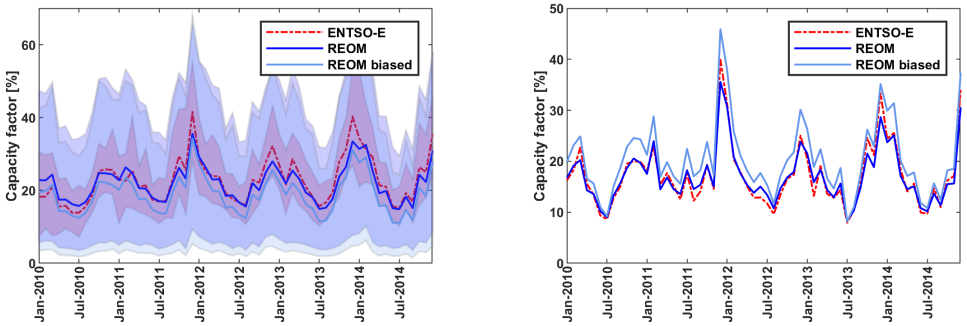

(A) (B)

FIGURE 4.1: Monthly capacity factors between 2010 and 2014 for ENTSO-E (dashed red), REOM (solid blue) and the biased REOM (solid light blue). Shown are results for the European average (A) and Germany (B). The 10% and 90% percentiles are shaded. Source: Henckes et al. (2018).

Averaged over the whole domain, a very good performance of the bias corrected REOM throughout the whole time span can be observed in Figure 4.1a, leading to an Europe-wide CF of 22.01%. Without bias corrections, this value would drop down to 18.95%. Still, REOM appears to slightly underestimate the ENTSO-E value of 22.85% CF by 3.6% in relative terms. Considering Staffell and Pfenninger (2016) suggesting that all ENTSO-E data is overestimated by 5% due to transmission and distribution losses would converge results even further. Figure 4.1b focuses on the evaluation period for Germany and exhibits two major points. First, it nicely illustrates the bias correction impact: ENTSO-E and the biased simulation are highly correlated but the model output shows a deviation pattern throughout the time span which is significantly reduced by the bias correction. Second, this deviation does not necessarily reveal the same direction trend as for the other European countries. In the case of Germany, the correction direction opposes the European average, showing a bias corrected (biased) average CF of 17.08% (20.38%) and 17.21% for ENTSO-E. This can also be observed in Figure 4.2 depicting the bias correction factors ϵ for all considered European countries. It is evident that the necessary correction increases for the Scandinavian and southerly countries compared to Central Europe. The same regions appear to be overestimated by trend while underestimations are found for Central Europe. Similar patterns are observed by Staffell and Pfenninger (2016) for their simulations based on MERRA-2.

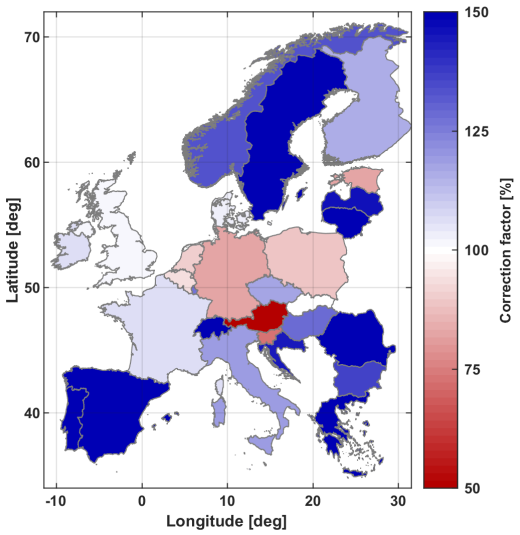

FIGURE 4.2: Bias correction factors (ϵ) for REOM in combination with COSMO-REA6 for the 21 considered European countries. The capacity factor correction is based on ENTSO-E data between 2010 and 2014. A value of 100% represents a perfect match between the simulation and observed value.

In addition to the overall European mean, Figure 4.1a shows the 10% and 90% percentiles. It is evident that the spread between the countries is far more pronounced for the simulated CF than in ENTSO-E. This is due to significant over- and underestimations in certain countries. Figure 4.3 gives insights to the mean absolute relative error for each country, revealing that the model still has problems to represent CF values in countries like Bulgaria and Sweden. This is in line with root mean square errors ranging between 1.45% CF for Germany and 6.78% CF for Bulgaria, leading to an average of 3.97% CF for Europe. A possible reason for the observed deviations between ENTSO-E and REOM, e.g. for Bulgaria and Sweden, are perhaps significant differences in the underlying assumptions of certain capacity portfolios. Both countries apply relatively few wind capacities leading to an increased sensitivity to differences in individual operation sites. However, further interpretation seems unreliable with respect to the available data sets for comparisons as ENTSO-E.

Beside the overall magnitude of wind power generations, the temporal patterns are important to asses. High Pearson correlation coefficients concerning ENTSO-E and REOM can be observed in Figure 4.4 for almost all European countries, ranging between 0.71 for Bulgaria and 0.98 for Germany. This leads to an overall mean value of 0.88 for the 21 countries. Noticeable seems the increase for Bulgaria due to the bias correction (c.f. Appendix, Figure D.2). In contrast to the MARE

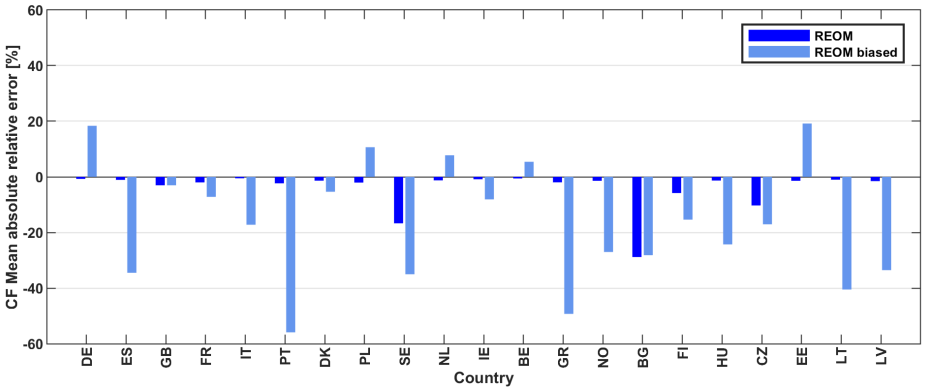

FIGURE 4.3: MARE [%] by country for monthly capacity factors of REOM and ENTSO-E during the time period 2010-2014.

(Figure D.2), the correlation is not significantly effected by the bias correction. This is expected, since the same correction is applied for all operation sites in one country. The spatial pattern in Figure 4.4 reveals a West-East dependency, perhaps triggered by the total amount of installed capacity in these regions – countries with the most pronounced wind power portfolios (e.g. Germany, Spain, United Kingdom and France) show the tendency of increased correlations.

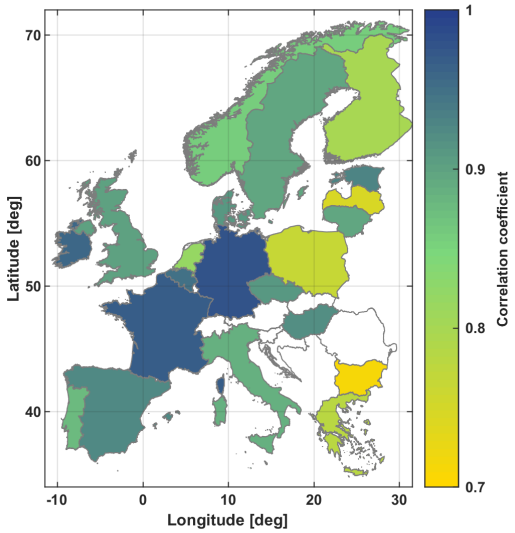

FIGURE 4.4: Pearson correlation coefficients by country between monthly capacity factors of REOM and ENTSO-E during the time period 2010-2014.

In Figure 4.5, the monthly averaged European CFs are presented. Except for a small local minimum in February not represented by the simulation, results follow closely the ENTSO-E shape. The evident underestimation in REOM is adjusted for by the bias correction: on average a very good fit is observed for *spring*

(March-April-May, MAM) and *summer (June-July-August, JJA)* months, while the *winter (December-January-February, DJF)* and *autumn (September-October-November, SON)* seasons still appear slightly biased. This can be observed in the error estimates yielding 2.97% CF for the MAE (MARE 12.8%) in DJF, 1.49% CF (6.9%) in MAM, 1.27% CF (5.8%) in JJA and 2.2% CF (9.9%) in SON, respectively.

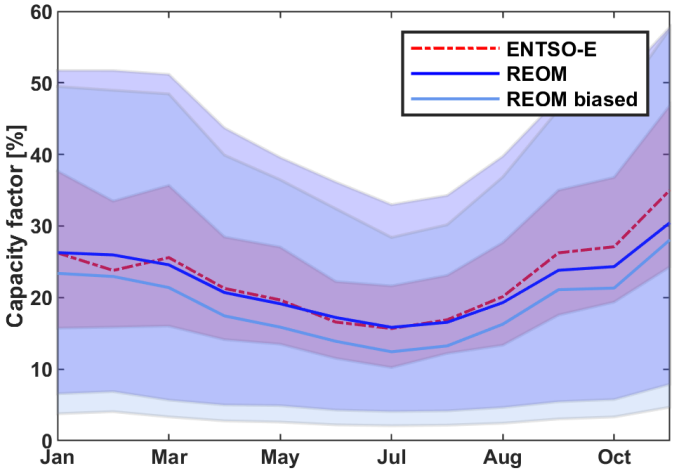

FIGURE 4.5: Wind capacity factors [%] across Europe monthly averaged between 2010 and 2014 for REOM and ENTSO-E. The 10th and 90th percentiles are shaded.

Regarding the inter-annual variability the model slightly underestimates the observed value of 8.1% CF *root mean square deviation (RMSD)* by 1.3% considering all countries. Looking at Germany or Spain the deviation decreases while it reaches a maximum of 4% CF underestimation in RMSD for Britain. The intra-seasonal RMSD for Europe indicates that winter months have the largest contribution (24.3% deviation) to these deviations whereas, in summer, the variability is better represented (8% deviation).

The second step contains an evaluation of the model performance of REOM in combination with COSMO-REA6 on an hourly basis. For this purpose, the hourly simulated wind power productions are compared to hourly means of data by EEX between 2010 and 2014 for Germany. Note that the EEX time series can not be seen as real-time measurements of power generated by the actual German wind park fleet. In contrast, the data set comprises a set of specific German wind parks, meant to represent the entire wind park portfolio of the country. Therefore, the wind power production time series obtained from the reference operation sites are extrapolated for Germany. Nevertheless, the time series can give further indications on the applicability of the model outcomes.

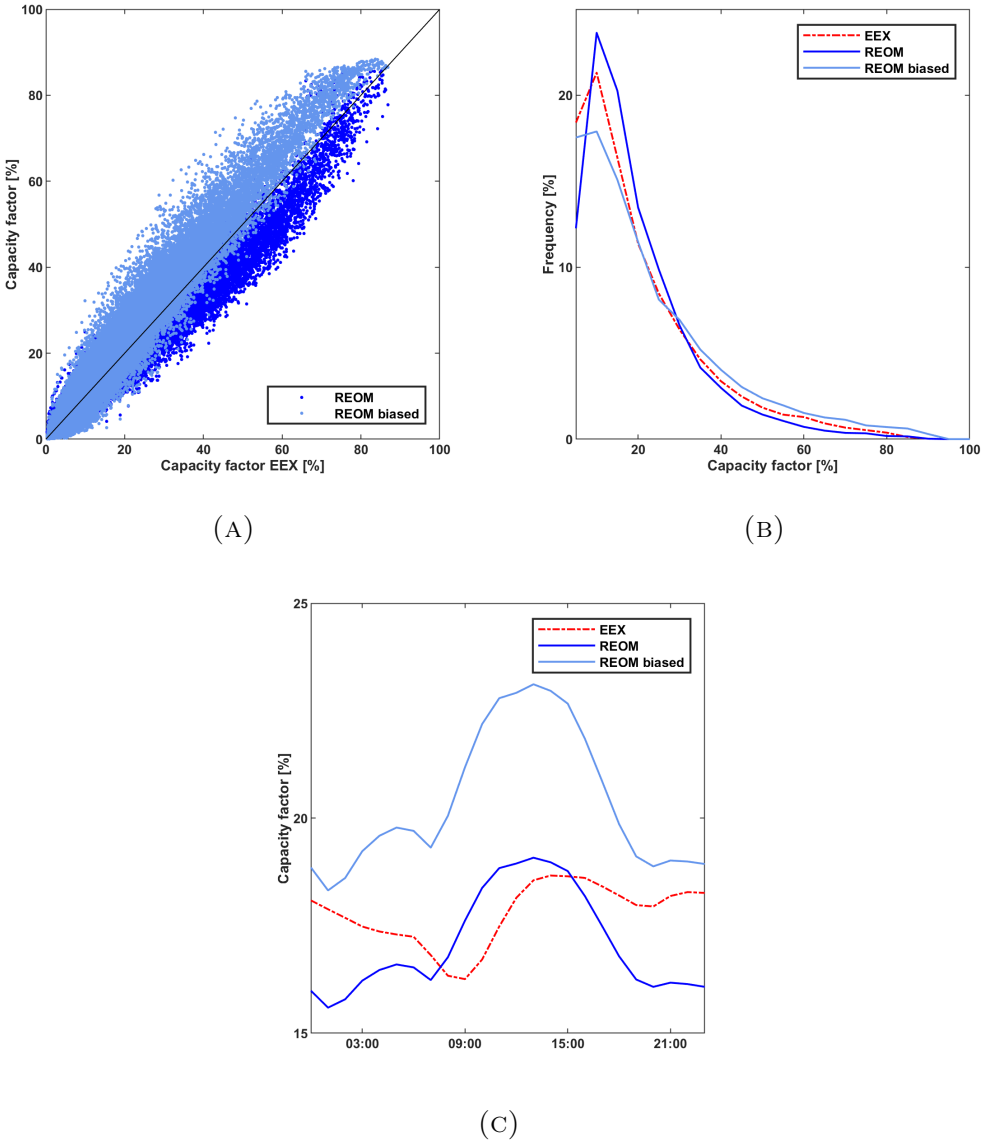

(A) (B)

(C)

FIGURE 4.6: Comparison of hourly capacity factors between 2010 and 2014 for EEX (red), REOM (blue) and the biased REOM (light blue), for (A) a scatter diagram, (B) the occurrence probabilities and for (C) the average diurnal cycle.

Regarding the comparisons for Germany, results suggest that REOM shows a strong overall performance. In line with previous findings for ENTSO-E, the German average CF (17.08%) is slightly underestimated by REOM, compared to 17.88% by EEX. Relative differences (3.9%) are very similar as found for Europe over the 5-year time span. The outcome appears very interesting concerning the usage of the EEX database as a benchmark for comparisons: assuming that ENTSO-E values are close to reality, the overall EEX average CF for Germany in the considered time period shows larger deviations than that of REOM.

Figure 4.6a compares each hourly CF of the control run to EEX, exhibiting a

very good fit throughout the time span which is in line with a very high observed correlation coefficient of 0.97. Again, the benefit of the bias correction arises, shifting values towards the line through origin. By this the *root mean square error (RMSE)* is decreased from 5.15% CF to 3.99% CF. This is similar with findings by Staffell and Pfenninger (2016), exhibiting an RMSE of 3.11% in their simulations. Furthermore, Figure 4.6b illustrates the occurrence probabilities of different capacity factors in the data sets. It is evident that low (<10%) and high CF (>30%) in the bias corrected simulation are partly shifted to CFs between 10% and 30%. The overestimation of low CFs seems to exceed the underestimation of high CF cases contributing to the overall negative deviation in average CFs.

In order to assess the intra-daily patterns, the 5-year average of the diurnal cycle of wind CFs is depicted in Figure 4.6c. In principal REOM is in good agreement with EEX, however showing slight underestimations during night times which are balanced by an extended mid-day maximum. In general the model in combination with COSMO-REA6 tends to overestimate the diurnal cycle with a pronounced mid-day maxima. The observed pattern of underestimations of variability in the model output compared to ENTSO-E continues with respect to the intra-daily timescale in Germany. REOM generates an RMSD of 13.3% CF, being 2% CF points below estimates from the benchmark.

From these findings regarding the evaluation of the bias corrected REOM wind power model, three main conclusion are drawn. First, the model shows good performance over the wide domain of Europe, including a high temporal correlation of 0.88 throughout the time period of 2010-2014, however values vary between 0.71 and 0.98 for single countries. The country-wise accumulated power generation levels by REOM are in good agreement with benchmarks, leaving a relative underestimation of 3.6% in average for Europe. Hereby, magnitude as well as the sign of deviations also vary between the countries. The application of bias corrections seems to significantly increase the accuracy of the model. Model performance appears to be best for spring and summer months. Second, the model underestimates inter-annual variability by 1.3% and intra-annual by 16.9%, respectively. For Germany the intra-daily variability is also lower than the estimations by EEX (13.6%). These deviations should be kept in mind when using the model outcomes for further analysis or simulations. Third, REOM seems to outperform the EEX estimations concerning wind power productions in Germany. Therefore, caution is appropriate using such data sets as benchmarks for validation purposes.

4.1.2 Long-term European wind power

In the following, results of the high resolution long-term run by REOM in combination with COSMO-REA6 are discussed. The hourly simulation between 1995 and 2014 again comprises the 21 European countries with significant amounts of wind power capacities on the 6 km x 6 km COSMO grid. Note that installed capacities by the end of 2014 are applied as Europe's wind park fleet for the entire 20-year time series – enabling comparisons of characteristics between different weather years. The long-term data set can be a valuable contribution to the research field, on one hand, to identify the crucial characteristics of European wind power, and on the other hand, to supply high quality data for further modeling and investigations, e.g. regarding cost-benefit or economic viability analysis. For instance, Obermüller (2017) takes advantage of the underlying high resolution and level of details for market value estimations of wind energy in Europe and Hagspiel et al. (2017) involve the data set to evaluate the regional cooperation benefits on firm capacity under security-of-supply aspects.

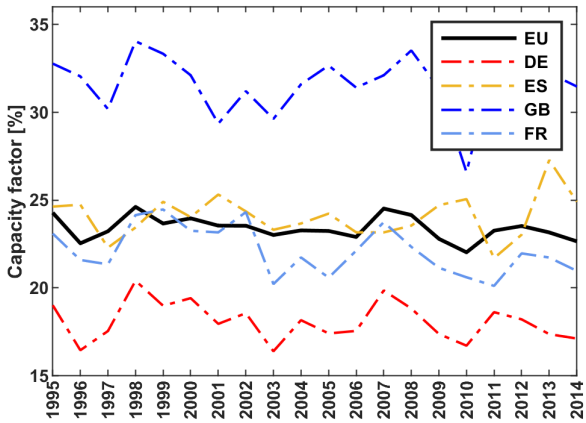

FIGURE 4.7: Capacity factors [%] across Europe yearly averaged for 1995 until 2014.

The yearly averages for Europe and specific countries between 1995 and 2014 are presented in Figure 4.7. An European average of 24.75% CF over the whole time span can be observed assuming a wind park fleet of 2014 while the inter-annual variability (RMSD) reaches ±0.7% CF. Looking at single countries the variability is stronger pronounced as for instance Germany experiences 18.1±1.4%. This appears due to a spatial smoothing effect when comprising a large domain as done for Europe – a key point for the appearance of potential balancing effects, further discussed in the following. Similarly, this can be observed for the variability on a day to day basis: the RMSD takes on values of 7.5% CF for Europe and 11% CF for Germany, resulting in 30.3% and 60.8% in relative terms. The estimated variability values

are exclusively induced by the underlying climate and weather characteristics, since a constant European wind park fleet is applied over the whole time horizon and eliminates potential impacts such as technological developments.

Strong inter-annual variability of average CFs leads to variations of up to 4.6% CF in case of Germany: the 20-year time series shows a minimum of 16.1% in 1996, whereas 1998 appears to yield the German maximum with 20.7% of wind power generation (Figure 4.7). That means that wind would have contributed 14.04 TWh (22% in relative terms) less power to the German energy system in 1996. At the same time, the maximum wind year of 1998 appears to obtain the maximum in deviation to the 20-year average annual generation, i.e. in relative terms 14.4%.

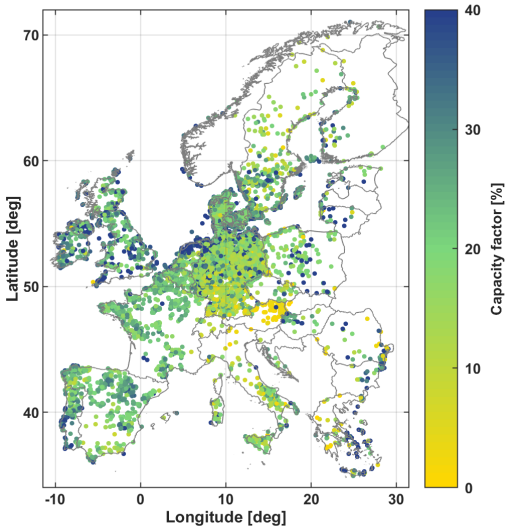

FIGURE 4.8: Capacity factors [%] across Europe between 1995 and 2014.

Further observing the different countries in Figure 4.7 indicates that the overall generation efficiency as well as the inter-annual patterns vary considerably within Europe. For instance, the poor wind years 2003 and 2010 for Germany and Britain are also reflected in the European average, Spain however, experiences one of its maximum years while it appears an average year for France. In contrast, 1997 emerges as a local minimum for Spain, Britain and France, whereas it turns out an average year for Germany. From this, several conclusion can be drawn: first, it seems critical to break down the European average wind power production to individual countries, even for those with large plant fleets. Second, even regarding the gross level of yearly averages exhibits the need of long-term data sets used as an input for energy system modeling. Third, the analysis already suggests that there may be potential for beneficial balancing effects between countries.

In contrast to Figure 4.7, the wind power generation time series are averaged over the full time span for each individual European operation site in Figure 4.8. Best wind operation sites can be found at the North Sea and coastal regions of Ireland, Britain, Germany and the Netherlands as well as Portugal. In addition, Britain, France, Spain, Belgium and the Netherlands show numerous inner-country locations with quite good performances. Besides punctual high inner-country CFs, Germany reveals a large number of lower efficiencies, in particular, towards the South. The same holds for Italy, Sweden and, especially Austria. Also noticeable are comparable high CFs for the Greek islands in the Mediterranean.

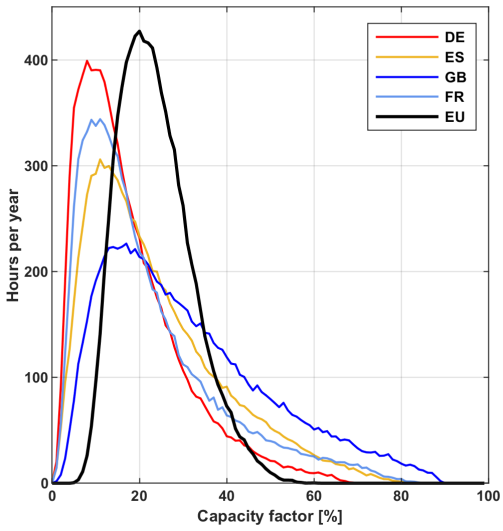

FIGURE 4.9: Distribution of hourly capacity factors [%] in Europe between 1995 and 2014.

Comparing the distribution of hourly wind generation for Europe and Germany in Figure 4.9 also reveals the previously mentioned smoothing effect. Europe experiences CF values between 0% and 68% whereas Germany exhibits wind generation of up to 88%. The probability of lower CFs is also significantly increased for an individual country as Germany. Therefore, on one hand, Germany is facing more extreme situations than the entire continent due to balancing effects between the adjacent countries. On the other hand, the probability for Europe as a whole to experience these extreme situations is very low.

Based on these distributions, two extreme conditions are defined to better quantify the occurrence probabilities:

- *Low wind*: situations within the 1st-percentile of the wind power distributions. Absolute threshold for Germany is at 2.27% CF (0.8 GWh), for Europe at 7.13% (8.54 GWh);

- *High wind*: situations above the 99th-percentile of the wind power distributions. Absolute threshold for Germany is at 69.83% (24.57 GWh), for Europe at 50.31% (60.29GWh).

These definitions serve as a basis for extreme situation analysis. Figure 4.10 highlights the number of extreme situations per year, i.e. the low and high wind cases. It appears that the inter-annual variation is, besides the yearly CF average, also large for the occurrence frequency of extreme conditions. As a consequence, Germany experiences, for instance, years with up to 185 cases (2002) of high wind, while only 24 cases are observed for 2006. Comparing the temporal evolution of annual average CFs and the occurrences of extreme situations for Germany reveals no clear link. The year 2011 serves as a suitable example: annual wind production is close to the German long-term mean (18.1% CF) with 18.62% CF, effectively an average year. However, the same year experiences exceptionally high frequencies of low wind situations while high wind conditions are met comparably seldom. Other years exhibit different patterns.

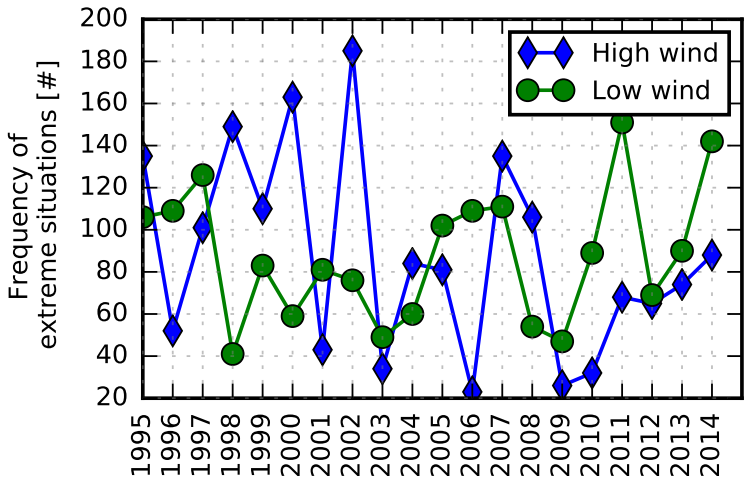

FIGURE 4.10: Frequencies of extreme situations between 1995 and 2014 with respect to German capacity factors. Source: Henckes et al. (2018).

When modeling energy systems, it appears to be very convenient to apply a representative wind year for computational cost and complexity reasons. However, the previous analysis emphasizes the challenge to obtain such a year which sufficiently represents all characteristics of the entire time period. Hence, from this the conclusion arises that it is impossible to adequately define a representative year. In particular, this is of high relevance when extreme events appear to play a critical role, i.e. in investigations concerning the reliability of future energy systems. Here, it seems to be crucial to apply long-term time horizons.

4.1.3 Balancing potentials in Europe and Germany

As previously mentioned, Europe as a whole experiences smoothing (balancing) effects, i.e. the continent faces very few situations with exceptionally low or high European average CF values. Hence, critical situations concerning system reliability can be reduced assuming sufficient transmission capacity available between the respective countries. Based on this approach, the correlation of average CFs for European countries in Figure 4.11a can be interpreted as the potential of European balancing effects between the countries.

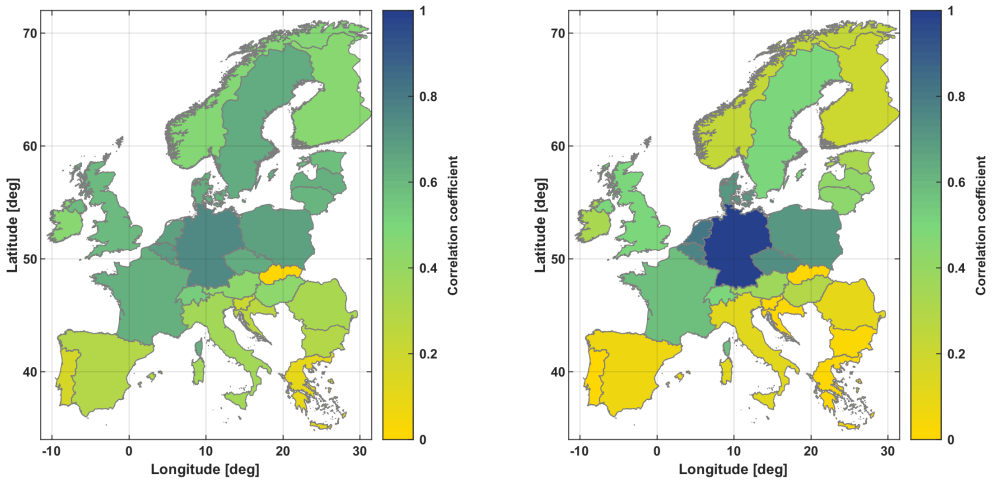

(A) (B)

FIGURE 4.11: Correlation of average wind power production by European countries with respect to the European average (A) as well as to Germany (B).

Figure 4.11a depicts the correlation coefficients of the European average wind power generation and each individual country. It is evident that Central Europe is strongly correlated to the European average with values of 0.76 for Germany (maximum), 0.7 for Belgium and 0.69 for the Netherlands and Poland. In particular for Germany, this is observed due to its location as well as its strong impact on the European average through its large wind park fleet. With increasing distance the correlation decreases, such as for Greece (0.11) or Portugal (0.18). These findings are in line with correlation patterns obtained by (Monforti et al., 2016) based on the time period 1961-2050 and 12 regional climate models. A similar pattern can be observed taking Germany as the comparison subject (Figure 4.11b). Consequently, this emphasizes the different situations regarding balancing effects for the different countries. In case of Germany, all countries are positively correlated and the expected distance dependency prevails by trend. Certainly it is beneficial for

Germany to be able to interact with low correlated and simultaneously geographically connected regions. Austria (0.38) and Norway (0.24) seem to be promising examples, in contrast to, for instance, the Netherlands (0.84) or Belgium (0.78). In contrast to the already existing high transmission capacities to Austria, the connection to Norway can only be accomplished via Denmark. However, with *NordLink*[1] a promising project is under way, with a scheduled commissioning by 2020.

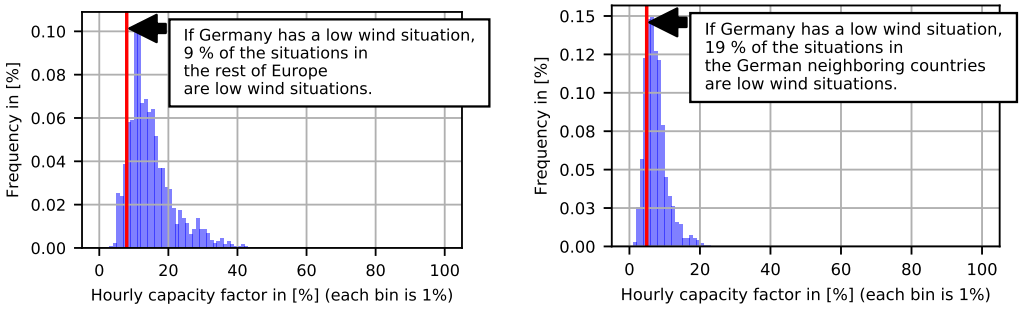

(A) Europe (B) Neighbors

FIGURE 4.12: Hourly capacity factor distribution for Europe (A) and neighboring countries (B) during low wind conditions in Germany between 1995 and 2014. The red lines show the 1st-percentile definition for low wind cases. Source: Henckes et al. (2018).

From this approach, the question arises how probable the benefit of balancing effects within Europe and neighboring countries are for Germany under low wind conditions and, hence, potentially critical situations for the electricity system. When Germany faces low wind conditions, balancing effects may contribute to the energy supply because there might still be wind power production available from uncorrelated regions, preferentially, from adjacent neighbors. For this purpose, Figure 4.12a and 4.12b illustrate the distribution of hourly CFs for the whole time horizon for Europe and Germany's neighboring countries. However, this time, only cases during low wind conditions in Germany are taken into account. The majority of cases in Europe and neighboring countries are also observed to be low compared to their 20-year median production value. Again applying the predefined low wind threshold of the 1st-percentile leaves only cases with simultaneously low production conditions in Germany as well as Europe and neighboring countries, respectively. It turns out that the production is critically low at once only in a small number of situations: for Europe, the CF is below the 1st-percentile in only 9% of the cases. As expected, the probability increases for the neighboring countries (19%). This demonstrates that, in all other cases (91% and 81%), beneficial balancing effects and

[1]NordLink is the first high voltage transmission line between Norway and Germany with 623 km and 1.4 GW capacity, https://www.tennet.eu/de/unser-netz/internationale-verbindungen/nordlink/

hence trading between the countries can be expected to take place. In further consequence, the joint probability of simultaneously low wind conditions for Germany and it's neighbors appear to be 0.19% (0.09% for Europe). In other words: not all countries experience extremely low wind conditions at the same time, enabling the potential of balancing effects under the assumption of sufficient transmission capacities.

The high spatial resolution of the underlying data set enables the possibility to extend the analysis of balancing effects to characteristics within Germany. In order to adopt the approach of spatial correlation for inner country analysis, the installed wind capacity and respective generation are aggregated on a grid of hexagons. Each hexagon contains the sum of internal wind park capacities, the average of their capacity factors and the correlation of their CF time series to the total German wind production. Figure 4.13 comprises the estimated parameters for Germany.

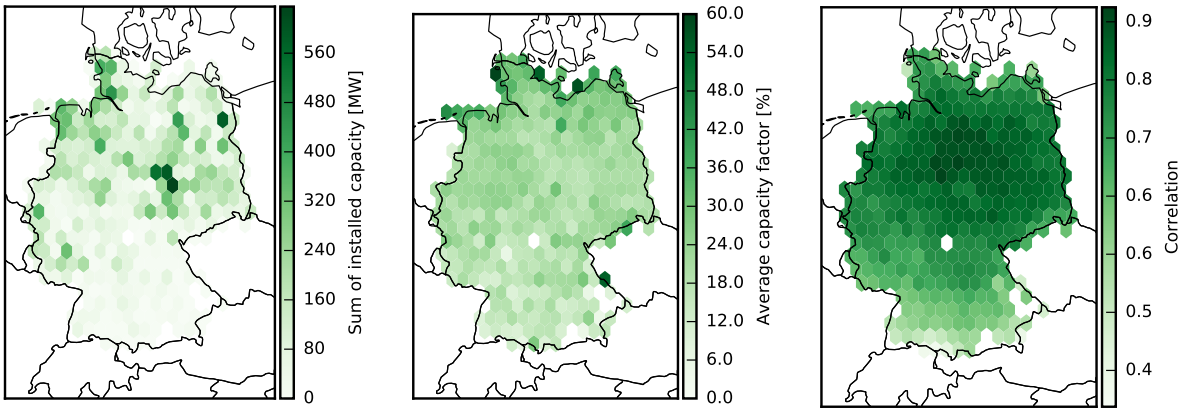

(A) Installed capacity (B) Capacity factor (C) Correlation

FIGURE 4.13: German wind power capacity (A), generation (B) and correlation of generation to the total German wind power production (C) between 1995 and 2014. Values inside a hexagon are summed up for capacities and averaged for capacity factors. Source: Henckes et al. (2018).

Certainly, German wind park facilities are mainly found in the North due to higher wind speeds, induced by lower surface roughness, and a corresponding subsidy scheme. Although the highest capacity concentration is located in the inner north-eastern part, more efficient wind production is achieved for the coastal regions, in particular, for the North Sea. This may be mainly triggered by stronger winds coming from the Northwest and evolving over sea with less surface roughness. Concerning the inner-country correlations, highest values are estimated for the North German plain where large amounts of installed capacities lead to an

implicit weighting of the correlation time series. Hexagons in this area take on values of up to 0.9, contrasting more southerly regions with weak correlations of e.g. 0.3. This results from both, different wind potentials and less installed facilities. From these findings, two conclusions can be drawn: first, with the wind park fleet from 2014, most efficient wind production per MW capacity can be obtained in the Northern windy regions. Under this aspect, coastal areas are favourable for two reasons: the slightly higher CF and simultaneously lower correlation to the rest of Germany. Second, Southern Germany may add valuable contributions to the German wind production due to its comparably very low correlation values. However, these regions appear to experience low CF and hence production efficiency at the same time. Here, a potential approach may be to apply more suitable turbine types and hub heights (e.g. smaller and lower turbines) with respect to the adjacent wind characteristics in order to improve the capacity factors.

4.2 Impact of VRE uncertainties to energy system modeling

In this Section, results concerning the impact of uncertainties on energy system modeling is presented (Study II). First, uncertainties of certain COSMO-REA6 parameters with respect to VRE power estimates are determined in Section 4.2.1. This is followed by the outcome of the sensitivity study (Section 4.2.2), which is then used as a basis for the generation of perturbed VRE power time series (Section 4.2.3). Finally, Section 4.2.4 highlights the results of the control, negatively and positively disturbed simulations by the investment model.

4.2.1 Error estimation of power output

Following the approach illustrated in Section 3.2.2, uncertainties of different COSMO-REA6 parameters, which are subject to the power conversion models (wind and PV), are being estimated. This is done by evaluation of comparisons between reanalysis data and observed time series with respect to the MARE and MAE (Equations 3.3 and 3.4).

Starting with wind power uncertainties, Figure 4.14a presents the result from the MARE estimation regarding COSMO-REA6 wind speed. Certainly, the error shows tremendous magnitudes of up to 870% for very small wind speeds. This seems reasonable, since wind speed measurements in these ranges are very challenging. Afterwards, the shape follows a stronger than exponential decrease with increasing wind speeds converging towards an error of about 20% for wind speeds exceeding

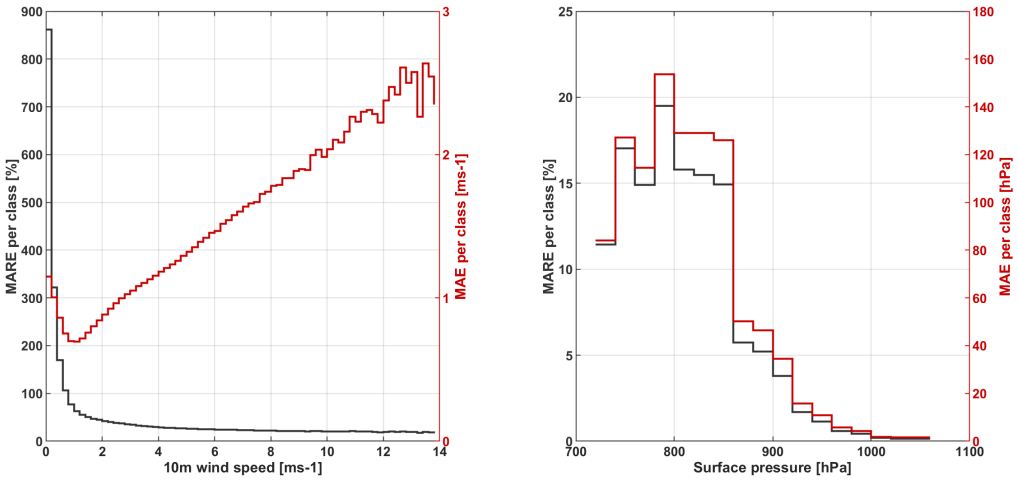

(A) (B)

FIGURE 4.14: Estimated MARE (black) and MAE (red) of 10 m wind speed and surface pressure from COSMO-REA6, for (A) 10 m wind speed and (B) surface pressure. Source: Henckes et al. (2019).

10 ms^{-1}. For surface pressure (Figure 4.14b), the reanalysis exhibits MAE between 0 and 160 hPa resulting in a MARE of up to 20% – starting with an MAE of 80 hPa for very low pressure, reaching a peak at around 780 hPa (160 hPa MAE) and then monotonically decreasing towards high pressure values. The error of these two parameters is applied using discrete values for each bin, since it is not possible to find any simple model fit.

To evaluate PV power uncertainties, the estimated MAE and MARE of direct and diffuse solar radiation are depicted in Figures 4.15a and 4.15b. For G_{dir}^{hor} the MAE from COSMO-REA6 reveals only slight variability with the absolute radiation value. This leads to an exponentially decreasing MARE with increasing radiation values from about 100% relative error for 120 Wm^{-2} to 20% for highest radiation values. Using the least square method to minimize the distance between the MARE values and an exponential model of the form

$$F_{MARE} = exp(-a \cdot x + b) + c \tag{4.1}$$

yields model coefficients of $a = 0.008\,W/m^2$, $b = 0.79$, and $c = 0.19$ (Figure 4.15a). The derived exponential function 4.1 is therefore used as an approximation for the uncertainty of G_{dir}^{hor}. In contrast, a linear relationship between the MAE and the diffuse radiation component is found, with regression coefficients of 0.255 for the slope and 20.46 Wm^{-2} for the offset. Since, there is no evidence for a good fitting model for the MARE, this linear approximation is used for the uncertainty

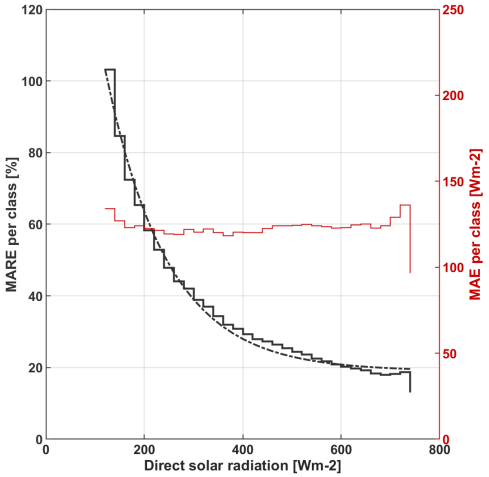

(A) Direct solar radiation

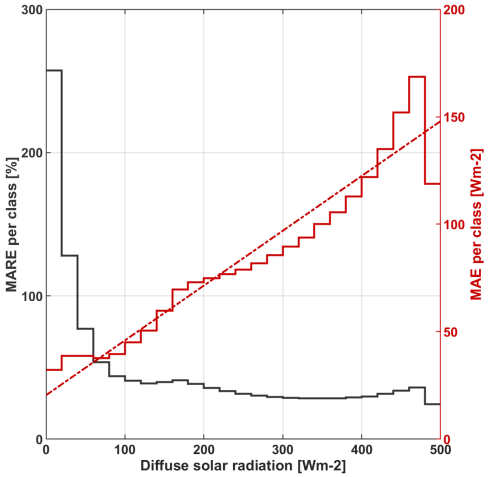

(B) Diffuse solar radiation

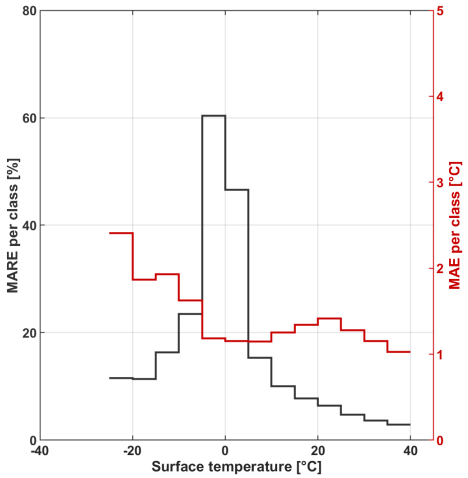

(C) 2 m temperature

FIGURE 4.15: Estimated MARE (black) and MAE (red) of direct (A) and diffuse (B) solar radiation and (C) 2 m temperature from COSMO-REA6. Dotted lines illustrate the respective model fit. Source: Henckes et al. (2019).

of G_{dif}^{hor}. Investigations of the 2 m air temperature error (Figure 4.15c) exhibits a roughly constant MAE between 1 and 1.4 K for $T_{2m} > 0$ K and an increasing MAE for decreasing negative temperatures, showing values up to 2.4 K. Consequentially, the MARE increases starting with about 10% for -20 °C, peaking at 60% around 0 °C and finally decreasing towards 0% for high temperatures. As discussed in Section 3.2.2, the error range of the surface albedo is approximated by the standard deviation derived from the 20-year COSMO-REA6 time series.

These estimated errors of COSMO-REA6 parameters are object to the following sensitivity study and selected parameters also to the perturbed inputs for the NEG

and POS simulations.

4.2.2 Sensitivity study

The results from the sensitivity study for the PV and wind power conversion models outlined in Section 3.2.2 are presented in the following. Regarding wind power, the reference turbine generates 8.9×10^3 MWh y^{-1} averaged over the 19-year time series from 60 SYNOP stations (Figure 3.4b). After disturbing each parameter for wind power modeling (wind speed & surface pressure) while keeping the other unchanged, the energy difference ΔE to the undisturbed reference case was calculated. In Table 4.1 the absolute [MWh y^{-1}] and relative energy differences [%] to the reference case are presented. It is evident that with 32.9 MWh y^{-1} (0.53%) the sensitivity of air density is neglectable compared to the wind speed quantity showing a ΔE value of 4698.4 MWh y^{-1} (62.8%). This is expected, since in contrast to air density, the energy output is proportional to the cubic wind speed. Looking at the spatial distribution of the absolute sensitivities (not shown here), values for wind speed range between 1461 and 6908 MWh y^{-1} and for air density between 11.7 and 93.8 MWh y^{-1}. Conversion to relative uncertainties in Figure 4.16 yields the expected North-South pattern for Germany, since the North is expected to experience stronger winds by trend. Certainly, with values ranging from 7.9% to 85.6% the wind speed sensitivity exceeds those of air density (0.1% to 5.0%) by far.

TABLE 4.1: Sensitivity of the wind model with respect to uncertainties of the input parameters being the surface wind speed (v_{hub}) and the air density (ρ). Absolute [MWh y^{-1}] and relative energy differences [%] to the reference wind turbine Enercon E-126 EP4 are given. Source: Henckes et al. (2019).

	ΔE [MWh y^{-1}]	$\frac{\Delta E}{E_{opt}}$ [%]
v_{hub}	4698.4	62.8
ρ	32.9	0.53

Concerning the PV power sensitivity study, the total yearly energy production by the reference panel is about 171.8 kWh y^{-1}. Looking at changes of produced energy amounts due to the substitution of the diffuse radiation model (KM or PM), only slight differences of less than 1% can be observed when applying an optimal tilt angle. The same holds for the tilt angle itself: analyses suggest that the total yearly energy generation is very similar with varying tilt angles in the range of the optimum angle. Here, very low sensitivity values of 0.1 kWh y^{-1} deg^{-1} compared to

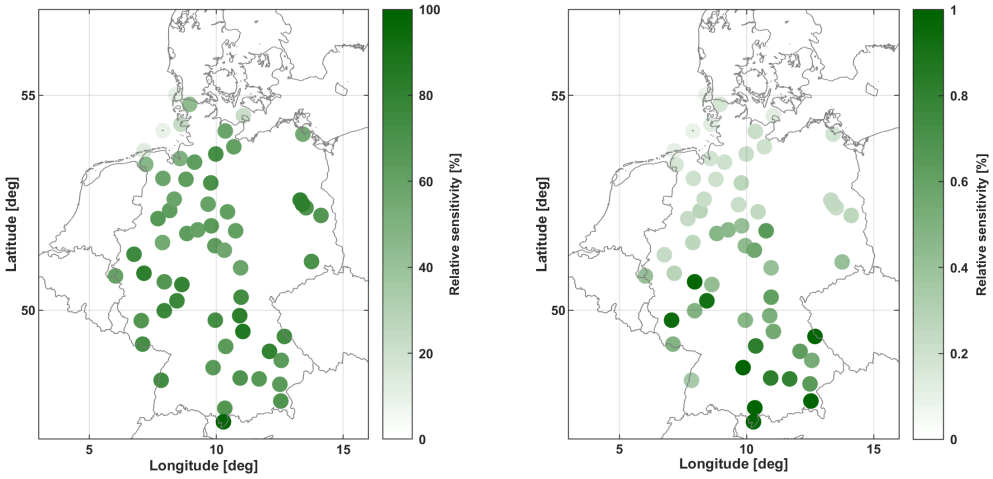

(A) Wind speed (B) Air density

FIGURE 4.16: Sensitivity of the wind power model with respect to uncertainties of the input parameters, in (A) surface wind speed (v_{hub}) and in (B) air density (ρ). Relative energy differences [%] at 60 SYNOP stations using the reference wind turbine Enercon E-126 EP4 are given.

the yearly overall production appear. From these findings the following conclusions are drawn: the choice of diffuse radiation model (e.g. KM or PM) and tilt angle are of minor importance for uncertainties in the PV power estimations. Therefore, the estimated optimal tilt angle (c.f. Appendix A) is used for all upcoming applications. In contrast to PM, as an analytical model the KM is not developed from empirical findings. This fact delivers the justification to make use of the Klucher scheme for further applications.

Similar to the wind analysis, each parameter for PV power modeling is disturbed while the others stay untouched. Then the energy difference ΔE to the reference case is obtained. Results exhibit that the direct and diffuse radiation are the largest error source in the model, showing relative sensitivities of 27.9% and 20.9%, respectively. Their absolute error of 47.8 kWh y^{-1} and 34.9 kWh y^{-1} appear to be one order of magnitude larger than the error of the other input parameters, being surface albedo and temperature. Table 4.2 gives an overview of absolute and relative sensitivity estimates for all parameters. The spatial distribution of relative energy differences in Germany is shown in Figure 4.17. Direct radiation and temperature reveal a North-South pattern, which seems to follow their respective climatological mean, e.g. less direct radiation and lower temperatures in the North compared to the South.

Hence, the second conclusion is that the dominant uncertainty source for PV is the direct solar radiation followed by the diffuse part. Similar properties are

TABLE 4.2: Sensitivity of the PV power model using radiation models KM and PM with respect to the uncertainties of the input parameters, being the direct radiation (G_{dir}^{hor}), the diffuse radiation (G_{dif}^{hor}) the surface albedo (α_{sfc}) and temperature (T_{2m}). Absolute and relative energy differences [kWh y^{-1}] to a southerly oriented reference PV panel with an area of 1 m^2 and an optimal tilt angle of 36° and 40° for the KM and PM, respectively, are given. Source: Henckes et al. (2019).

	KM		**PM**	
	ΔE [kWh y^{-1}]	$\frac{\Delta E}{E_{ref}}$ [%]	ΔE [kWh y^{-1}]	$\frac{\Delta E}{E_{ref}}$ [%]
G_{dir}^{hor}	47.8	27.9	48.6	28.3
G_{dif}^{hor}	34.9	20.4	34.6	20.2
α	2.2	1.3	2.6	1.5
T_{2m}	0.9	0.6	0.9	0.6

observed for wind speed, when the wind power model is applied. Concerning the spatial patterns of sensitivities, it appears reasonable to assume no major differences in uncertainties for different locations in Germany. In conclusion, only the uncertainties exhibiting maximal impact on the power conversion models are considered when perturbations are applied to each location in the NEG and POS simulations.

4.2.3 Perturbed VRE power

After estimating COSMO-REA6 parameter uncertainties and elaborating which of these are of major significance, the next step is to apply the errors to the 20-year COSMO-REA6 time series in order to generate the perturbed simulations NEG and POS. This Section outlines the impacts of the applied perturbations on the outcome of REOM, i.e. power generation of wind and PV, and depicts the effect arising in the set of generated typedays, which are finally used as an input for the RPSM simulations.

First of all, differences between the original CF data set generated by REOM and the resulting typedays through clustering are determined. For this purpose, the outcome of the control simulation (CON) is investigated. In Figure 4.18, the histograms of the entire and clustered CF data set are compared. For onshore wind, a very good representation can be assumed for most CF values, although the cluster distribution shows slightly too few values for both ends of the spectrum,

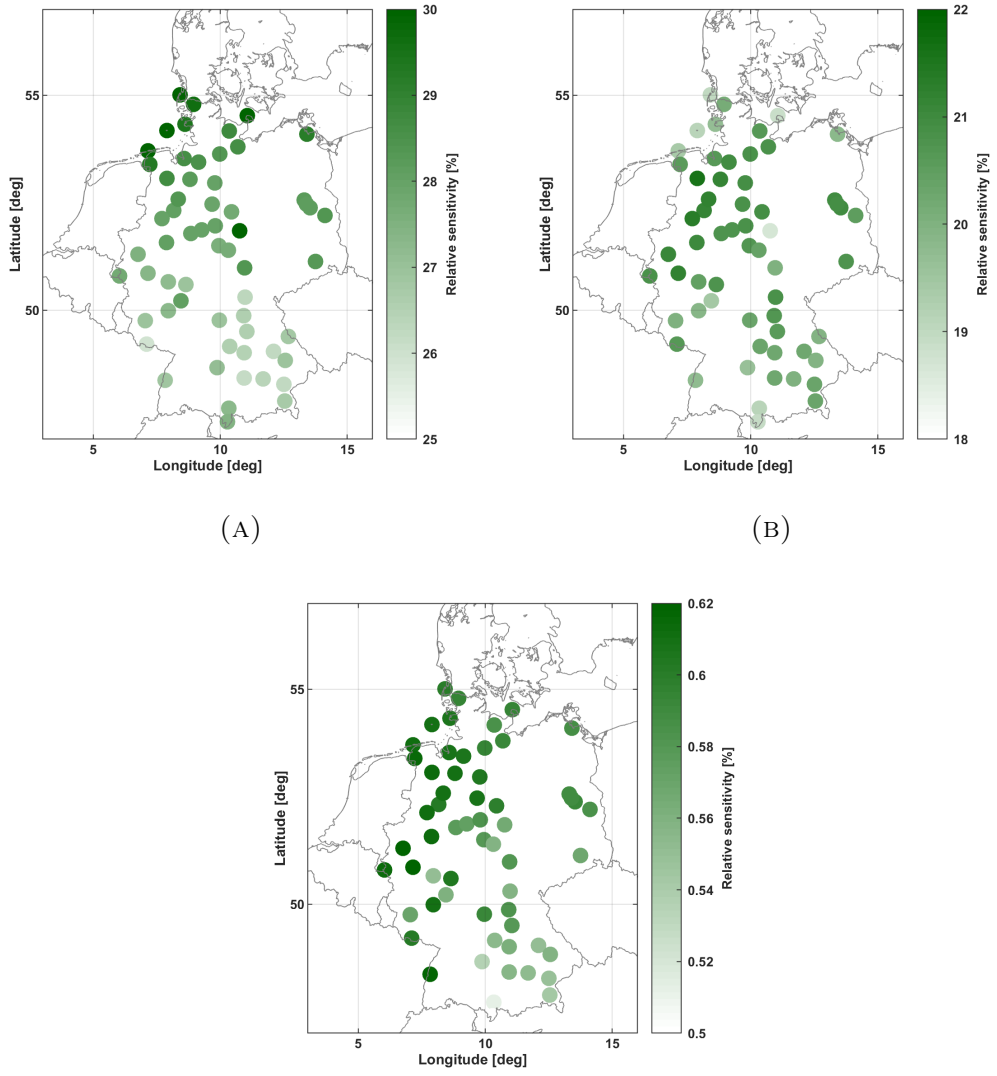

(A) (B)

(C)

FIGURE 4.17: Sensitivity of the PV power model (using KM) with respect to uncertainties of the input parameters, in (A) direct (G_{dir}^{hor}), in (B) diffuse (G_{dif}^{hor}) radiation and in (C) 2 m temperature (T_{2m}). Given are relative energy differences [%] at 60 SYNOP stations using a southerly oriented reference PV panel with an area of 1 m^2 and an optimal tilt angle of 36°.

i.e. no generations and rated generations. The same can be observed for offshore locations, however the fit in between gets worse: the 5-10% cases seem to be shifted to CF above 20%. In case of PV, the typedays appear to represent the entire data set very well. Furthermore, mean values are in perfect agreement and only for the offshore sites the standard deviation is underestimated by about 11.2%, expressed in full load hours 3532 h for the entire and 3137 h for the typeday data set, respectively. Even due to the temporal clustering process, it might occur that the spatial pattern

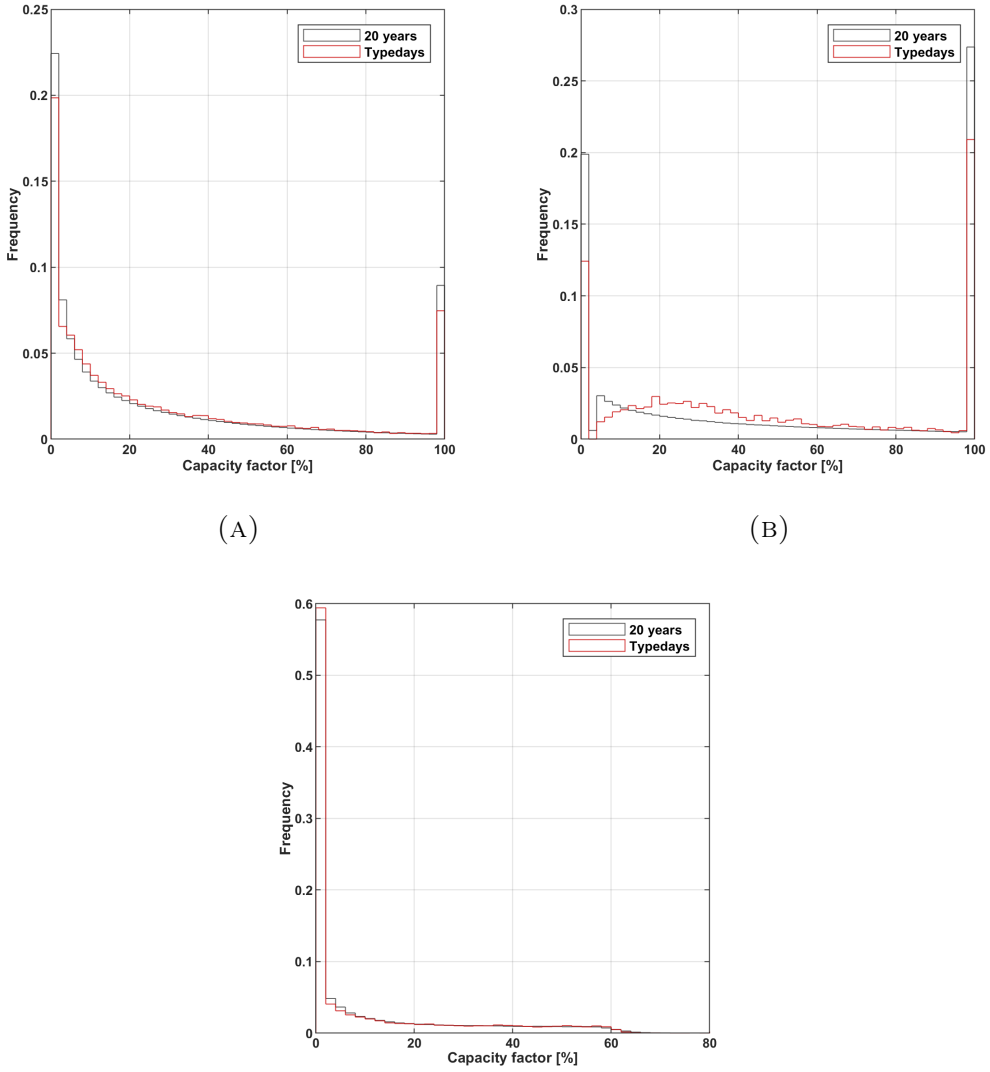

FIGURE 4.18: Histograms of occurrence probabilities for capacity factors [%] of (A) wind on- and (B) offshore as well as (C) PV in Germany, for the original 20-year time series (black) and for the clustered 20 typedays (red).

of CF is modified. While those changes are negligible for PV, a few onshore wind locations experience differences of up to 11.4% in mean CF. However, the majority of wind sites show comparable values in both data sets.

Regarding the demand, the main features are conserved nearly perfectly after the clustering process. The total yearly demand for Germany estimated from the typedays in combination with the occurrence frequencies yields 481.35 TWh, which very well corresponds to the 5-year average of ENTSO-E data (480.47 TWh). Looking at the mean (54.5 GWh) and standard deviation (10.28 GWh) also yields an almost perfect agreement for the 5-year time series and the clustered data set.

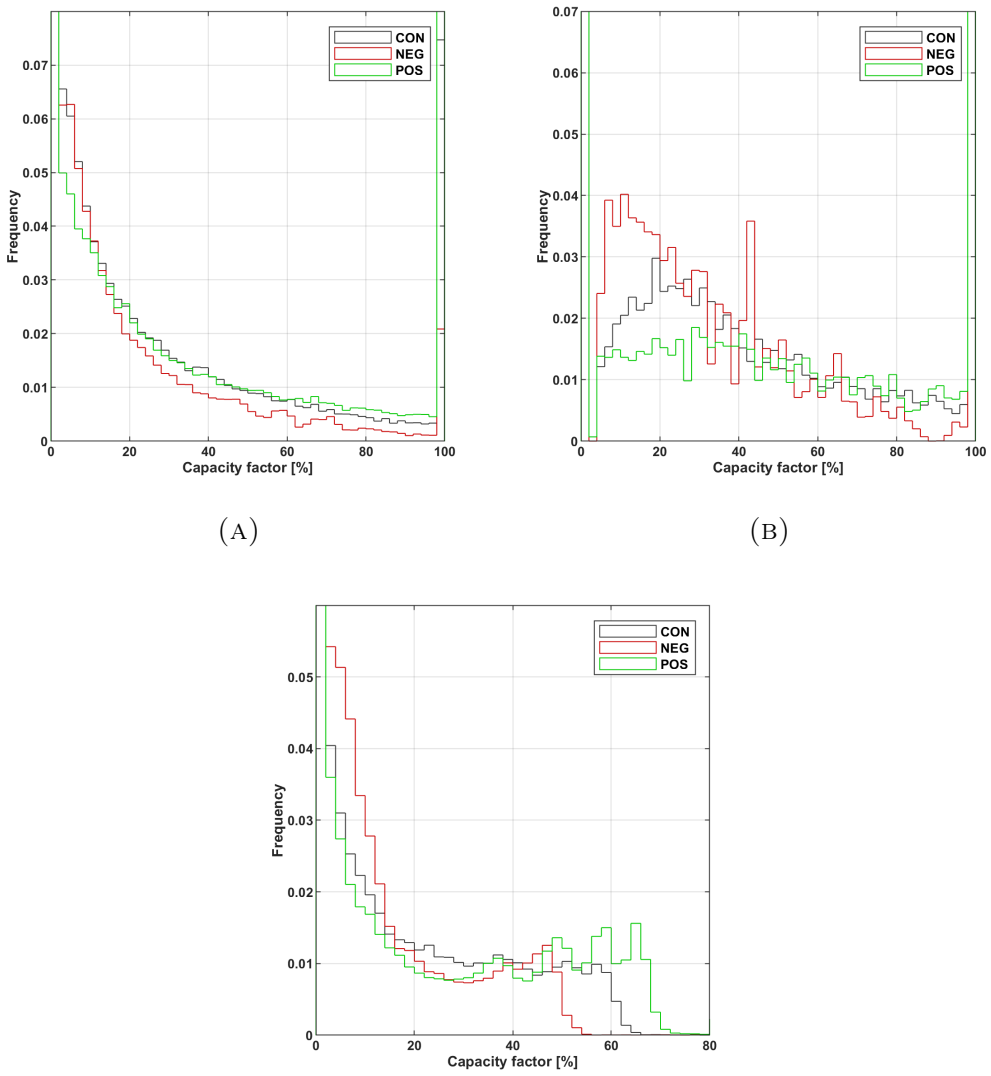

FIGURE 4.19: Histograms of occurrence probabilities for capacity factors [%] of (A) wind on- and (B) offshore as well as (C) PV in Germany based on 20 typedays in the CON (black), NEG (red) and POS (green) simulations.

Figure 4.19 depicts the CF histograms for the control (CON), negatively perturbed (NEG) and positively perturbed (POS) simulations based on the 20 typedays. As expected, all three technologies exhibit a significant shift to (a) a higher probability of small CFs and (b) a smaller probability of high CFs by trend when comparing CON and NEG. The inverse is observed for the POS simulation. Certainly, the differences in the distributions show some distinct characteristics for each technology type. For instance, the negative perturbations lead to 50% more cases with no generation for onshore and 25% for offshore sites, whereas there are no changes evident for PV. In contrast, the NEG run contains less rated generation

cases (onshore ~1/3, offshore ~1/2). For PV, the maximum of mean CFs drops from about 64% (CON) to 56% (NEG). A reversed pattern is present for the positively perturbed simulation: the rated CF cases increase by 50% onshore, by more than 1/3 offshore and for PV the maximum rises to 72% CF.

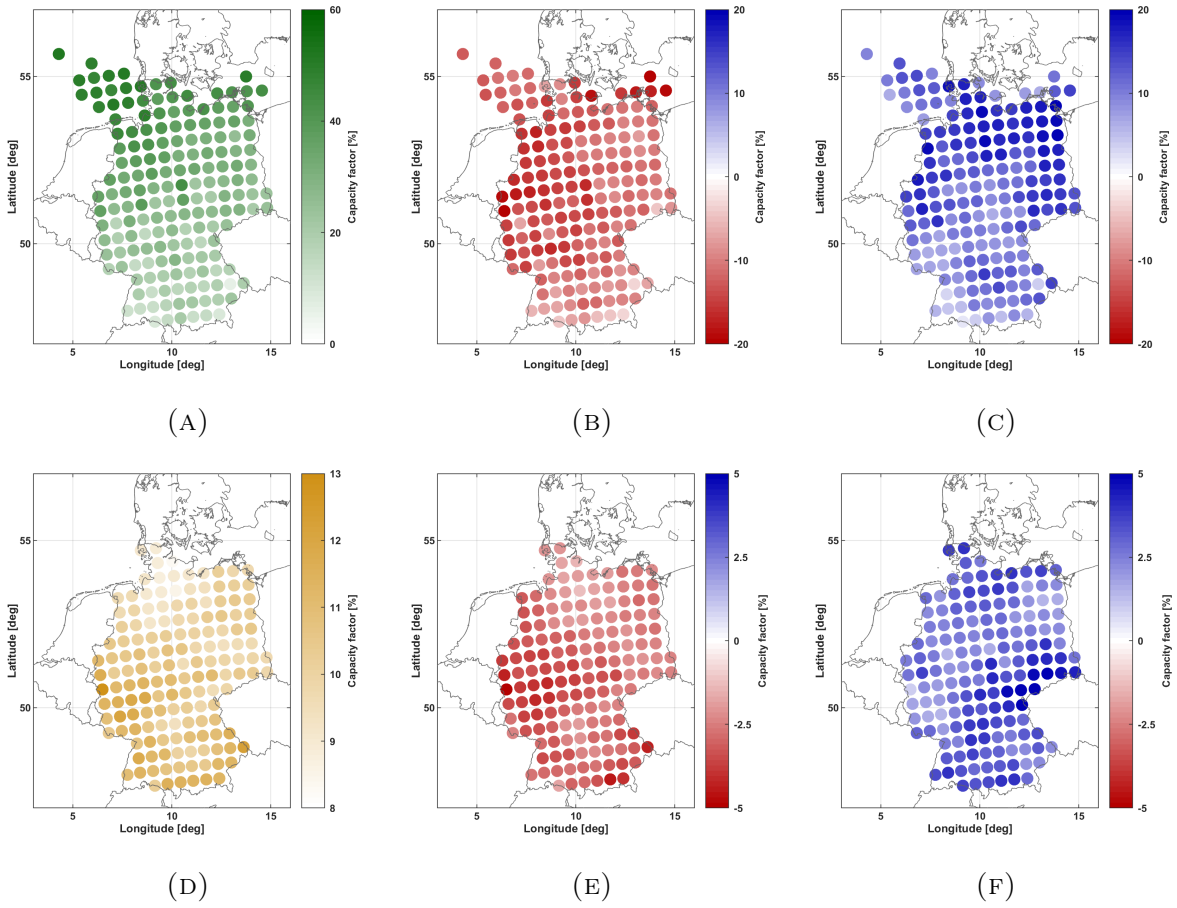

FIGURE 4.20: Mean wind capacity factors [%] of 20 typedays, for (A) the control (CON) simulation and (B) the residual to the negative (NEG−CON) and (C) positive (POS−CON) simulations. The same is shown for PV in (D)-(F). Source: Henckes et al. (2019).

Figures 4.20a and 4.20d contain the wind and PV capacity factors at each operation site in Germany averaged over the 20 typedays. In general, regarding the overall spatial pattern of wind generation in the control run, a North-South decline appears due to less topography and, hence, stronger winds in the Northern part of Germany. Capacity factors range between 6.6% near the Alps to 54% in coastal regions for onshore sites and between 41.7% and 55.5% for offshore areas. Here, the Baltic Sea experiences slightly lower values compared to the North Sea. Since the examined values are averages over time, these results emphasize that German offshore wind sites exhibit highly competitive generation potentials at any times. PV draws a different picture, showing comparably low mean values between 8.5

and 12.6% CF. A spatially almost homogeneous distribution can be observed with slightly higher generation potentials in the South. Table 4.3 yields further information about the minima, maxima and mean values of all simulations. It is remarkable that the wind site with the minimum offshore CF for NEG (28.5%) is still exceeding the PV maximum in POS (16.5%) and even the mean onshore value for the control run (27.4%).

The remaining graphs in Figure 4.20 (b, c, e and f) show the residuals of the perturbation simulations to the control run. Note that positive numbers mean that the perturbed case exceeds the control run. Investigating the spatial pattern of differences in wind CF reveals that the impact of the negative perturbations is highest in the Western part of Germany and the Baltic Sea, while for POS the strongest signals can be observed in the North-east. In case of PV, larger differences prevail in the West and close to Austria for the NEG simulation and in the East for POS. In general, when comparing the mean values in Table 4.3, the NEG simulation

TABLE 4.3: Wind and PV capacity factors [%] for the control (CON), negatively (NEG) and positively (POS) perturbed simulations averaged over 20 typedays. Given are maximum, minimum and mean values. Source: Henckes et al. (2019).

	CON	NEG	POS
Minimum			
Wind onshore	6.6	3.6	12.6
Wind offshore	41.7	28.5	54.8
PV	8.5	6.1	11.3
Maximum			
Wind onshore	54.0	49.1	71.7
Wind offshore	55.5	45.8	66.6
PV	12.6	9.1	16.5
Mean			
Wind onshore	27.4	15.7	39.4
Wind offshore	47.3	33.3	57.5
PV	10.3	7.5	13.4

appears to contain only about 57% points of the onshore potentials as in CON, 70.4% for offshore and 72.8% for PV respectively. In contrast, the POS simulation exhibits 143% of the onshore, 121% of the offshore and 130% of the PV potential found in the control run.

4.2.4 Impacts on energy systems

The following Section finally investigates the impact of initial errors, inherent to the underlying meteorological data, on the resulting investment planning by the RPSM. Thereby, as a first step, results for the undisturbed CON simulation are discussed and then compared to outcomes by the negative and positive realizations of the model chain. Certainly, total numbers regarding the CON simulation with respect to reality must be treated with caution, since the model setup is simplified and abstracted from several energy system processes in order to isolate the effects of interest. Therefore, the analysis focuses on the one hand on the development of the system over the whole time horizon as well as on relative differences to the perturbation runs on the other hand.

Undisturbed system characteristics

First of all, the cost-optimal development of generation capacities under a strong decarbonization target (90% reduction in 2050 with respect to 1990) until 2050 are analyzed. Figure 4.21 depicts the composition of installed capacity for electricity generation in the unperturbed case for the time span of interest. Germany's combined capacity raises from 168.8 GW in 2014 to 316.6 GW in 2050. Thus, the system experiences almost a doubling (+87.7%) of total installed capacity due to the CO_2 emission target – even when assuming a constant level of yearly electricity demand.

Driven by the gradually decreasing CO_2 emission target, the system experiences a corresponding reduction of lignite and coal from decade to decade, from about 11.6% capacity share in 2014 down to 0.9%, and 13.5% to 2.8%, respectively. As a result in 2050, coal remains with 8.9 GW mainly for capacity provision reasons, while lignite almost exits the market. This is caused by higher specific CO_2 emissions for lignite than for coal as well as slightly higher FOM costs (c.f. Appendix, Tables C.6 and C.11). However, due to comparably low generation costs, the remaining lignite is continuously employed to a high extend over the entire time span (between 42% and 71% CF) while still fulfilling the emission constraint (c.f. Appendix, Table C.12, Figures D.5 and D.6). The electricity generation share of lignite (coal) is consequently reduced from 28.33% (20.37%) to 2% (0.5%).

The reduction of fossil-based technologies is complemented by a market exit of nuclear facilities, yet contributing with 15.3% of the German energy generation in 2014, forced by the phaseout precondition. Since biomass and hydro are rather expensive (c.f. Appendix, Tables C.10 and C.11) and in addition constrained concerning capacity expansion, the remaining technologies to absorb the emerging

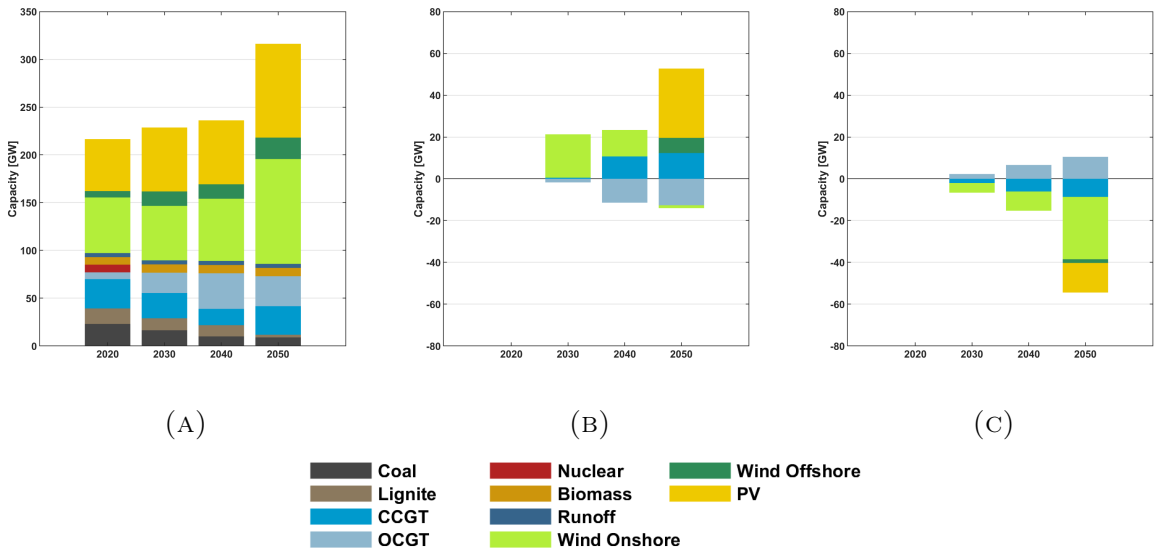

FIGURE 4.21: Development of the installed capacity [GW] composition in the control simulation (A) and its residuals to the negative (B) and positive (C) simulation. Residuals are defined as the perturbed minus the control run. Source: Henckes et al. (2019).

generation residual are variable renewable energy sources and gas. The latter is increased from about 30 GW in 2014 to 61.3 GW in 2050, while their ratio shifts from *combined cycle gas turbine (CCGT)* dominant to an even extent with capacities of *open cycle gas turbines (OCGT)* (Figure 4.21a) in order to supply comparably cheap backup capacities. However, the main expansion occurs for VRE technologies as the model needs to meet the CO_2 emission targets. Wind onshore (offshore) increases from 34.2 to 109.7 GW (1 to 22.4 GW) and PV expands from 38.8 to 98.2 GW. This leads to a raise of the generation share to 50.7% (prior 18.9%) for onshore wind, 11.2% (prior 0.9%) for offshore wind and 16.8% (prior 7.0%) for PV in 2050.

With respect to spatial allocation, Figure 4.22a and 4.22d show the operation sites and assigned generation capacities of wind and PV facilities for Germany in 2050. Except for two sites in the Southeast the model builds assets mainly in northern regions, in particular in the Northwest and the North Sea. Nevertheless, the Baltic coast experiences expansion of wind on- and offshore capacity to a significant extent. Values of up to 3.9 GW per grid point can be observed for onshore and 4.4 GW for offshore spots. By this the model obviously follows the most profitable energy generation profiles, located offshore and in the northern German plain. In addition, it illustrates that the area availability constraint takes effect. At the same time, PV draws a different and more distributed picture: main capacities can be found in western Germany close to the Netherlands and Belgium. Here, the area

potential constraint is responsible for the gap located over North-Rhine-Westphalia. Additional generation capacities are built in the Northeast close to the Baltic Sea coast. The capacity maximum is located close to the Dutch border with about 3 GW.

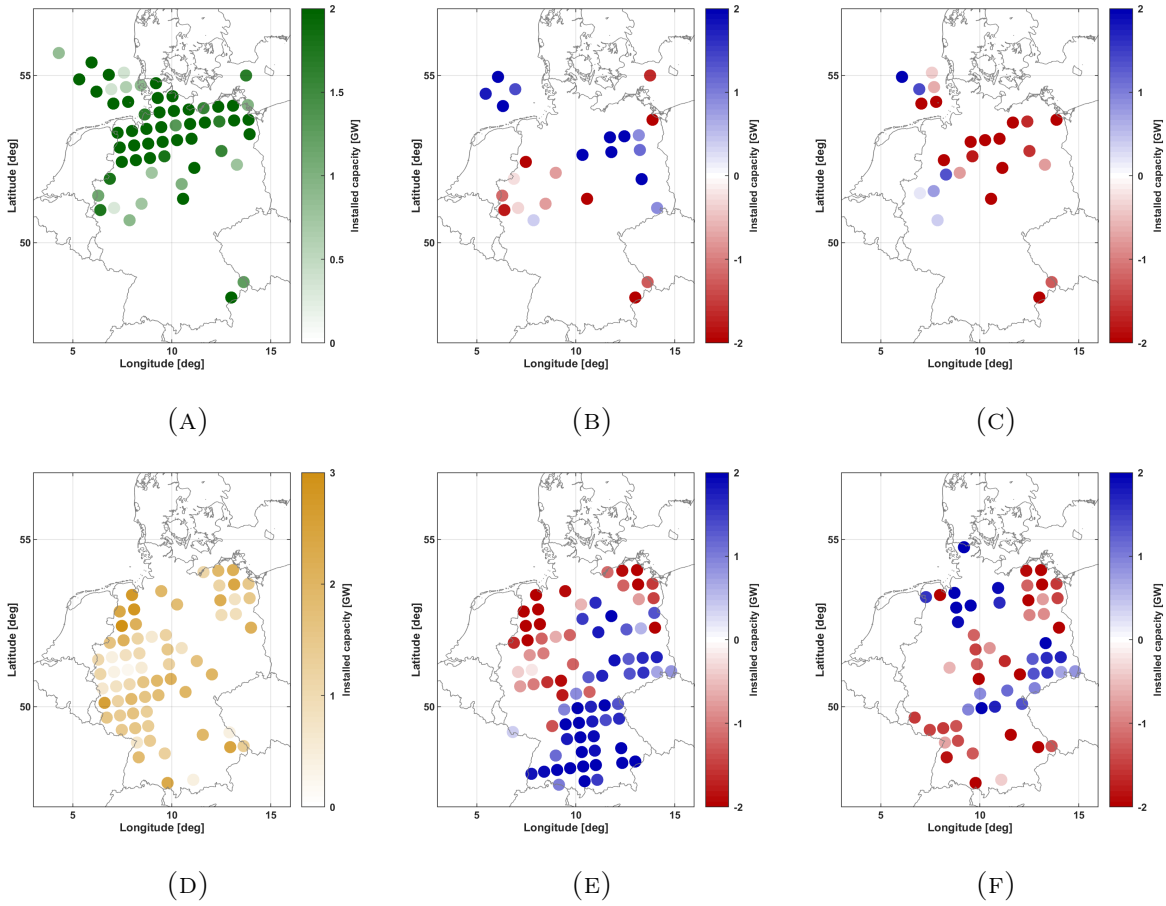

FIGURE 4.22: Spatial distribution of installed wind capacities for the control simulation in 2050 (A) and its residuals to the negative (B) and positive (C) simulation. Residuals are defined as the perturbed minus the control run. The same is presented for installed PV capacities in (D)-(F). Source: Henckes et al. (2019).

Perturbed systems

Now the effect of applied perturbations is analyzed by comparing to both, the NEG and POS realizations. Figure 4.21b and 4.21c depict the absolute differences of installed capacities of both simulations for the time span of interest.

In case of NEG, it is evident that significantly lower wind speeds and accompanied lower energy generation yield a strong expansion of onshore wind facilities to be able to still meet the tightened CO_2 targets in 2030 and following decades (Figure 4.21b). Here, onshore wind is preferred in contrast to offshore wind and

PV, since it causes almost half of the so called levelized cost of energy (LCOE, c.f. Appendix B) with respect to the other two. This expansion accounts for additional 20.8 GW (36.4%) in 2030 and 12.7 GW (19.5%) in 2040. Although wind power capacities are increasing, their electricity generation is still decreasing (c.f. Appendix, Figure D.5b) and not sufficient to compensate the CF or efficiency reduction. In 2020 this can partly be handled by coal, lignite and nuclear contributions. Afterwards however, the specific CO_2 content of the residual generation (non-VRE) has to decline to fulfill the emission constraint. The coal and lignite reduction is realized by a switch from OCGT to CCGT capacities and accompanied generation (c.f. Figure 4.21c and Appendix, Figure D.5c). In 2050 this is complemented by a strong extension of PV capacity to a total of 131.3 GW (33.2% more than CON) as well as offshore wind capacity up to 29.7 GW (32.3% more than CON) in order to meet the emission targets under low VRE generation potentials.

Figure 4.21c presents the equivalent for the positive perturbation case. In this scenario, more generation can be gained per MW of given installed VRE capacity (c.f. Appendix, Figure D.6c). Consequently, the model is able to employ less onshore wind facilities while meeting the decarbonization target, namely 4.6 GW in 2030, 9.2 GW in 2040 and 29.8 GW in 2050. The remaining 79.9 GW of onshore wind capacity account for about 72% of that observed in the undisturbed results in 2050. Still, the results suggest a strong enhancement of onshore wind generation for the positive scenario compared to CON (c.f. Appendix, Figure D.5c), which leads to less required CCGT capacity and hence a transition to OCGT backup capacity (Figure 4.21c). In 2050, the same holds true for PV and wind offshore power: in the POS simulation respective capacity can be reduced while generation is slightly increased due to higher CF profiles.

Now the question is whether the German electricity system experiences any allocation effects accompanied with the perturbation scenarios. Figure 4.22b shows the difference in spatial distribution of installed wind power capacities for the negative compared to the undisturbed case in 2050. As discussed earlier, the NEG outcomes reveal essential raises in wind on- and offshore generation capacities in order to compensate the downgrade of capacity factors. This is accomplished by expansions in comparably good wind sites which still have area potential available, such as the Northeast and the North Sea. Here, capacity is increased mainly between 2 GW to 3.2 GW for onshore sites and 1.4 GW to 3.1 GW for the North Sea spots. As observed in Section 4.2.3, grid points in the West of Germany and the Baltic Sea experience strongest reductions of wind CF values for the NEG case, which lowers their relative competitiveness (Figure 4.20b). Therefore, these regions face dismantling of installed capacities mainly between -0.7 GW and -3.8 GW for onshore sites

and -1.66 GW for the Baltic Sea area. However, reduced relative competitiveness cannot be observed for the two southern sites (Figure 4.20b), showing less installed capacity in the negative scenario (Figure 4.22b). In line with findings from Figure 4.13c, this can perhaps be explained by the assigned temporal diurnal profiles (typedays) which may appear uncorrelated to the rest of Germany (in particular to the Northwest) and can therefore be of major value to the system despite their low productivity.

Figure 4.22e shows the equivalent for installed PV capacity in the negative perturbation scenario. The previously discussed strong expansion of PV facilities is mainly accomplished in southern and eastern Germany (mainly between 1 GW and 4 GW per grid point). The choice of operation sites is driven by the respective rate of change in profitability. For instance, the concentration of capacity expansion in south-central and eastern Germany is related to comparably less CF reduction (c.f. Figure 4.20e and Appendix Figure D.6) taking place. The system reacts to the altered CF situation by a pronounced reallocation of PV facilities in the Northwest (showing worst CF for NEG) and Northeast towards the South and East. Hence, dismantling of up to -3 GW per operation site can be observed.

Figure 4.22c depicts the change in spatial distribution of installed wind capacities for the POS simulation with respect to CON in 2050. The strong decrease in onshore capacity due to the increased wind capacity factors observed previously, is distributed to various operation sites mainly located in north-central and north-eastern Germany peaking at -3.7 GW. Besides the general decline in wind capacity, an additional effect takes place for the positive perturbation case. For some high wind onshore and offshore sites, the increase of wind speeds by the positive perturbation raises the number of hours exceeding the cut-out wind speed. As a result, these sites face reduced profitability (Figure 4.20c) leading to further dismantling of capacity. However, through reallocation to adjacent spots, which show comparably higher CF, this reduction is compensated. Hence, grid points in the West and at the North Sea experience expansions of up to 1.3 GW for onshore and 3.2 GW for offshore sites in the POS scenario (Figure 4.22c).

Comparing the positive simulation to the undisturbed scenario with respect to installed PV capacity in 2050 draws a rather heterogeneous picture (Figure 4.22f). Due to comparably smaller CF enhancements by the positive perturbation of direct solar radiation in northeastern and southwestern as well as central Germany (see Figure 4.20f), the profitability of respective operation sites is lower than for example in the Northwest of the country. Consequently, the model reallocates PV capacities accordingly, while accomplishing a slight decrease of total PV capacity as seen before for the POS scenario.

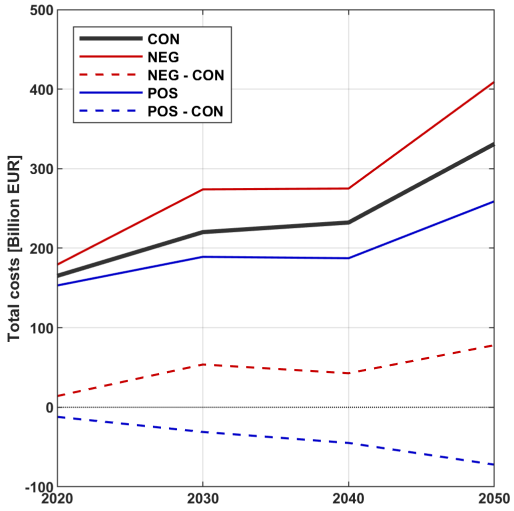

FIGURE 4.23: Development of system costs in [bn EUR] for the control (black), negatively (red) and positively (blue) perturbed simulations. Respective residuals are presented as dotted lines and are defined as the perturbed minus the control run.

The development of total system costs (defined as the sum of capital investment cost, operation and maintenance costs and variable generation costs) in Figure 4.23 exhibits an increase from about 165 Billion (bn) EUR in 2020 to 331 bn EUR in 2050 for the control simulation, accounting for a relative difference of about 100%. Both perturbed simulations follow this development, but with different rates of increase. In 2020 the German energy system costs in the NEG (POS) case about 14.1 bn EUR (12.1 bn EUR) more (less) than for CON, resulting in 8.5% (-7.3%) in relative terms. This difference is increased for 2050 yielding +78 bn EUR (+23.6%) for the negative and -72,2 bn EUR (-21.8%) for the positive simulation.

4.3 Climate change impact on European energy markets

The subsequent Section outlines results with respect to Study III: impacts of climate change to VRE resources in Europe (Section 4.3.1), associated power production profiles (Section 4.3.2) and finally the European power sector (Section 4.3.3). The underlying simulations are based on Section 3.3.

4.3.1 Future changes of VRE resources

The upcoming analysis concentrates in a first step on potential future changes of VRE power related parameter, namely surface wind speed, global radiation and temperature. Conclusions from the sensitivity study in Section 4.2 suggest, that wind speed and radiation are the dominant parameters to consider. Hence, less attention is payed to surface temperature changes, nevertheless, associated Figures can be examined in the Appendix.

To asses climate change towards the end of the 21st century, the historical HIST simulation covering the period of 1970-1999 and the future projection RCP85 from 2070-2099 are compared. Differences are often determined using residuals between both simulations – within these analyses always defined as RCP85 minus HIST. Consequently, positive numbers indicate an increase of the respective quantity in the future. Besides a description of the present climate, future changes of annual and seasonal means are discussed in order to evaluate the overall VRE future potential in Europe. Additionally, potential changes of the variability on different time scales are investigated, being inter-annual, intra-annual and inter-daily. The inter-annual variability is calculated by the standard deviation of annual means of the respective 30-year period. Variability within a day is processed similarly. For intra-annual variability, the seasonal mean of the winter months (DJF) is subtracted from that of the summer months (JJA).

Wind speed

Figure 4.24a shows the climatology of 10 m wind speeds for the HIST simulation in Europe. Due to the reduced surface roughness and lacking topography, wind speeds are generally higher over the oceans than on land. Offshore areas reach mean values of up to 7 ms^{-1} in the Mediterranean, 8 ms^{-1} for the Baltic Sea, while highest wind speeds can be observed close to the Irish coast (10 ms^{-1}). The European mainland experiences mean wind speeds mainly between 3 and 6 ms^{-1}. Following the RCP85 scenario winds tend to decrease until the end of the 21st century almost for the entire continent (Figure 4.24b). Changes of about -3 to -6% are observed for central and southern Germany as well as for Belgium, the Netherlands and Britain (c.f. Tobin et al., 2018). Most parts of the North Sea and adjacent onshore regions to the Baltic Sea show decreases of 2% to 3% compared to present mean conditions, while the Baltic Sea itself faces nearly no changes. Stronger offshore signals can be found close to the French and Spanish coasts and, in particular, in the Mediterranean region. Only the Baltic Sea coasts of Finland and Sweden as well as the coastal areas of Greece exhibit increases of up to 8%. These spatial patterns fit very well to

estimations of future energy output potentials by Moemken et al. (2018) using the ensemble mean of simulations by RCA4 in combination with multiple GCMs. Yet, their analysis reveals higher relative differences, which is due to the amplification by the energy conversion process (cubic dependency) not processed to this point. In general, Tobin et al. (2016) also agree on these findings, however determining opposing signals for eastern Europe.

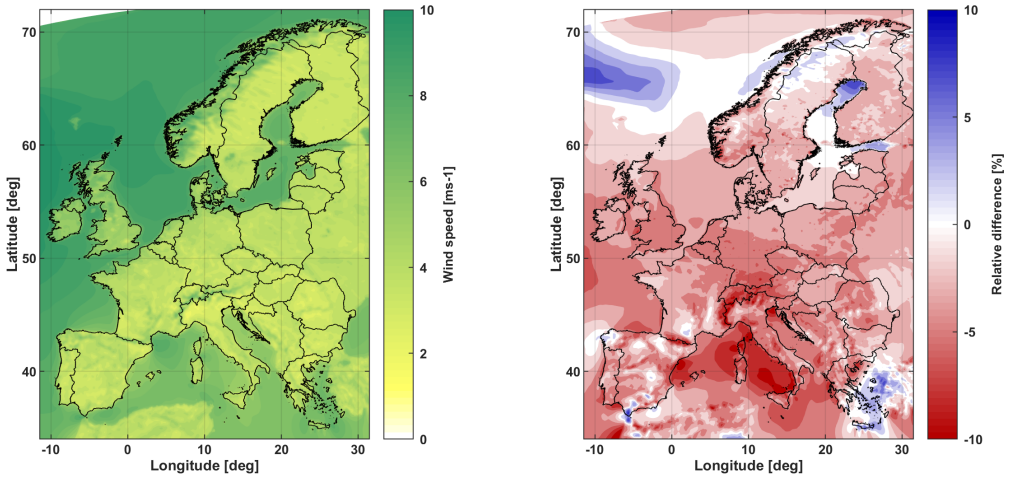

(A) (B)

FIGURE 4.24: Climatological mean of surface wind speed for (A) the HIST simulation (1970-1999) and (B) the relative difference to the RCP85 run (2070-2099). Residuals are defined as RCP85 minus HIST.

The intra-annual variability depicted in Figure 4.25a, basically the difference between winter and summer months, is quite strong in Europe with values mainly in the range of 2 to 4 ms^{-1} for offshore and 0.5 to 2 ms^{-1} for continental regions. This is due to more pronounced low pressure systems in winter months by trend, crossing mainly central and northern Europe. For the future, RCA4-ECEARTH projects a slight enhancement of this seasonality over vast parts of Germany and France (2-20%), but in particular higher values for the spacious region of the British Isles with 10-30% (c.f. Mideksa and Kallbekken, 2010) and the French Mediterranean coast with up to 25% (see Figure 4.25b). These changes can be attributed to decreases of the summer mean (Figure 4.25d) clearly exceeding changes appearing in winter (Figure 4.25c), especially in Britain and the Mediterranean (c.f. Mideksa and Kallbekken, 2010). Negative differences are estimated on the Iberian Peninsula (due to higher summer wind speeds) and southern and eastern Europe including the Baltic Sea (due to stronger decreases in winter). According to Moemken et al. (2018) these observations can be confirmed by ensemble mean analysis.

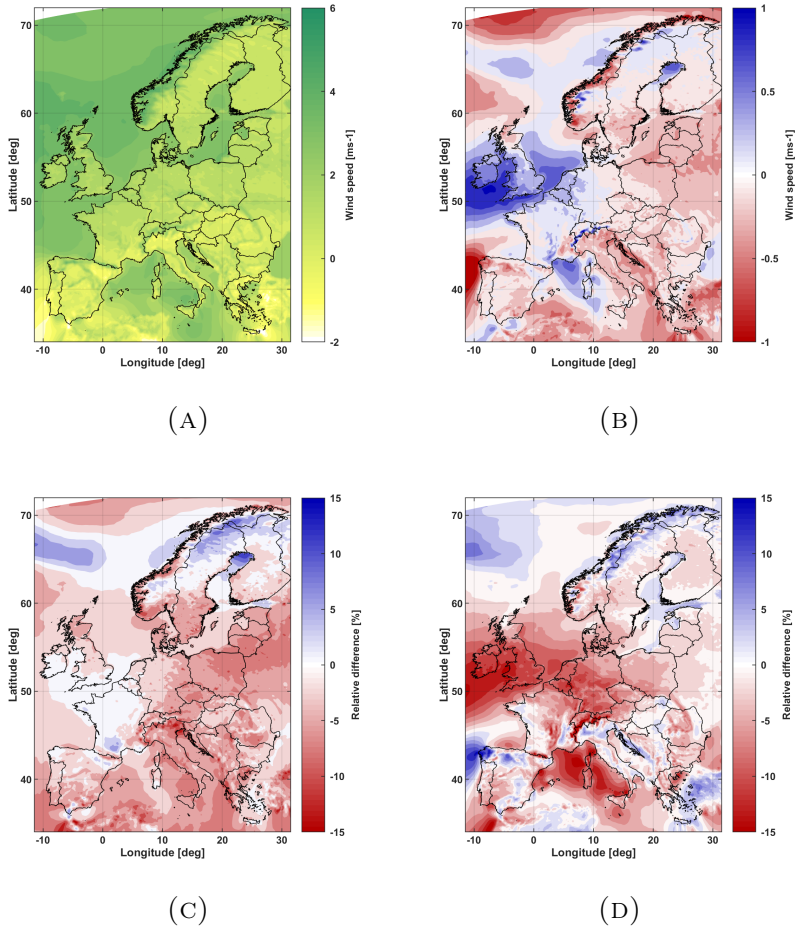

FIGURE 4.25: Intra-annual variability of surface wind speed [ms^{-1}] (winter minus summer) for (A) the HIST simulation (1970-1999) and (B) the residual to the RCP85 simulation (2070-2099). In addition, the relative difference of (C) winter (December-February, DJF) and (D) summer (June-August, JJA) between both simulations are shown. Residuals are defined as RCP85 minus HIST.

Future changes in inter-annual and inter-daily variability are presented in Figure 4.26. The residual pattern of variability between the years occurs rather unstructured, in particular for regions South of Scandinavia, with estimated negative changes of about 15% for the Iberian Peninsula and southwestern France as well as the British Isles (Figure 4.26a) and about 30% decrease for the Baltic Sea. Most parts North of 60° latitude experience a strong enhancement of up to 60% in inter-annual variability. Ensemble means of the RCA4 simulations seem to show similar and robust results (Moemken et al., 2018). For the inter-daily variability, they estimate mainly positive robust changes at the end of the 21st century for central Europe, the North Atlantic, Scandinavia and large parts of eastern Europe of up to 5% and an opposing trend on the Iberian Peninsula and the Mediterranean.

These findings are not entirely confirmed by the single RCA4-ECEARTH simulation, showing a different sign of changes for eastern Europe and varying tendencies in the Mediterranean region (Figure 4.26b). Since these areas of disagreement to the ensemble means are of rather low importance with respect to wind energy, the choice of the RCM-GCM configuration still appears adequate. In addition, higher values of changes can be determined here, perhaps again due to the different quantities examined (surface wind speeds vs. energy output).

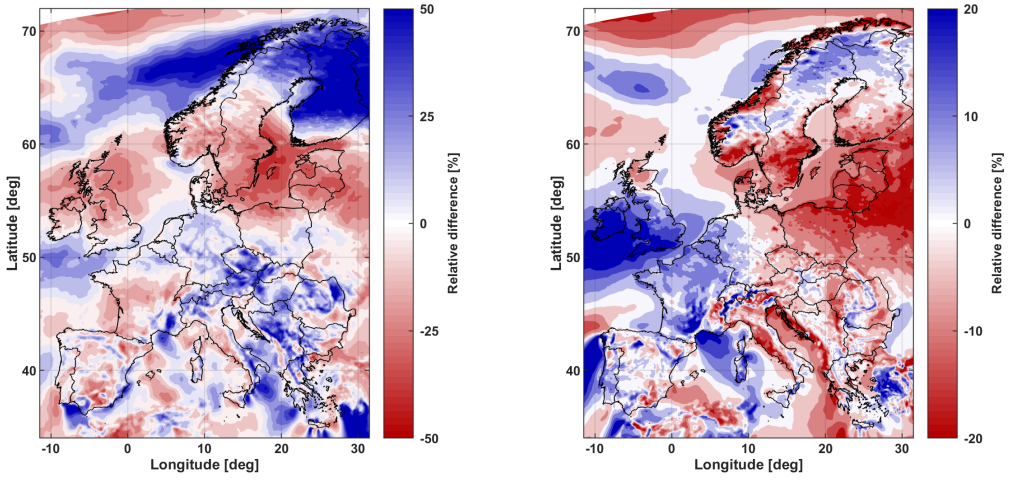

(A) (B)

FIGURE 4.26: Relative differences [%] of inter-annual (A) and inter-daily (B) variability in surface wind speed between the HIST (1970-1999) and RCP85 (2070-2099) simulations. Residuals are defined as RCP85 minus HIST.

An interesting additional feature of the study by Moemken et al. (2018) appears to be the analysis concerning future changes in occurrence probabilities of 100 m winds with respect to wind power related wind speed ranges. They detect robust results indicating an enhancement of winds below 3 ms^{-1} (cut-in) for large parts of Europe and a decrease in the Baltic Sea and Aegean. At the same time, a decrease for high winds (>20 ms^{-1}, cut-out) is suggested by the ensemble means for the Mediterranean and the North Atlantic, yet for most parts of the European continent, no clear tendencies are observed. Noticeable is the strong decline estimated for the North Atlantic and adjacent coasts for the rated power generation range (between 11 and 20 ms^{-1}).

In conclusion, an increased inter-daily and seasonal variability enhances the differences of power supplied by wind energy in the future within a day or a year. This yields a more pronounced challenge of handling future European energy systems with high shares of wind power and may foster the need for backup plant

capacities. The climatology of wind speeds is projected to slightly decrease by about -3% to -6% over most parts of the continent, triggering expectations of a decline in wind power potentials towards the end of the 21st century.

Global solar radiation

Regarding global solar radiation at the surface, results comparing the HIST and RCP85 simulations by the RCA4-ECEARTH realization are mostly in good agreement to ensemble mean analyses processed by Jerez et al. (2015), using combinations of five RCM and five GCM. Figure 4.27a depicts the future changes of the climatology mean in relative terms. The Iberian Peninsula, France, southern Germany and Britain show weak positive signals below 5%, with maximum changes found for northwestern France. Most remaining parts of the continent and the North Atlantic experience a decrease of radiation towards the end of the century, mainly between -2% and -5% and peaking with about -15% in Scandinavia.

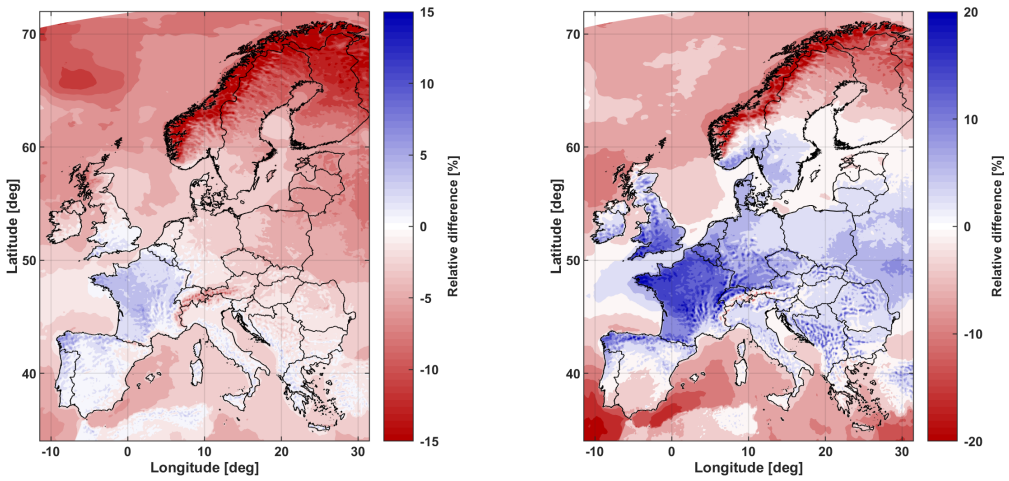

(A) (B)

FIGURE 4.27: Relative differences [%] of the climatological mean (A) and intra-annual variability (B) of surface global solar radiation between the HIST (1970-1999) and RCP85 (2070-2099) simulations. Residuals are defined as RCP85 minus HIST.

The variability between winter and summer shows clearer tendencies for the future. Winter months experience a decline prevailing almost over the whole domain, except for the Mediterranean and Iberian Peninsula with about +2% (c.f. Appendix, Figure D.14a). In most parts of Europe these decreases clearly exceed those observed for summer months (c.f. Appendix, Figure D.14b) leading to an increase of intra-annual variability between 4% and 17% (Figure 4.27b). Again,

largest signals can be found in northwestern France where radiation reveals essential enhancements of about 10% in summer. The Mediterranean region and most parts of the Atlantic undergo slight decreases in intra-annual variability of -2% to -5% with a peak of 10% at the Spanish coast. In addition, Scandinavia faces reductions of up to 20%. Inter-daily variability appears to show very similar patterns to those discussed above (Figure D.14d), showing slightly weaker magnitudes though.

According to Jerez et al. (2015), their ensemble mean surface temperature exhibits 3 to 5 K raise over the whole domain for the end of the century, in agreement with the single model results in (c.f. Appendix, Figure D.15). They derive a resulting change in PV power potential of about -3% for southern and eastern Europe, with highest impact in summer for southerly regions while impacts in winter can be neglected.

4.3.2 Renewable power production profiles

In this Section, the effect on CF time series related to the clustering algorithm is presented first, followed by results concerning the VRE potentials for historical and climate change conditions.

Evaluation of the clustering step

Both previously analyzed time series are object to REOM and the clustering algorithm, leaving two sets of spatially clustered European regions, each containing 20 typedays. Each typeday consists of 3-hourly daily time series regarding capacity factors for wind on- and offshore and PV as well as demand. As for Section 4.2, first the difference between the full 30-year and clustered data set is examined, using the example of the HIST simulation. Afterwards, the impact of climate change is estimated by comparing both sets, i.e. HIST and RCP85. By that, the effect of climate change signals observed in Section 4.3.1 can be traced towards the typeday patterns, which in fact are finally the main drivers for the RPSM simulation outcomes.

In general, the spatio-temporal clustering method reproduces the distributions of occurrence frequencies quite promising, with best results accomplished for PV (Figure 4.28). For both, wind on- and offshore the method slightly underestimates situations with maximum production. The same can be observed for the low generation range between 0% and about 10% CF. These cases seem to be shifted towards higher CF values. At the same time, 0% CF cases are overestimated in the clustered data set for wind onshore production. This in combination leads to a considerable relative difference of -12% (-3.3% CF) for onshore wind potential, +2% (0.9% CF)

for offshore wind and -2.1% (0.2% CF) for PV in Europe. As expected, the standard deviation within a year is decreased by the application of a clustering algorithm, i.e. -12% for onshore, -4% for offshore wind and -8.2% for PV, respectively.

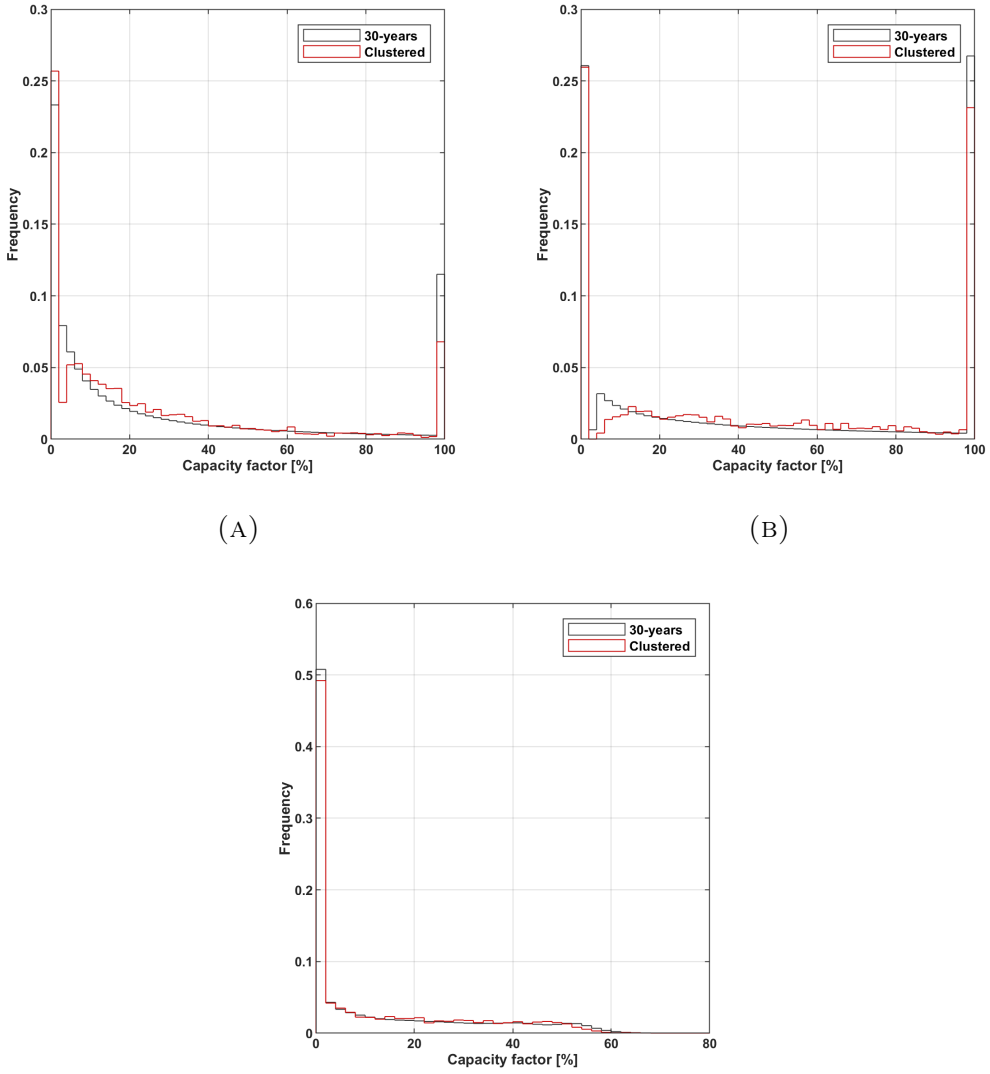

FIGURE 4.28: Histograms of occurrence probabilities for capacity factors [%] of (A) wind on- and (B) offshore as well as (C) PV in Europe, for the original 30 year time series (black) and for the clustered 20 typedays (red).

In particular, the onshore difference needs to be kept in mind, since lower VRE capacity factors may mitigate their potential to contribute to an energy transition with respect to strong decarbonization targets. Yet, further investigations would be required to be able to outline an appropriate reason for this behaviour, laying outside the scope of this thesis. In addition, the slight decline in variability throughout

the year is also of importance when it comes to reliability related aspects, such as backup capacity planning.

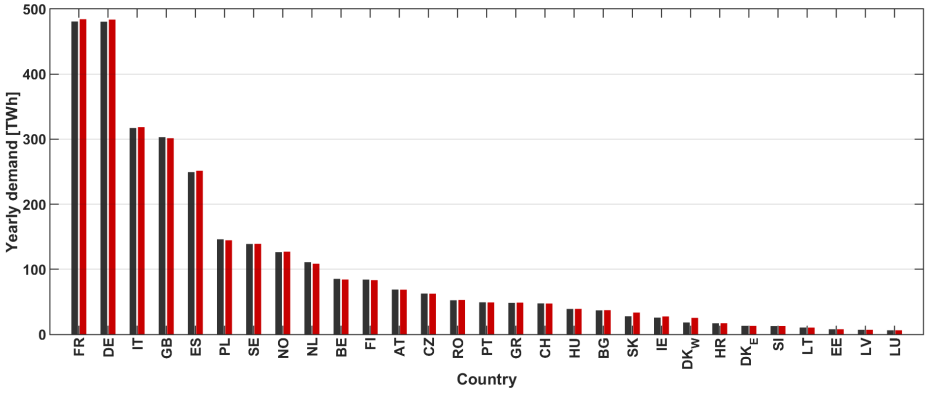

FIGURE 4.29: Average of total yearly demand for ENTSO-E between 2010 and 2014 (black) and for the clustered simulation results (red).

Figure 4.29 illustrates the yearly average demand from ENTSO-E and extrapolations to yearly values from the clustering results (using typeday occurrence frequencies) for each European country. It is evident that the yearly total load is captured very well, showing only slight considerable deviations. An underestimation of 2.1% is found for the Netherlands to be the maximum deviation in Europe. The differences in hourly averages of demand are observed to be of the same magnitude. Also, the standard deviation is well represented, with a deviation maximum in Germany estimated at about +8.5% in relative terms.

Future changes of VRE potentials

Comparing the occurrence distributions of CF in the HIST and RCP85 data sets for Europe as a whole (not shown) reveals no clear pattern of difference, e.g. shifts within certain ranges of capacity factors. Exceptions are the deviations at both ends of the spectrum: the future run tends to exceed the HIST run in the probability of cases with no generation for all VRE sources (in particular for onshore wind) and contains less situations with capacity level productions at the same time (especially for offshore wind). This is in line with the general picture of declining wind speeds and global solar radiation over most parts of Europe as seen in Figures 4.24b and 4.27a. Also this agrees with the analysis by Moemken et al. (2018) concerning the analysis of different power curve ranges (cut-in, cut-out and rated speed). Their estimated increase of low wind situations ($v < 3\,\mathrm{ms}^{-1}$) over large parts of Europe contributes to the increase of 0% CF cases, whereas the strong decline of wind speeds at rated production level ($11\,\mathrm{ms}^{-1} < v < 20\,\mathrm{ms}^{-1}$) for the North Atlantic and adjacent coasts lowers the probability of situations showing 100% CF.

Figure 4.30a shows the results for the HIST simulation regarding temporal averaged (over all typedays) wind generation potentials in Europe, spatially distributed to the clustered regions in each country. Certainly, highest values are observed for offshore areas closely following the climatology of the resource (c.f. Figure 4.24a): CFs in the North Sea exceed those found for the Baltic Sea, i.e. about 65% CF for the British coasts, Germany and Denmark, whereas 40% close to Finland and 60% in Sweden and Latvia. At the Portuguese coast 50% can be observed while values in the northern Adriatic Sea drop down to about 28% CF. For onshore wind, the best regions are found in Ireland and Norway (˜58%), followed by Britain (43-48%). Germany appears quite diverse ranging between comparably low 15% in the South and 40% in the Northwest. The combination of all clustered regions per country yields the country-based total averages depicted in Figure 4.30c. Note that onshore and offshore CFs are contributing to the respective country. A clear general pattern emerges: Europe's wind power potential experiences a strong Northwest to South gradient as already observed in Figure 4.24a. A major reason for the distinct difference between northern countries (North Atlantic coasts) and the Mediterranean region is the higher offshore potential. This is in line with the low combined potentials of Spain and Portugal (about 21% CF) compared to for example France, since these two countries have no or only few available offshore spots in the North Atlantic (due to water depths). Best total production potentials are estimated for the British Isles with about 52%, the Netherlands and Denmark 46%, and Norway 42% CF. In contrast, worst average CF are yielded for Slovenia (15%), Finland (18%) and Romania (19%).

Respective residuals (RCP85 minus HIST) are also provided in Figures 4.30b and 4.30d. The general pattern follows the future changes found for the wind resource (c.f. Figure 4.24b) – most countries experience a relative decline between 5% to 10% for wind power production in the RCP85 scenario, which corresponds roughly to a doubling of magnitudes observed for the wind resource itself. Strongest decreases are estimated for Italy with -18% in relative terms, mainly due to strong signals in northern regions (-31% to -40%), complemented by -12% for the Adriatic Sea. This is followed by Greece (-13%), Czech Republic (-11%) and France (-10%). For the latter, very contrasting onshore signals show up ranging from -52% in the South to +77% in the Northwest. Contributions of available areas for power generation in the North Atlantic are mainly of a negative nature, with relative changes between -5% and -16% East and Southwest of the British Isles. The decline tendency of wind speeds in the range of rated power production observed by Moemken et al. (2018) is perhaps responsible for this behaviour.

In contrast to vast parts of Europe, some regions show a different picture than

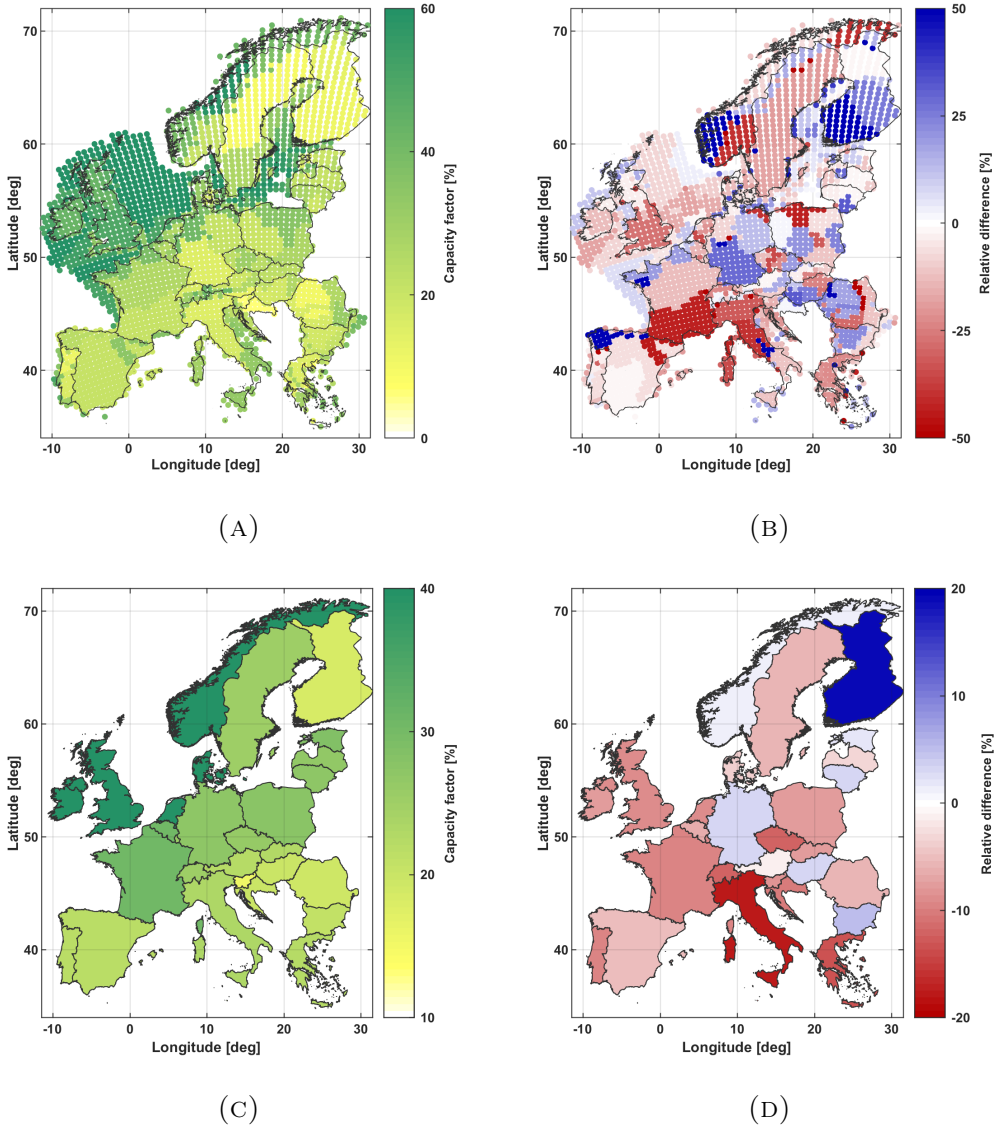

FIGURE 4.30: Spatial distribution of wind capacity factor potentials [%] averaged over all typedays for the HIST simulation (A) and relative differences [%] to the RCP85 run (B). In addition, country-based averages [%] (on- and offshore combined) of the HIST simulation (C) and the respective differences [%] to RCP85 (D) are depicted.

expected from the climatological mean of the wind resource. For instance, this includes Germany, Austria and Bulgaria with rather weak but positive future changes in wind power potential between 3% and 5%. In case of Germany, the contributing regional values reveal large variations of -38% at the Baltic coast to +28% of relative change in the South. A similar difference can be observed for the German North Sea (-15%) and Baltic Sea (+26%) offshore areas. That means that the strongest changes are found for regions with the lowest wind power potential in Germany and vice versa. The strongest enhancement of CF is estimated for Finland with a

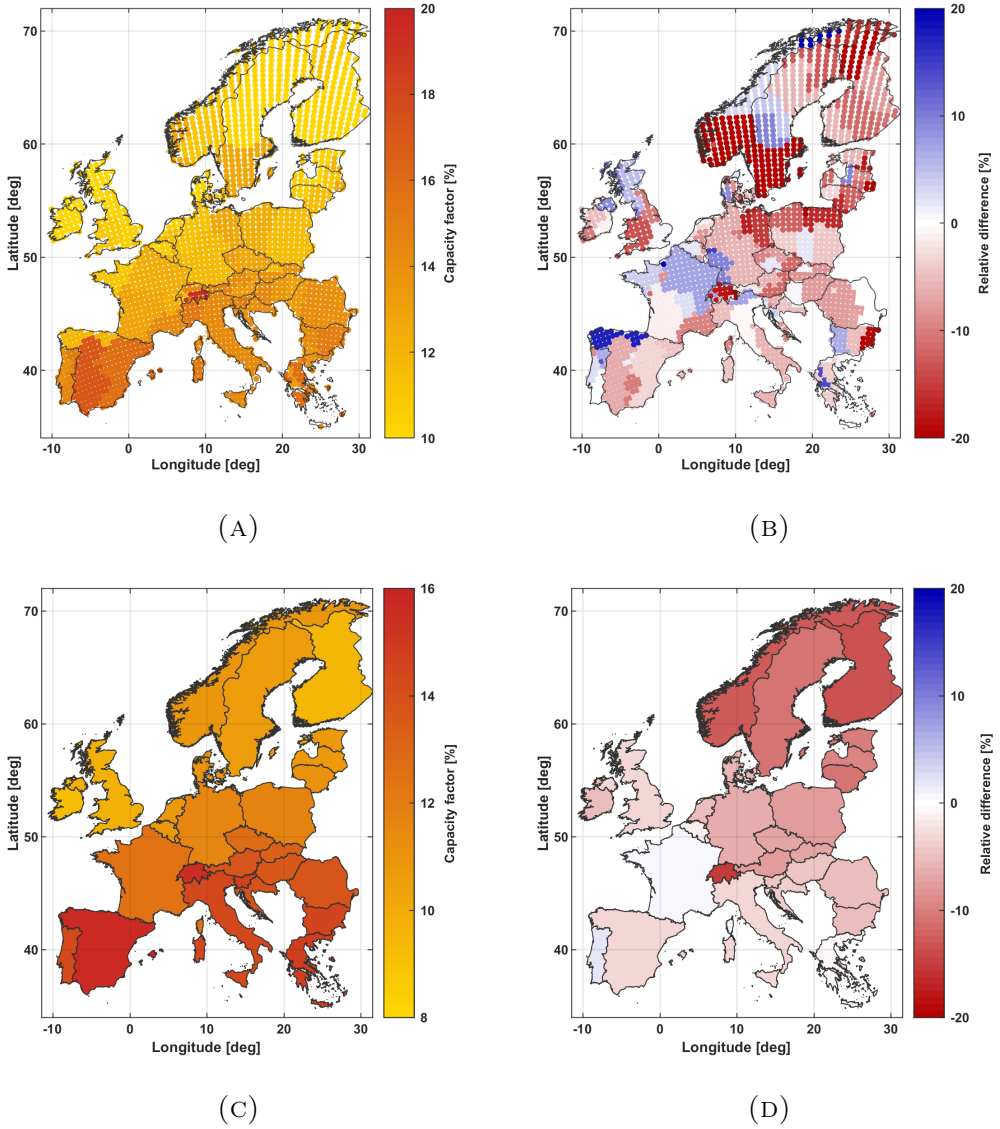

FIGURE 4.31: Spatial distribution of PV capacity factor potentials [%] averaged over all typedays for the HIST simulation (A) and relative differences [%] to the RCP85 run (B). In addition, country-based averages [%] of the HIST simulation (C) and the respective differences [%] to RCP85 (D) are depicted.

relative change of +20% for the end of the century, mainly caused by differences in the South. Since Figure 4.24b would suggest a decline, the actual reason stays unclear. A possible explanation could be given by changes with respect to the essential wind speed ranges for power production. In general, the huge differences observed for certain countries can partly be attributed to the different outcomes of both simulations concerning the spatial clustering process.

Figure 4.31 contains equivalent plots as presented before, here for European PV

power production potentials. The principal pattern of average CFs in the historical simulation closely resembles the North-South gradient inherent to the direct solar radiation (see Figure 4.31c), which implies a strong latitude dependency and acts as a main driver for PV production (c. Section 4.2.2). Consequently, highest production potentials are estimated for the Mediterranean region (14% CF) led by Spain with 15.8% CF as a country average. Switzerland showing a strong potential of 15.6% in average exceeds even the eastern Mediterranean countries due to enhanced radiation in the Alps. For central Europe as well as for Scandinavia, 10% to 13% PV potential are observed, whereas Finland and the British Isles form the European minimum between 9% and 10%. Compared to the wind power potential, PV reveals only little differences between clustered regions within a country (Figure 4.31a). Most pronounced variations can be found for Switzerland, where values appear to range between 11% in the South and 20% in the Northeast, followed by Spain (12%-17%) and France (11%-14%). For most parts of Europe however, the inner-country variability is even lower leading to a rather homogeneous overall picture for PV power generation.

According to Jerez et al. (2015), the impact of ambient surface wind speed on the PV power output is negligible and thus not further examined here.

The relative differences for future PV potentials in the RCP85 scenario are presented in Figure 4.31d. A clear pattern of a Southeast to Northwest gradient of a declining PV power potential emerges, very similar to the changes observed for the global radiation resource (c.f. Figure 4.27a). Hence, rather weak signals are estimated for the high potential Mediterranean region, with values of about -3% relative change for Italy, Spain as well as Croatia and +1% for France (smallest European change). Here, Spain and France experience a diverse pattern of enhancements in northern areas contrasted by decreases in the South (Figure 4.31b). The future projection suggests a relative decline of PV potential for central and eastern Europe in the range of -6% (Germany) and -7.5% (Poland). Most cluster regions at the Baltic Sea coasts exhibit strong decreasing values, peaking with -21.9% in southern Sweden, -21.4% in northeastern Poland and -17.1% in northeastern Germany. On a country-based average, this leads to the strongest decreases in the northern Baltic Sea regions and Norway, with values down to -13% (Finland and Norway) in relative average differences compared to the historical time period. However, changes in Switzerland exceed those observed for the North (-15.2%) following the estimated decline in future global solar radiation in the Alps. This may be additionally triggered by clearly stronger signals for increasing surface temperatures in the Alps towards the end of the century.

4.3.3 Impacts on the energy system

Finally, this Section analyzes the results for the last modeling step – simulations of the European energy system under energy transition towards high shares of VRE, driven by a 90% decarbonization target at the end of the century (2100). Hereby, the focus lies on climate change related differences in the European electricity system for two model setups, i.e. the HIST simulation indicates a future energy system assuming historical climate conditions and the RCP85 assuming the RCP 8.5 future scenario to take place. In contrast to Section 4.2, the RPSM is run in *Greenfield* mode. Therefore, the following analysis investigates the optimal system configurations in 2100 under certain conditions, realized by the model by neglecting any temporal capacity development aspects.

Note that in the following, Denmark is separated into a western (DK_W) and eastern part (DK_E) with respect to energy system aspects, as it is common practice in the research community due to the geographic and corresponding energy market constellation (e.g. Peter and Wagner, 2018). In addition, offshore power is distinguished between 50 m and 150 m technologies, accounting for their technical limitations regarding water depths limits. Although, when only referring to offshore wind power in the following sections, a union of both technologies is meant.

Energy system under historical conditions

The estimated cost-optimal future energy system in Europe, experiencing historical climate conditions, is represented by the installed capacity composition in Figure 4.32a. In addition, Figure 4.33a depicts the resulting electricity generation by technology and country, while Figure 4.33c shows only VRE generation in Europe. No fossil-based technologies are present in Europe due to the pre-set general phaseouts of lignite and coal. For the historical climate scenario, a total of 1175 GW capacity is installed in Europe in 2100, generating 3074 TWh of electricity. France (17.6%), Germany (14.8%) and Britain (11.1%) are the leading countries with respect to total electricity generation in Europe.

In order to meet the CO_2 emission target, VRE capacities contribute with 494.7 GW (42.1%) to the overall European plant fleet and are therefore the main drivers for an energy transition towards a decarbonized system. Here, onshore wind parks supply the main part of about 297.0 GW (25.3%), offshore wind sites add 121.6 GW (10.4%), whereas PV shows a surprisingly low total capacity of only 76.1 GW (6.5%) (Figure 4.32a). The bulk wind power capacity is invested in Germany (83.0 GW), Britain (63.2 GW), France (55.0 GW) and Italy (38.2 GW). With respect to generation, VRE technologies contribute with an even higher share of

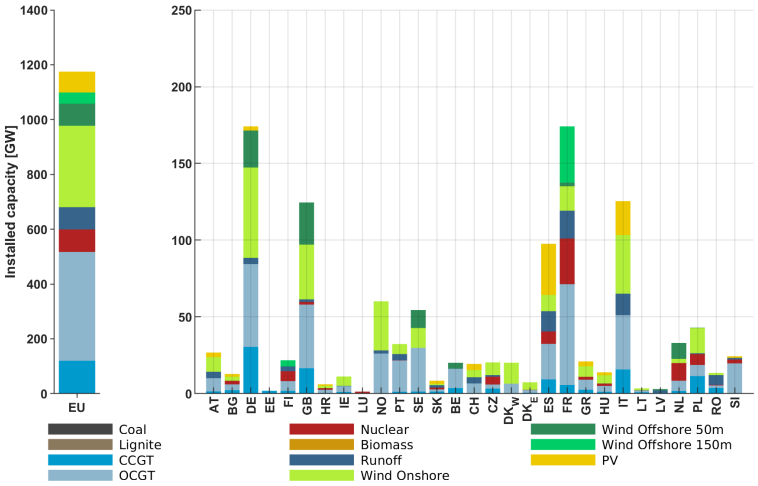

(A)

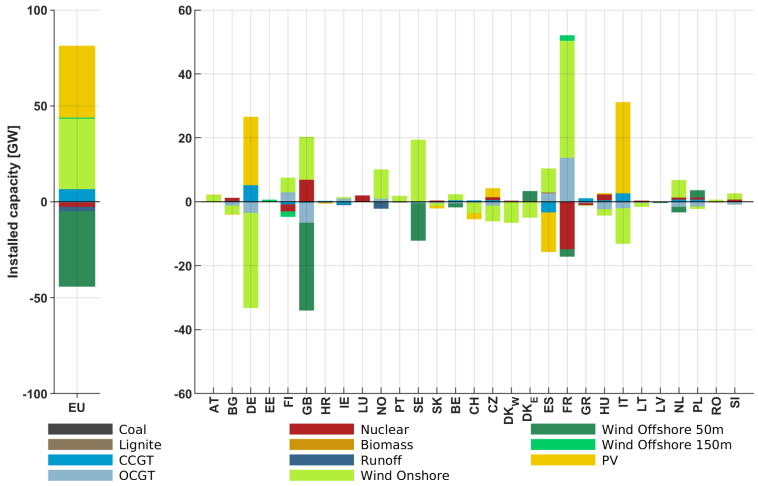

(B)

FIGURE 4.32: Installed capacity [GW] composition under historical conditions (A) and its residual to RCP85 future scenario conditions (B). Residuals are defined as RCP85 minus HIST.

51.0% to the overall European electricity supply. Following the spatial distribution of wind capacity, the main contributors for European VRE electricity generation appear to be Germany with 19.7% (308.5 TWh), Britain 16.3% (254.7 TWh), France 13.4% (209.7 TWh), Norway 8.6% (143.4 TWh) and Italy 7.8% (121.3 TWh) (Figure 4.33c). Among these, Italy is the only country with a significant share of PV power supply (28.4 TWh). The others contribute mainly through onshore wind, and, in case of Germany, Britain and France, this is complemented by large offshore wind capacity amounts.

In contrast to expectations and (Peter, 2019), PV seems not to play a major role accomplishing the transition to a decarbonized energy system (Figure 4.32a). This is probably due to comparably high net transfer capacity (NTC) assumptions

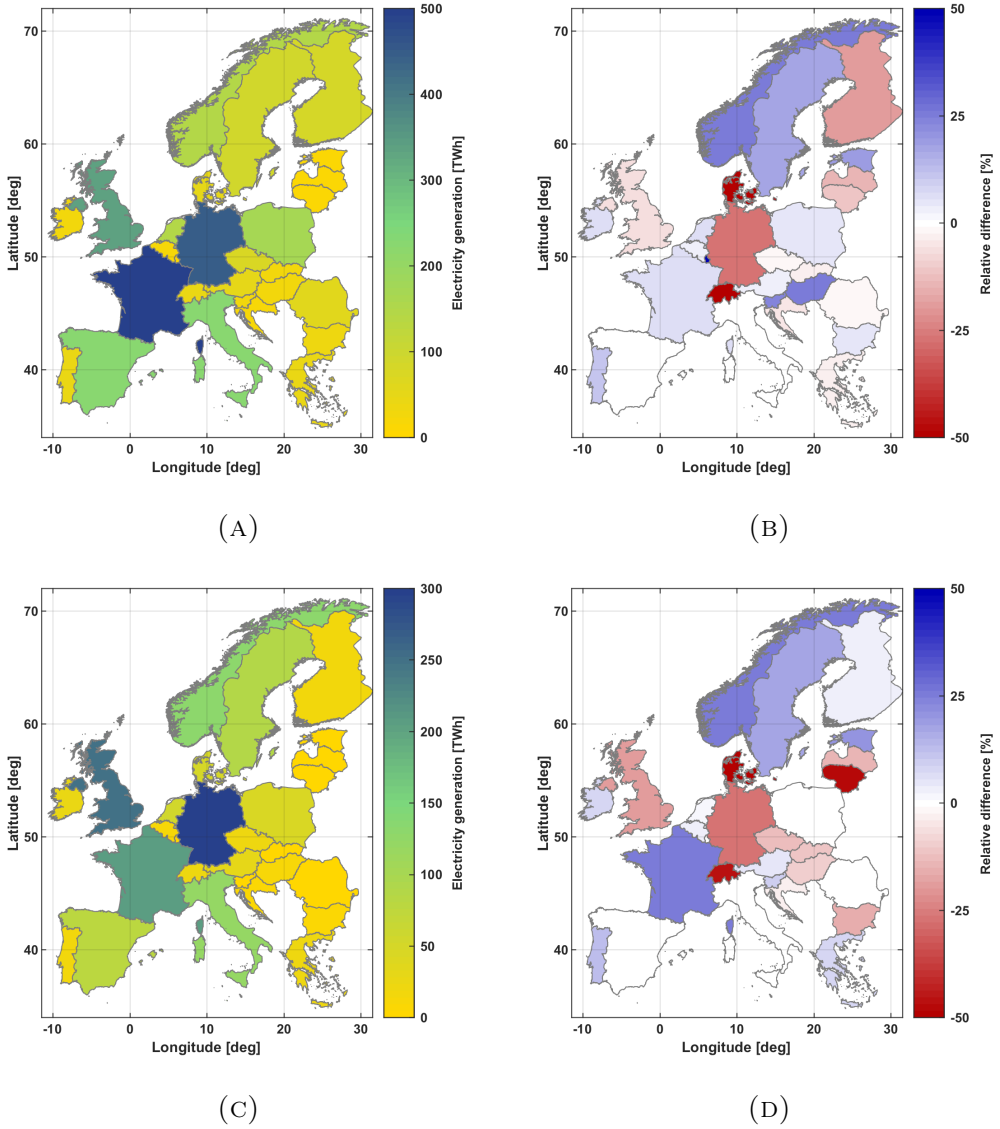

FIGURE 4.33: Total electricity generation [TWh] under historical conditions (A) and its residual [%] to RCP85 future scenario conditions (B). Equivalently for VRE technologies only, in (C) and (D). Residuals are defined as RCP85 minus HIST.

enabling the possibility of pronounced exchange effects between the countries. In combination with a strong competitiveness of the wind technologies, the system is able to distribute the cost-effective wind generation from Europe's best wind spots to satisfy demand under cost-optimal conditions wherever it is needed – leaving PV as a rather redundant technology for most regions. The system's behaviour therefore appears still reasonable, given the cost-minimizing approach for the whole European system.

Nuclear power still remains in several countries, and does not experience a phase-out of the technology. The European nuclear capacity of about 82.1 GW (7%) is

mainly found in France (29.8 GW), the Netherlands (11.5 GW), Spain (8.1 GW), Poland (7.1 GW) and Finland (6.5 GW), providing a base-supply of about 19.9% of the total European electricity demand (c.f. Appendix, Figure D.16a). Besides run-of-river with 81.3 GW (6.9%), Gas accounts for the residual capacity with a total of 517 GW (44%) installed in Europe. The latter is mainly used to provide flexibility in a VRE dominant system and is hence necessary for system reliability. Therefore, being the more flexible technology, OCGT (397.3 GW) clearly exceeds the CCGT capacity (119.7 GW). Despite their large capacity amounts, OCGT facilities only contribute with 1.6% to the overall European generation (c.f. Appendix, Figure D.16a). The remaining demand is satisfied by run-of-river (13.5%). These findings are comparable to results by Peter (2019).

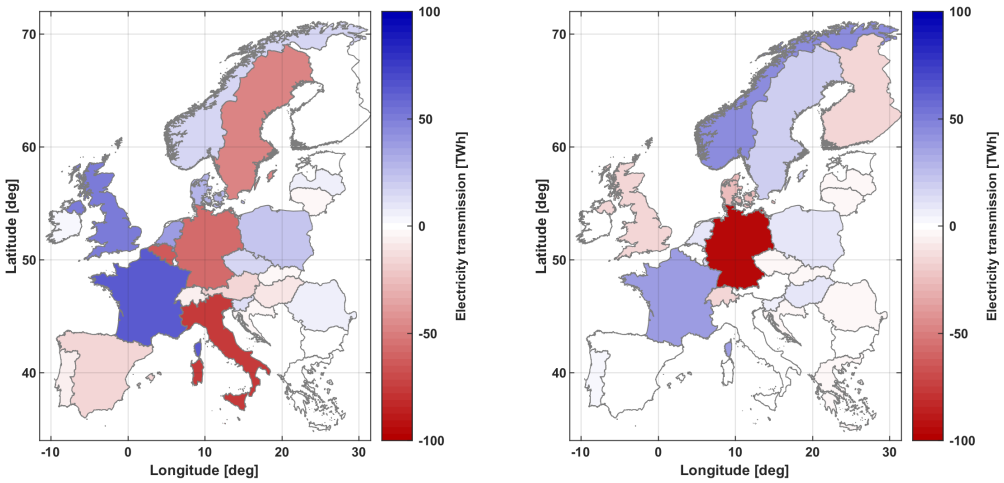

(A) (B)

FIGURE 4.34: Net electricity exchange under historical conditions (A) and its residual [%] to RCP85 future scenario conditions (B). Positive values indicate a net export. Residuals are defined as RCP85 minus HIST.

Figure 4.34a shows the net electricity exchange for each country under historical climate conditions. Positive values indicate a net export for the respective country. It appears that in particular Britain (52.7 TWh), Denmark (38.2 TWh) and Norway (18.7 TWh) are able to cover their electricity needs by high shares of VRE and still exporting large amounts to the European system (c.f. Appendix, Figure D.16a) under cost-optimal conditions. France as the leading export country with 66.3 TWh, generates besides VRE and hydro a large part via nuclear plants. The same can be observed for the remaining prominent exporting countries, such as the Netherlands, Poland and Czech Republic. In contrast, Italy (-76.4 TWh), Belgium (-63.1 TWh), Germany (-55.9 TWh) and Sweden (-46.4 TWh) are the main importing countries

under historical climate conditions. They have high VRE shares as well as a nuclear phaseout in common. Hence, it seems that they experience a turning point in competitiveness of the remaining available VRE operation sites, probably mainly with respect to nuclear electricity generation.

The resulting overall system costs for Europe in the historical scenario account for 1807 bn EUR, where 95% are allocated to capital investment costs and 2.5% to operation and maintenance as well as variable fuel costs. The main contributors to capital costs are nuclear (492 bn EUR) and onshore wind capacity (438 bn EUR). FOM and fuel costs appear to be one magnitude smaller with a maximum of 10.4 bn EUR for onshore wind (FOM costs) and 23.9 bn EUR for CCGT (fuel costs). The marginal electricity generation costs, which can be interpreted as the associated electricity price, amount to an European average of 43.6 EUR/MWh in 2100.

Energy system under climate change conditions

Finally, the differences between the energy system under historical (HIST) and strong climate change conditions (RCP85) are investigated in the upcoming section. As discussed before, the only differences between the two simulations are changes in the wind and radiation resource, leading to local changes in the wind and PV power potentials. Hence, the analyses estimate the impact of climate change on the European electricity sector at the end of the century under a strong decarbonization target, focusing on VRE technologies.

Figure 4.32b shows the residual for 2100 between the model results with respect to installed capacity per technology accumulated per country as well as Europe as a whole. For Europe 38.8 GW less offshore wind capacities are installed in the RCP85 scenario compared to HIST, which accounts for about -32%. That leads to a reduction in electricity generation by offshore parks of about -33%. Looking at the spatial distribution of wind capacities (c.f. Appendix, Figure D.17b) reveals that the main differences can be found in the North Sea territory of Britain and in the Baltic Sea close to the southern coast of Sweden. In both countries, offshore technologies are abandoned completely for the RCP85 case. This can be directly attributed to a decline in capacity factors in these regions between -11% and -15% (Figure 4.31b). Here, it appears that the competitiveness of offshore wind is falling below those of other supply options. Exceptions are Germany, the Netherlands and France where offshore facilities are still operating to the same degree as for the HIST scenario. For the latter, a small surplus can even be observed, since adjacent capacity factors rise for the climate change driven case (Appendix Figure D.17b).

The reduction of offshore capacities in the climate change scenario with respect to the historical conditions is compensated by a rise of onshore wind and PV operation sites, accounting for a surplus of 36.8 GW (+12.4%) and 37.5 GW (+50%), respectively. The expanded capacities generate 19.1% and 33.5% more electricity for the RCP85 simulation than for HIST. In case of onshore wind power, main regions for expansions are found to be the northern French Atlantic coast with about 36.6 GW (+230%), Northwest Sweden with 19.4 GW (+150.3%) and northern Britain with 13.5 GW (+37.7%) (Figures 4.32b and Appendix, D.17b). This is due to the enhanced CF potentials of about +15% and +20% for onshore wind power in these regions (Figure 4.30b). The same holds true for the observed reallocation of onshore facilities from South to North in Britain compared to historical conditions. Similar behaviour is predicted for Spain (from the Pyrenees to the Atlantic coast), Czech Republic and Poland (from West to East) as well as Norway. In the climate change scenario, the system invests half of the onshore capacities in northwestern Germany compared to the HIST case, leading to a residual of -29.7 GW (Figure 4.32b). Here, Germany is a good example for a region which faces a total enhancement of onshore CF, averaged over the entire country, but a reduction at essential competitive operational sites in the RCP85 future, such as in the Northwest (Figures 4.30d and 4.30b).

The difference in PV for the climate change scenario is mainly accomplished by an expansion of 21.4 GW (+88.7%) in southwestern Germany, where PV capacity factors are enhanced by about 10% leading to sufficient competitiveness of the operation sites (Figure 4.31b). Even though southern Italy experiences a CF decrease of about -5% under climate change conditions, PV facilities are expanded almost all over the country, summing up to 28.5 GW (+56.3%) (Figure 4.32b). This is slightly mitigated by -12.4 GW (-59.1%) less PV capacity observed for Spain. Here, best PV power spots located in the Central West face reductions of about -10% CF compared to the historical case (Figure 4.31b), leading to a convergence of the value of these regions to the total European energy system. Potentially, the observed reallocation of PV capacity from western to central Europe is driven by the greater range of trading possibilities to other European regions.

The combination of less offshore wind but more onshore wind and PV leads to an overall surplus of 35.4 GW of VRE capacities in total for the climate change scenario, contributing with 45.1% to the total European capacity mix. By that, VRE technologies supply 52% of the European energy demand under climate change conditions, considering the cost-optimal assumption, which accounts for about 1% raised share compared to the HIST case. As it is illustrated in Figure 4.33d, major positive changes in VRE generation in the RCP85 case are observed for France (+155 TWh,

+73.9%), Norway (+48.1 TWh, +35.8%) and Sweden (20.3 TWh, +22.9%). For the latter two this directly leads to a surplus in total generation compared to the historical case (Figure 4.33b). In contrast, Germany (-95.7 TWh, -31%), Britain (-61.6 TWh, -24%) and Denmark (-27.2 TWh, -41.6%) experience significantly less VRE expansion under climate change conditions, due to changes in the wind resource in these regions. In consequence, France replaces Germany as the main VRE electricity supplier to the European energy system, followed by Britain.

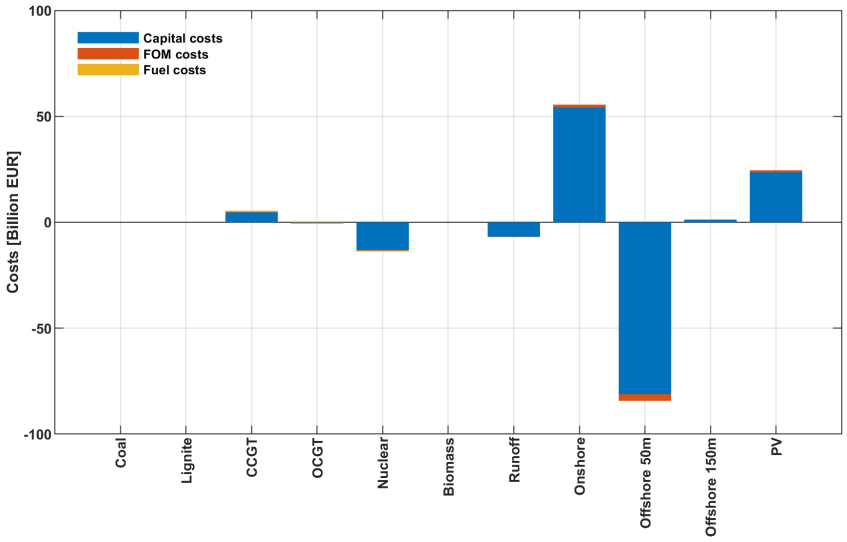

FIGURE 4.35: Residual of costs [bn EUR] per technology in Europe between the HIST and RCP85 simulation. Residuals are defined as RCP85 minus HIST.

Besides changes in VRE technologies, considerable differences for other technologies are only estimated for France and Britain (Figure 4.32b). In the climate change scenario, the system composition allows France to reduce the nuclear baseload plants and their generation down to a half of the HIST case. This is most likely possible due to the strong expansion of the onshore wind share, which is accompanied by a need of more variable backup capacity. Consequently, the flexible OCGT technology is raised for France (13.8 GW, 21%). By that, France even experiences a slight surplus in the total electricity generation and, hence, remains the leading producer (581.5 TWh). For Britain the opposite is prevalent: the strong negative difference in offshore wind supply, due to reduced offshore potentials, is partly compensated by onshore wind facilities. However, it seems that there are insufficient amounts of onshore sites to be able to compete with the nuclear technology in order to cover for the missing offshore generation. Hence, the system invests in nuclear plants (+6.9 GW) and is able to reduce OCGT capacities (-6.3 GW).

Concerning the overall system cost under climate change conditions, almost no difference to the historical reference scenario is obtained (-1.1%). Since the main observed changes of investments between both simulations are attributed to a substitution of offshore wind capacities to onshore wind and PV, the differences in investment costs of each technology balance each other (Figure 4.35). Due to the strong expansion of onshore wind capacity, an increase of 54.2 bn EUR (+12.4%) capital costs (investment) is evident, passing nuclear as the leading contributor. Investments in PV generate a surplus of 23.6 bn EUR (+49.5%) in RCP85, while less offshore facilities lead to a saving of -80 bn EUR (-31.7%). The marginal generation costs can also be preserved, accounting for 43.8 EUR MWh^{-1} (+0.5%).

Chapter 5

Conclusions & outlook

The upcoming Sections summarize and discuss outcomes and conclusions from Study I, II and III. This is complemented by an outlook for the research field based on the presented studies, trying to classify the results and conclusions with respect to the overall picture.

5.1 Conclusions

Study I

In the scope of this study, a long-term wind power data set with a high spatio-temporal resolution is developed for Europe and further analyzed with a focus on Germany. Results are partly published in Henckes et al. (2018). Since renewable energy, and in particular wind power, is gaining more and more importance in present as well as future energy systems, it appears essential to better understand and anticipate wind power characteristics. The study contributes to present research in three main aspects.

First, the novel wind and PV power conversion model REOM is developed in order to convert the meteorological resource data (wind speed, solar radiation) into renewable power supply. Its application to the unique high resolution (hourly, 6x6 km) reanalysis COSMO-REA6 yields a novel long-term (1995-2014) wind power data set for the entire European Union, featuring a location specific assessment at a high level of details. By that, the widely known issue of missing and/or poorly resolved long-term wind power information is approached. The data set can be used for a wide range of questions and analysis in this field, as it is already applied in Obermüller (2017), and complements existing data sets, such as by Staffell and Pfenninger (2016) or Gonzalez et al. (2016). In addition, REOM is further used for Studies II and III as well as Peter and Wagner (2018) and can easily be applied to higher resolutions. Investigations in this study show that COSMO-REA6

outperforms other common reanalyses due to its high resolution and that REOM exhibits a good performance.

Second, a detailed analysis of the annual variability as well as the frequency of extreme conditions in European wind power is examined for the novel data set. Results suggest that long time spans are necessary to gain robust wind power time series for follow-up energy system analysis. Since various years within the 20-year time horizon show significant differences in annual variability and its combination with occurrence probabilities of extreme events, it appears impossible to choose a single weather year as a representative, containing all essential characteristics. Therefore, it is highly recommended to pay particular attention to the choice and selection procedure when a reduction of input data for energy system modeling is required.

Third, the investigation of potential balancing effects in Europe, with a focus on Germany, reveals that balancing effects and the potential for beneficial electricity transmissions between Germany and other countries is prevalent in almost all situations. The estimated small share of critical cases with simultaneously low wind conditions in Germany and neighboring countries accounts for a considerably low probability of 0.2%. This joint probability reduces to 0.1% when all European countries are taken into account. In particular, such a statistical assessment of balancing effects in European wind power is of major importance for transmission extension approaches in the EU and emphasizes the need for further investments in transmission capacities.

Study II

Study II is related to Henckes et al. (2019) (submitted in April 2019 to *ENERGY*) and tries to shed light on uncertainties in energy system modeling. To the best of the authors' knowledge so far there are no investigations focusing on the impact of errors introduced by the meteorological input data on investment simulation outcomes under high shares of VRE power supply. Since reanalysis products are a very convenient and widely used meteorological data source, the effect of their bias range to error margins in a low carbon German electricity system by 2050 is investigated. From this approach, three main insights are obtained.

First, a sensitivity study of the energy conversion models in REOM is processed. Hereby, the following question is addressed: How sensitive is the conversion modeling, processing from wind or solar radiation to wind or PV power generation, to the meteorological input quantities. The study reveals that for wind power, the model is very sensitive to the wind speed itself, while air density can be neglected. This appears reasonable, since the power output shows a cubic dependency on the

wind resource. In case of PV power, the dominant quantities are direct and diffuse radiation, whereas the other quantities (temperature, wind speed and albedo) as well as the choice of the diffuse radiation model are of minor importance.

Second, the assessment of error margins, induced by uncertainties in the underlying meteorological data set, indicates strong impacts on the overall composition of the cost-optimal energy system. Large spreads are observed, in particular, for the VRE plant fleets when reasonable reanalysis errors are applied. Errors in wind speed of about ±20% for all grid points lead to average perturbations in German wind power potentials (CF) between -43% and +43% for onshore sites and between -29% and +21% for offshore locations. In case of direct radiation, the incoming errors range between 20% for high values and 100% for low values, which leads to a difference in capacity factors of -27% to +30%. These VRE potential differences combine to generate a difference in the German electricity system between -36% and +33% with respect to wind power capacities and -14% and +33% for PV. Regarding total system costs, the error margin accounts for approximately -22% to 24%.

Third, besides the differences with respect to the overall installed capacities and electricity generation, the optimal spatial allocation of VRE facilities differs substantially. The system shows a pronounced reaction to the altered spatial VRE potential situation and adapts allocation accordingly. Both, the observed essential impacts on error margins and allocation effects show how important the accuracy of the meteorological input data is, especially, with respect to energy systems under high shares of VRE power supply. Results in this study suggest that an error analysis of the input data prior to subsequent energy system applications is essential and imply that such energy system model results should be treated with caution. Moreover, initial errors of the most important meteorological quantities are transferred to a doubling in onshore wind CF, while the error is conserved and passed for offshore and PV capacity factors with the same magnitude. These CF errors in turn are fully retrieved in the final energy system error margins (e.g. capacity or generation mix).

Study III

Finally, in Study III the impact of altered European VRE power potentials induced by climate change at the end of the 21st century on the European energy system is examined. The investigation carried out in the scope of this thesis tries to contribute to existing research (e.g. Peter and Wagner, 2018) by looking into details of VRE effects at any step of the modeling chain – from the changed meteorological

quantities over resulting VRE power potentials to the responding electricity system. In order to focus on margins of change attributed to changes in wind speed and solar radiation, the investment modeling system is kept rather simple, so that impacts can be isolated and more easily interpreted.

In order to assess climate change impacts, historical (1970-1999) and future projection (2070-2099) simulations by a GCM-RCM combination (EC-EARTH and RCA4) from the EURO-CORDEX project are compared. Here, the strong RCP 8.5 scenario from the IPCC is assumed. Then, all methods and tools developed in the framework of this thesis find application yielding a comprehensive model chain: REOM is used to convert the respective quantities to power output in both scenarios, followed by a reduction of dimensions using clustering techniques and, finally, the cost-optimization of the electricity system by RPSM under strong European decarbonization targets.

First of all, climate change impacts on the climatological mean and variability of surface wind speed and global solar radiation are examined. Results suggest a slight decrease for the wind resource over vast parts of Europe between -3% and -6% in the future climate change scenario compared to historical conditions. Also, the inter-daily (+5%) and seasonal variability (+10% to +30%) is observed to increase in many European regions. The latter is mainly induced by a dominant decrease of wind speeds in summer months compared to observed winter reductions in the future scenario. In case of global solar radiation, only Spain and France exhibit considerable increases of about +5%, whereas the rest of continental Europe experience a decline between -2% and -5%, with strongest signals to be found in Scandinavia (-15%). Except for Scandinavia, the intra-annual and inter-daily variability are found to increase for most parts of the continent. These findings, yielded by a single GCM-RCM combination, are mainly in agreement with ensemble mean observations by Moemken et al. (2018) and Jerez et al. (2015).

Second, the previously mentioned changes in the respective resource under strong climate change conditions lead to considerable alterations for the resulting European VRE power potentials. A relative decline of about 5%-10% in wind CF is estimated for most European countries and offshore areas, which corresponds to a doubling of the observed wind speed changes. However, the analysis reveals that signals of future changes in CF vary essentially for certain regions, e.g. -52% for southern and +77% for northern France. A reduction of potential PV capacity factors can also be observed for almost the entire European continent. Here, southern regions with strong PV potentials exhibit rather weak changes of approximately -3%, while this decline increases towards the North reaching about -10% for the future RCP 8.5 scenario. Again, strong local differences are evident, with

peaks located at the Baltic Sea coasts (approx. -20%).

Third, the impact of the discussed changes on the investment model outcome are rather small and negligible with respect to overall system quantities. Both simulations (HIST and RCP85) yield similar capacity and generation shares for VRE and non-VRE technologies as well as average overall system cost and average electricity price. This is due to the system's ability to adjust to climate change driven differences in VRE potentials, without the need of great restructuring of the overall composition. However, these adjustments contain substantial changes concerning spatial VRE capacity allocation and shares within the VRE technologies. Three main aspects provide for the system's ability to adapt to climate change conditions with negligible financial impacts: First, the approach of a perfect foresight assumption enables a perfect anticipation of variations in VRE conditions. Second, net transmission capacities appear to be sufficiently large to be able to facilitate a pronounced electricity distribution over the continent, so that regions can benefit from balancing effects in VRE power supply. Third, although results suggest that the European overall VRE potentials decline in the future scenario, the domain contains changes of both signs. Hence, the system is apparently still able to allocate sufficient VRE capacity at highly competitive operation sites by the end of the 21st century, in order to meet the emission targets with VRE expansion at comparable costs. In conclusion, climate change has an effect on the local conditions with respect to VRE electricity productions, but would not bring the system to a critical point, where it is necessary to invest in inefficient VRE sites or even conventional technologies.

5.2 Overall picture and outlook

As mentioned in the Introduction, one of the biggest challenges of the 21st century is expected to be climate change and its impacts on ecosystems and socio-economic aspects (IPCC, 2014). As a result, decarbonization policies (e.g. Paris climate agreement) try to tackle the threat in order to mitigate climate change risks. Following Bloomberg (e.g. 2018), amongst other adaption strategies, pronounced VRE expansion is necessary. Therefore, a comprehensive understanding of VRE power supply characteristics and its sources, such as wind speed and solar radiation, is essential.

Due to the lack of reliable long-term VRE data sets, a novel high resolution wind power production data set is created for Europe and analyzed with respect to unique characteristics. The COSMO-REA6 reanalysis is used as a meteorological basis. It can be concluded from analyses, that the applied meteorological data set should be

based on long-term time series containing all essential characteristics. Furthermore, investigations emphasize the potential of balancing effects within Europe in order to capitalize on the present and future wind power potentials to tackle the challenge of a decarbonization development. Here, an extension of the detailed analyses by PV power would be of great interest, in order to comprise the whole VRE picture. Further investigations of local balancing effects of regions with strongly heterogeneous distributions in wind and PV power supply can also contribute to improve our understanding of the future role and possibilities concerning renewable energies.

The application of reanalysis in this context is quite common for this research field and subsequent VRE power generation data sets are often used for further energy system modeling (Staffell and Pfenninger, 2016). It has been shown for Germany, that reanalysis data sets contain non-negligible biases leading to substantial uncertainties in subsequent power conversion and energy system modeling. This high sensitivity of energy system models to input data should be kept in mind and respective outcomes treated with caution. From these findings, an adequate calibration of the input data is suggested in order to yield more robust data for further derivation of reliable results regarding energy system simulations. In addition, the present study could be extended to the entire European domain and results further validated by an application to a real case study in order to sharpen the potential impacts of initial errors.

It has been shown, that future VRE resources under strong climate change conditions (RCP 8.5) undergo substantial changes on local scales until the end of the 21st century. These affect potential local VRE power supplies at least on a similar magnitude. Averaged over a large domain like Europe however, they reveal only weak differences to historical climate conditions. This demonstrates how essential an appropriate spatial resolution is in this context. Additionally, enhanced variability on different temporal scales are observed for the climate change scenario at the end of the century. Both, the reduction in average VRE supply as well as its enhanced variability may lead to more pronounced challenges for future energy systems, e.g. with respect to system reliability.

The electricity system adapts to climate change driven changes in VRE potentials mainly by considerable alterations in the allocation of VRE facilities. This approach does not generate any additional cost nor raise electricity prices considering Europe as a whole. The adaption strategy shows once again the need for sufficient investments in transmission capacities within and between the countries to enable balancing effects. In addition, this study assumes the welfare and cost-optimal approach, which emphasizes that the challenge of climate change mitigation

in the energy sector urgently requires a common European answer. Also, the model finds the cost-optimal solution under the perfect foresight assumption, which can be translated to an anticipation as of today of future climate changes. That indicates the importance of comprehensive actions with respect to adaptation from this day forward.

The present simplified energy system is able to meet the 90% decarbonization target by employing about 50% of the plant fleet with VRE technologies. The impact of climate change to such a system may be enhanced, when further VRE expansion is required. This may be the case, when additional system components are considered (c.f. Peter, 2019). As such, the heat and traffic sector increase CO_2 emissions, so that additional emission-free power generation is required. Since a share of 100% VRE seems possible (e.g. Connolly et al., 2016), the European system appears to have tremendous upside potential to tackle these challenges. Furthermore, the feedback between climate change and the different sectors of the energy system, e.g. concerning the demand side (Mideksa and Kallbekken, 2010), is a crucial and interesting field for further promising research.

In order to be able to provide adequate advice for policymakers, in particular natural and economic sciences need to improve the overall understanding of all essential system components and their behaviour in the future. Therefore, this thesis has the aim to foster the interdisciplinary cooperation of the different research subjects in order to better understand the connections and it tries to contribute to the overall picture. Besides this work and the two corresponding publications in close cooperation with the EWI (Henckes et al., 2018; Henckes et al., 2019), the developed models and data sets are also used in other studies (Obermüller, 2017; Peter and Wagner, 2018; Peter, 2019) and are meant to serve as a basis for future research in related projects by the Institute for Geophysics and Meteorology at the University of Cologne.

Appendix A

Optimal tilt angle of PV systems

Based on the radiation data of COSMO-REA6, the optimal tilt angle, with respect to the maximum of producible energy, is determined for south-oriented PV systems at each location implemented in REOM. First, radiation data is averaged to a one year time series for every location. Then, the total solar flux on a tilted plane is calculated for various tilt angles. In the final step, the tilt angle providing the largest cumulative flux is selected. Note: this part is subject to the publication Henckes et al. (2019).

As depicted in Equation 2.10, the total flux on the tilted plane is the sum of direct, diffuse and reflected solar radiation on the tilted plane. The direct fraction depends on the sun's zenith and azimuth angle, and the tilt angle θ_{tilt} of the plane. The diffuse contribution G_{dif}^{tilt} was determined using two simplified models by Klucher (1979) (KM) and Perez et al. (1986) (PM). G_{ref}^{tilt} is the radiation that reaches the plane after being reflected by the surface and depends on θ_{tilt} and the surface albedo A. The latter was set to 0.2 (Klucher, 1979).

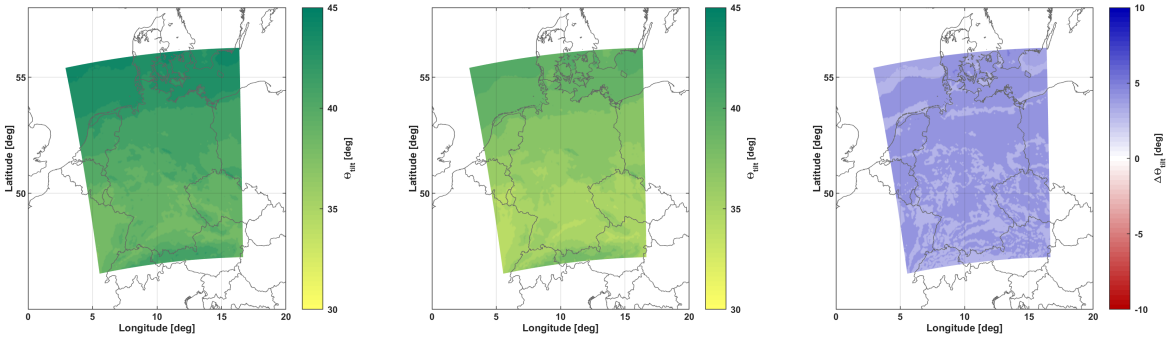

(A) (B) (C)

FIGURE A.1: Optimal tilt angle for southerly oriented PV panels in Germany, determined using either (A) the Perez (PM) or (B) Klucher model (KM). In addition, the residual PM minus KM is shown (C). COSMO-REA6 radiation data serves as a basis and an uniform albedo of 0.2 is assumed. Source: Henckes et al. (2019).

Figure A.1 shows the optimal tilt angle for entire Germany for both models and their difference. In both, the tilt angles are about 10° smaller than the latitude, which is due to the contribution of diffuse radiation. On average, it contributes between 25% to 75% to the total radiation in Germany, depending on the location. Significant patterns, such as the strip of low tilt angles at about 48.5°North 9-12°East in the KM, correspond to patterns found in the averaged direct radiation on an horizontal plane. Hence, the horizontal stripe corresponds to an area of low direct solar radiation.

Appendix B

Levelized costs of energy

Levelized costs of energy (LCOE) is a measure of the total costs of building and operating a power plant over an assumed lifetime[1]. This allows a comparison of different power plant technologies featuring different lifetimes, capital and operational costs and capacities. It can be seen as an extension of the capacity factor and full load hour quantities by the specific technology costs. The LCOE is calculated by dividing the overall lifetime costs by the energy production of a power plant

$$LCOE = \frac{\sum_{y=1}^{\lambda} \frac{C_y^{inv} + C_y^{fix} + C_y^{var}}{(1+r_d)^y}}{\sum_{y=1}^{\lambda} \frac{G_y}{(1+r_d)^y}}$$

with the investment costs C^{inv}, operation and maintenance costs C^{fix}, fuel costs C^{var} and the electricity generation G in year y as well as the systems' lifetime λ. For the present analyses, the discount rate r_d is assumed to be 0.08.

[1] https://www.energy.gov/sites/prod/files/2015/08/f25/LCOE.pdf

Appendix C

Tables

TABLE C.1: Constants to determine the clear-sky indices for the horizon (F_1) and for the sun's near ambience (F_2) (Source: Perez et al., 1986).

ϵ-class	1	2	3	4	5	6	7	8
ϵ range	1.000-1.065	1.065-1.2300	1.230-1.500	1.500-1.9500	1.950-2.800	2.800-4.500	4.500-6.200	6.200-∞
F_{11}	-0.008	0.130	0.330	0.568	0.873	1.132	1.060	0.678
F_{12}	0.588	0.683	0.487	0.187	-0.392	-1.237	-1.600	-0.327
F_{13}	-0.062	-0.151	-0.221	-0.295	-0.362	-0.412	-0.359	-0.250
F_{21}	-0.060	-0.019	0.055	0.109	0.226	0.288	0.264	0.156
F_{22}	0.072	0.066	-0.064	-0.152	-0.462	-0.823	-1.127	-1.377
F_{23}	-0.022	-0.029	-0.026	-0.014	0.001	0.056	0.131	0.251

TABLE C.2: Corine land cover categories and their resulting distances to large wind plants according to German Federal Ministry of Environment, Nature Conservation and Nuclear Safety. (Source: McKenna et al., 2015)

ArcGIS code	CLC 2000 code	Description	Large wind plants?	Distance to large wind plants [m]
Built-up area				
Urban area				
1	111	Continuous urban area	No	1000
2	112	Non- continuous urban area	No	700
Industry, trade and traffic areas				
3	121	Waters	No	400
4	122	Road and Railway network	No	200
5	123	Harbour area	No	400
6	124	Airports	No	1000
Waste disposal and construction areas				
7	131	Decomposition area	No	0
8	132	Disposal and overburden stockpile	No	0

Continued on next page

Table C.2 – continued from previous page

ArcGIS code	CLC 2000 code	Description	Large wind plants?	Distance to large wind plants [m]
9	133	Construction areas	No	0
Artificially made, not agriculturally used grassed area				
10	141	Urban grassed area	No	0
11	142	Sport and leisure facility	No	0
Agriculture				
Arable land				
12	211	Non-watered arable land	Yes	-
13	212	Regularly-watered arable land	Yes	-
14	213	Rice field	Yes	-
Permanent crops				
15	221	Wine cultivated area	Yes	-
16	222	Fruit/berry fruit stocks	Yes	-
17	223	Olives groves	Yes	-
Grassed area				
18	231	Grassland and meadow	Yes	-
Heterogeneous agricultural area				
19	241	Annual cultures in connection with permanent crops	Yes	-
20	242	Complex lot structures	Yes	-
21	243	Agriculturally used area with natural vegetation with significant size	Yes	-
22	244	Areas used for agriculture and forestry	Yes	-
Forests and nature related areas				
Forests				
23	311	Deciduous forests	Yes	-
24	312	Coniferous forests	Yes	-
25	313	Mixed forests	Yes	-
Bush vegetation				
26	321	Natural grassed area	Yes	-
27	322	Heather and bog heather	Yes	-
28	323	Sclerophyllous plants	Yes	-
29	324	Forest/bush	Yes	-
Open spaces without or with less vegetation				
30	331	Beaches, dunes, sands	Yes	-
31	332	Areas used for agriculture and forestry	Yes	-
32	333	Areas with sparse vegetation	Yes	-
33	334	Fire areas	Yes	-
34	335	Glacier/permanent snow area	Yes	-
Wetland				
Wetland in inland				
35	411	Bogs	Yes	-
36	412	Peat bog	Yes	-
Wetland on the coast				
37	421	Salt marsh	Not known	0
38	422	Salines	Not known	0
39	423	Areas lying in the intertidal zone	Not known	0
Expanse of water				
Expanse of water in the inland				
40	511	Watercourse	No	0
41	512	Expanse of water	No	0
Marine waters				
42	521	Lagoons	No	0
43	522	Estuary	No	0
44	523	Sea and ocean	No	0

Table C.3: Overview of GCM and RCM model configurations considered for comparisons.

RCM/GCM	Referred to as	Scenario	Variable	Available period	Used period
RCA4					
CNRM-CM5	RCA4-CNRM	historical	sfcWind	1970-2005	1980-2005
EC-EARTH	RCA4-ECEARTH	historical	sfcWind/rsds	1970-2005	1980-2005
	HIST	historical	sfcWind/rsds	1970-2005	1970-1999
	RCP85	rcp8.5	sfcWind/rsds	2006-2100	2070-2099
HadGEM2-ES	RCA4-HadGEM2	historical	sfcWind	1970-2005	1980-2005
MPI-ESM-LR	RCA4-MPI	historical	sfcWind	1970-2005	1980-2005
IPSL-CM5A-MR	RCA4-IPSL	historical	sfcWind	1970-2005	1980-2005
CCLM4-8-17					
CNRM-CM5	CCLM4-CNRM	historical	sfcWind	1970-2005	1980-2005
EC-EARTH	CCLM4-ECEARTH	historical	sfcWind	1970-2005	1980-2005
HadGEM2-ES	CCLM4-HadGEM2	historical	sfcWind	1970-2005	1980-2005
MPI-ESM-LR	CCLM4-MPI	historical	sfcWind	1970-2005	1980-2005

Table C.4: Overview of GCM name, institution and spatial resolution.

Model name	Institution	Horizontal resolution [km x km]	Vertical level
CNRM-CM5 (CNRM Coupled Global Climate Model V.5)	Centre National de Recherches Mètèorologiques (CNRM), France	256×128	31
EC-EARTH (EC-Earth Consortium)	European Consortium (EC)	320×160	62
HadGEM2-ES (Hadley Centre Global Environment Model V.2, Earth System)	Met Office Hadley Centre, United Kingdom	192×145	38
MPI-ESM-LR (MPI Earth System Model, low resolution)	Max Planck Institute (MPI) for Meteorology, Germany	192×96	47
IPSL-CM5A-MR (IPSL Coupled Model V.5 incl. NEMO, medium resolution)	L'Institut Pierre-Simon Laplace (IPSL), France	144×143	39

TABLE C.5: Remaining set of 21 European countries in Section 4.1 including the used ISO-3166-1 (Alpha-2) code.

Country	ISO code
Belgium	BE
Bulgaria	BG
Czech Republic	CZ
Denmark	DK
Estonia	EE
Finland	FI
France	FR
Germany	DE
Greece	GR
Hungary	HU
Ireland	IE
Italy	IT
Latvia	LV
Lithuania	LT
Netherlands	NL
Norway	NO
Poland	PO
Portugal	PT
Spain	ES
Sweden	SE
United Kingdom	UK

Table C.6: Technical characteristics of technologies.

Technology Unit	Efficiency [$MWh_e l/MWh_t h$]	Lifetime [a]	Capacity value	CO_2 emission factor [t/TJ]	Area power density [MW/km^2]
Black coal	0.41	45	0.84	93.1	-
Lignite	0.38	45	0.86	113.1	-
CCGT	0.60	30	0.86	55.9	-
OCGT	0.40	25	0.86	55.9	-
Nuclear	0.33	60	0.92	0.0	-
Biomass	0.30	30	0.85	0.0	-
Runoff river	0.90	60	0.59	0.0	-
Wind onshore	1.00	25	0.05	0.0	8
Wind offshore 50 m	1.00	25	0.05	0.0	12
Wind offshore 150 m	1.00	25	0.05	0.0	12
PV	1.00	25	0.00	0	25

Table C.7: Installed capacities [MW] of all technologies in 2014.

Technology	Installed capacities [MW]
Lignite	19601
CCGT	24428
OCGT	5519
Nuclear	10734
Biomass	7144
Runoff river	4252
Wind onshore	34275
Wind offshore 150 m	0
Wind offshore 50 m	916
PV	32648

Table C.8: Planned capacities [MW] for all technologies. Values for renewable technologies follow the EEG 2014 targets.

Technology	2014	2020	2030	2040	2050	2060	2070
Black coal	0	5719	0	0	0	0	0
Lignite	0	0	0	0	0	0	0
CCGT	0	6499	291	0	0	0	0
OCGT	0	3475	192	0	0	0	0
Nuclear	0	0	0	0	0	0	0
Biomass	0	710	1000	0	0	0	0
Runoff river	0	0	0	0	0	0	0
Wind onshore	0	19685	14500	0	0	0	0
Wind offshore 150 m	0	0	0	0	0	0	0
Wind offshore 50 m	0	5584	8500	0	0	0	0
PV	0	15568	12500	0	0	0	0

Table C.9: Dismantled capacities [MW] for all technologies.

Technology	2014	2020	2030	2040	2050	2060	2070
Black coal	0	5440	6591	6462	1056	0	0
Lignite	0	3347	3724	755	8970	2805	0
CCGT	0	263	6519	13446	10699	291	0
OCGT	0	1890	2399	1294	3602	0	0
Nuclear	0	2676	8058	0	0	0	0
Biomass	0	0	194	4289	2661	0	0
Runoff river	0	0	0	0	0	0	0

TABLE C.10: Specific investment cost trends [EUR/KW] of technologies.

Technology	2014	2020	2030	2040	2050	2060	2070
Black coal	1613	1613	1500	1450	1425	1425	1425
Lignite	1550	1550	1550	1550	1550	1550	1550
CCGT	711	711	711	711	711	711	711
OCGT	400	400	400	400	400	400	400
Nuclear	6000	6000	6000	6000	6000	6000	6000
Biomass	3297	3297	3293	3290	3287	3287	3287
Runoff river	3000	3000	3000	3000	3000	3000	3000
Wind onshore	1656	1602	1548	1512	1476	1476	1476
Wind offshore 50 m	3493	3168	2473	2236	2061	2061	2061
Wind offshore 150 m	3749	3460	2581	2300	2099	2099	2099
PV	1188	936	774	702	630	630	630

TABLE C.11: Fixed FOM costs [EUR/KW/a] of technologies.

Black coal	45
Lignite	54
CCGT	28
OCGT	17
Nuclear	97
Biomass	165
Run off river	60
Wind onshore	13
Wind offshore 50 m	93
Wind offshore 150 m	93
PV	15

TABLE C.12: Variable (fuel) cost trends [EUR/MWh$_{th}$] of technologies.

Technology	2014	2020	2030	2040	2050	2060	2070
Black coal	13.0	13.0	15.0	16.0	17.0	17.0	17.0
Lignite	3.1	3.1	3.1	3.1	3.1	3.1	3.1
CCGT	23.0	30.0	31.0	33.0	33.0	33.0	33.0
OCGT	23.0	30.0	31.0	33.0	33.0	33.0	33.0
Nuclear	8.5	8.5	8.5	8.5	8.5	8.5	8.5
Biomass	21.0	20.7	21.2	21.8	22.4	22.4	22.4

Appendix D

Figures

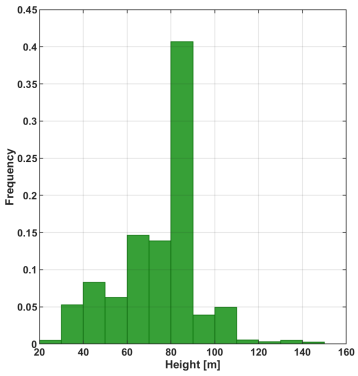

(A) Hub height [m]

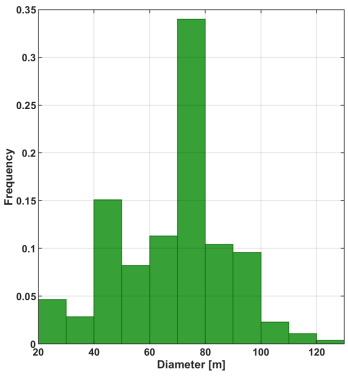

(B) Rotor diameter [m]

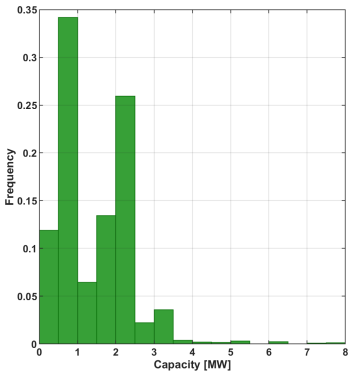

(C) Turbine capacity [MW]

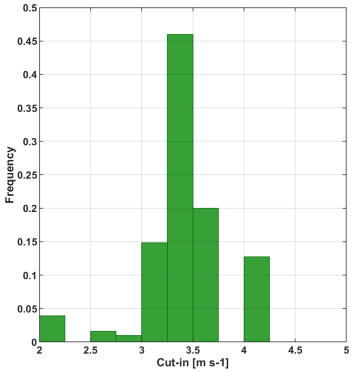

(D) Cut-in wind speed [ms^{-1}]

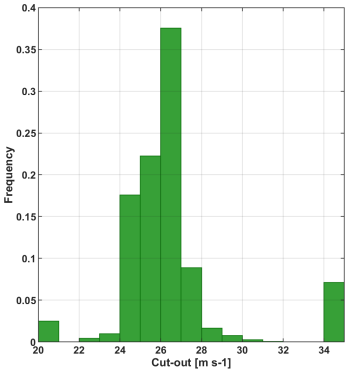

(E) Cut-out wind speed [ms^{-1}]

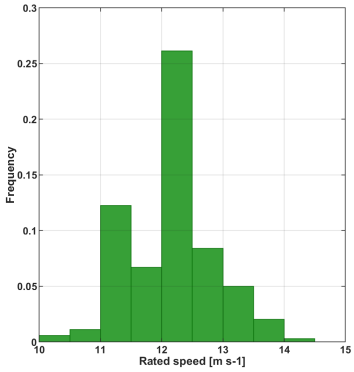

(F) Rated wind speed [ms^{-1}]

FIGURE D.1: Histograms of turbine specific parameters for all wind parks in Europe by the end of 2014. The database *The Wind Power* serves as the basis. Parks with either missing location or commission date are excluded.

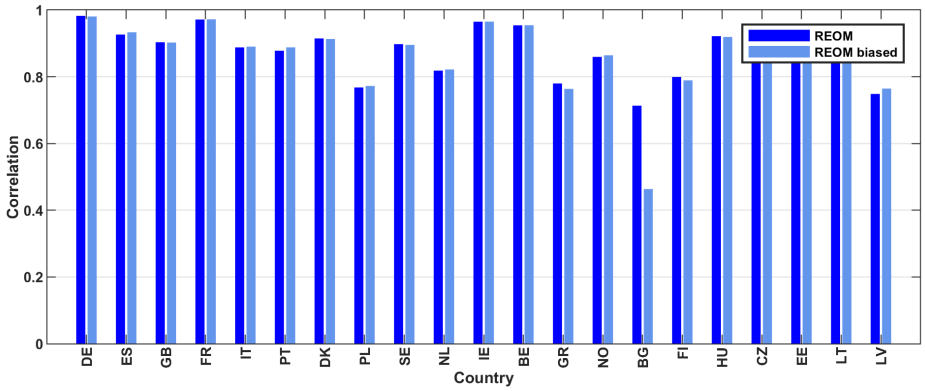

FIGURE D.2: Pearson correlation coefficients by country between monthly capacity factors of the corrected and uncorrected REOM simulations and ENTSO-E during the time period 2010-2014.

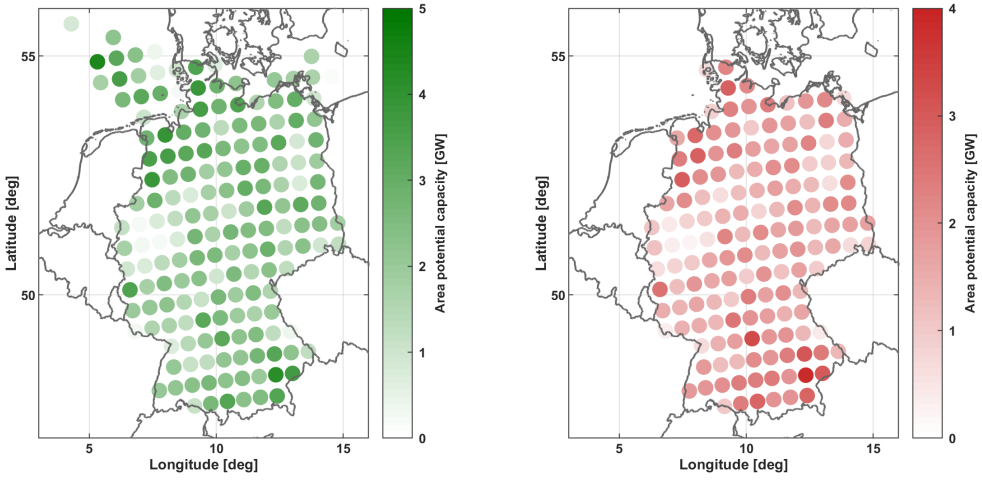

(A) HIST, wind (B) HIST, PV

FIGURE D.3: Area potentials [GW] for each grid point in Germany, for (A) wind and (B) PV power.

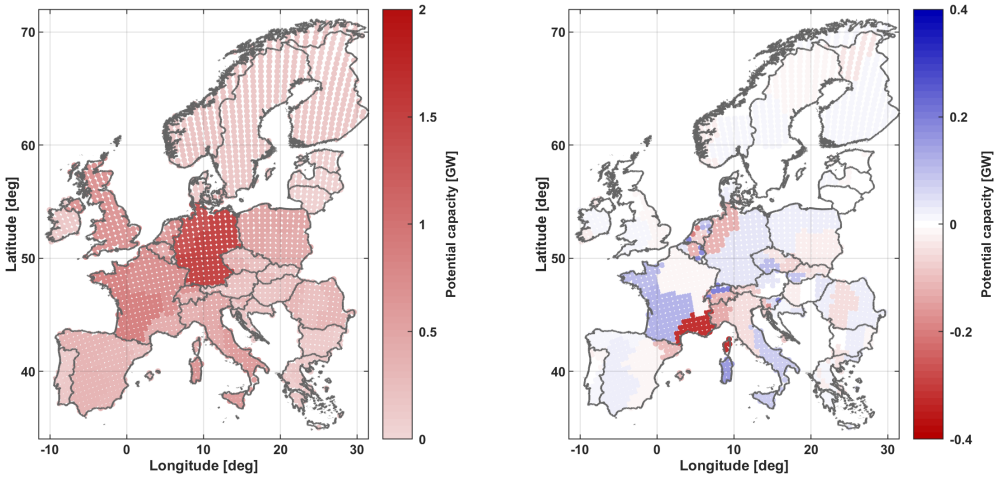

(A) (B)

FIGURE D.4: Area potentials [GW] for European PV power with respect to a method used in RPSM (A) and the residual to a simpler approach (B).

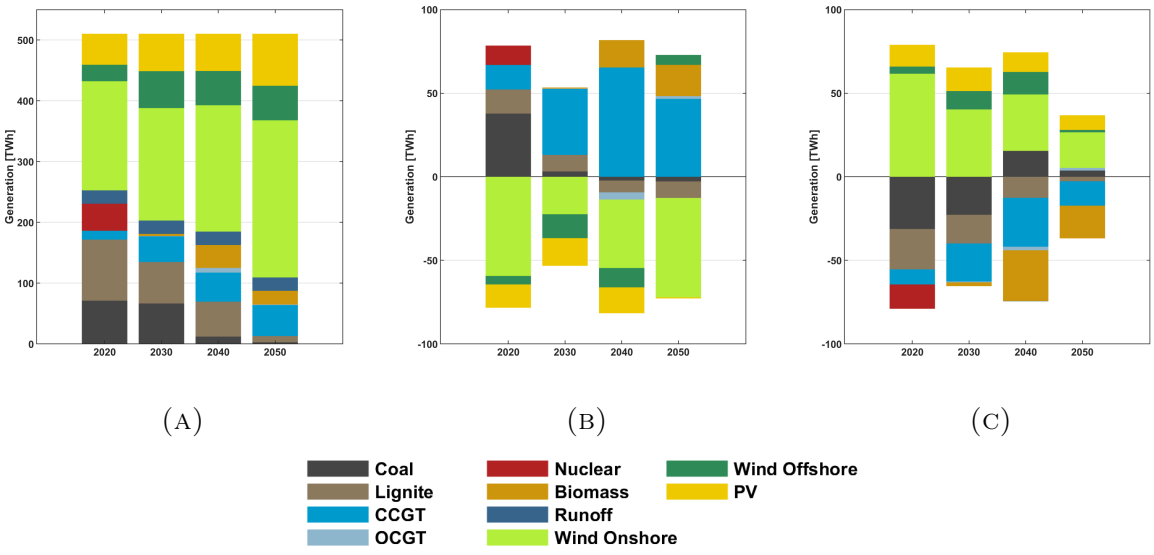

(A) (B) (C)

FIGURE D.5: Development of the electricity generation [TWh] shares in the control simulation (A) and its residuals to the negative (B) and positive (C) simulation. Residuals are defined as the perturbed minus the control run.

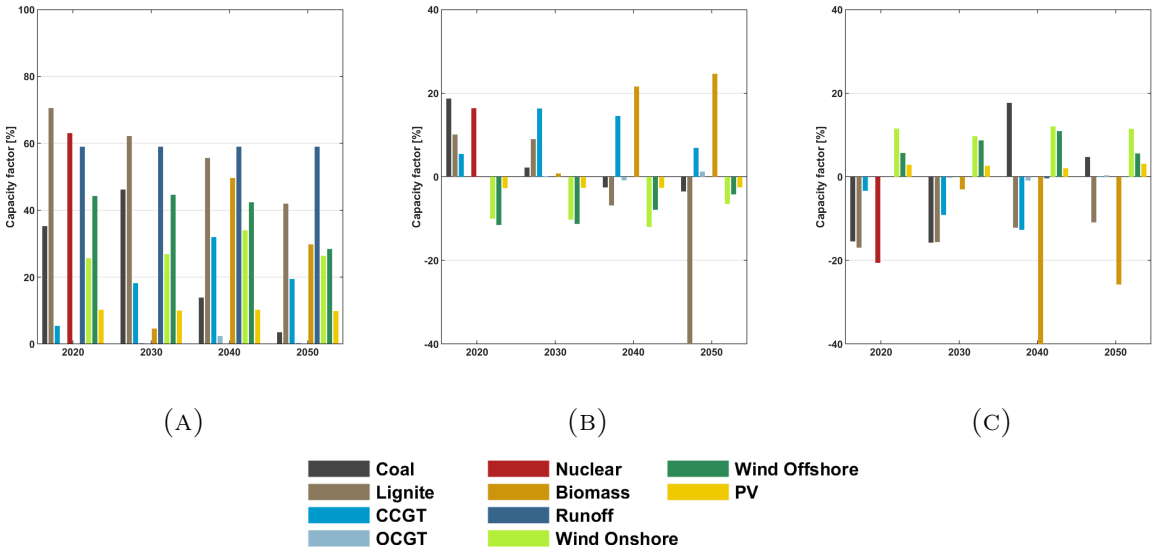

(A) (B) (C)

FIGURE D.6: Development of the capacity factors [%] in the control simulation (A) and its residuals to the negative (B) and positive (C) simulation. Residuals are defined as the perturbed minus the control run.

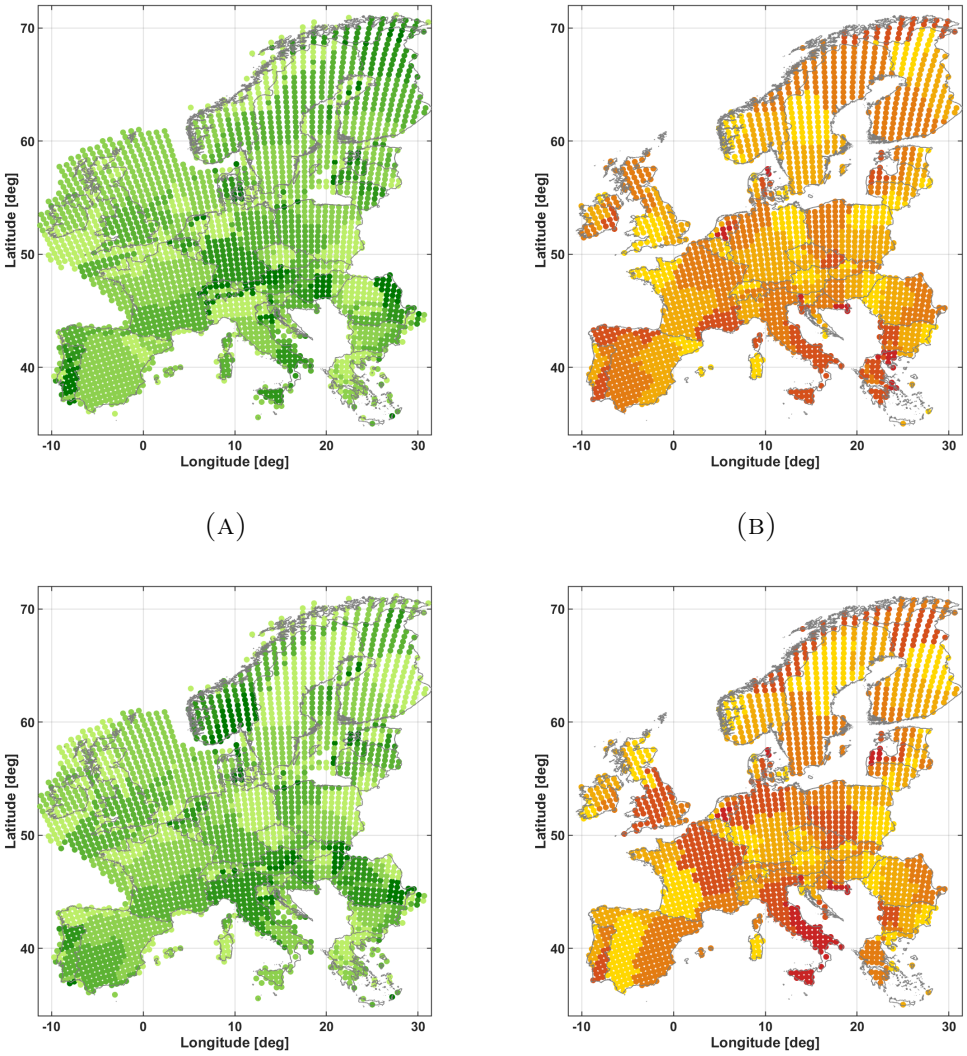

(A) (B)

(C) (D)

FIGURE D.7: Spatial distribution of the capacity factor clusters in Europe, in (A) for wind and (B) for PV in the HIST simulation and in (C) for wind and (D) for PV in the RCP85. Grid points of the same color within a graph belong to the same cluster.

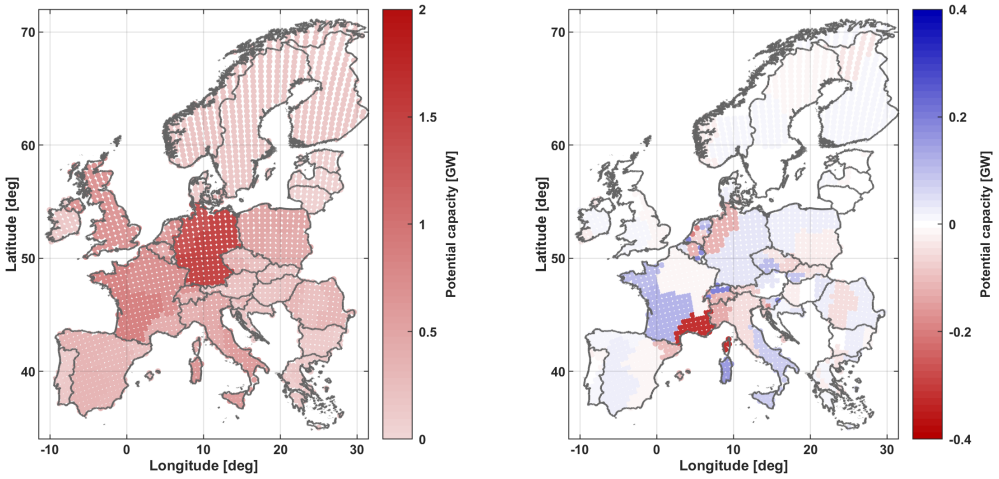

(A) (B)

FIGURE D.8: Area potentials [GW] for European PV power with respect to a method used in RPSM (A) and the residual to a simpler approach (B).

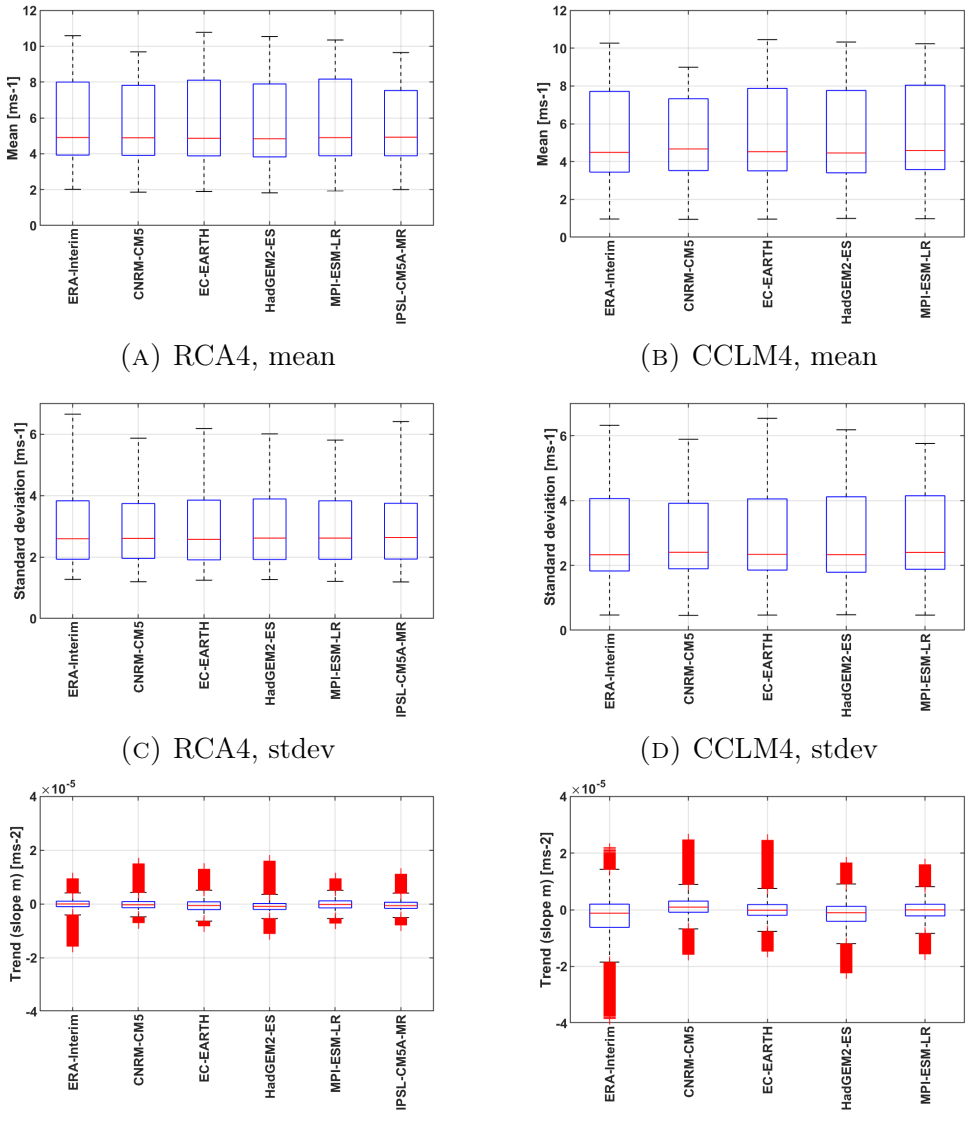

(A) RCA4, mean

(B) CCLM4, mean

(C) RCA4, stdev

(D) CCLM4, stdev

(E) RCA4, trend

(F) CCLM4, trend

FIGURE D.9: Boxplots of mean, standard deviation and trend of 3-hourly surface wind speeds for multiple GCM driven and ERA-Interim driven historical simulations with two RCM between 1980 and 2010. Median (red line), 25th and 75th percentiles (blue box), extreme data (dashed whiskers) and outliers (red cross) are presented.

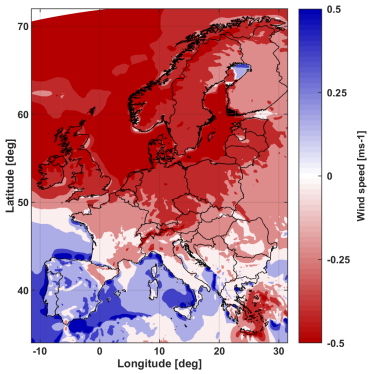

(A) CNRM, mean

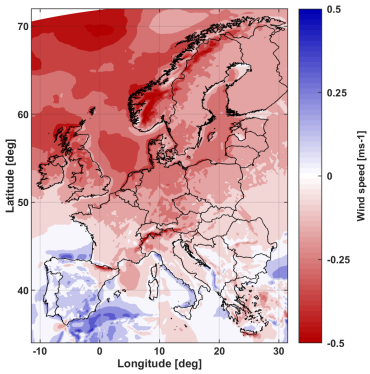

(B) CNRM, stdev

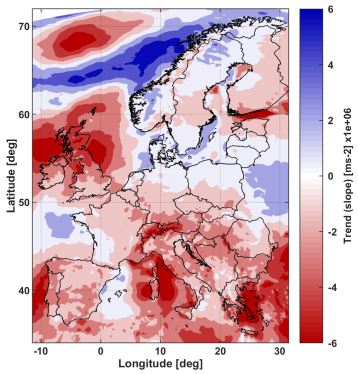

(C) CNRM, trend

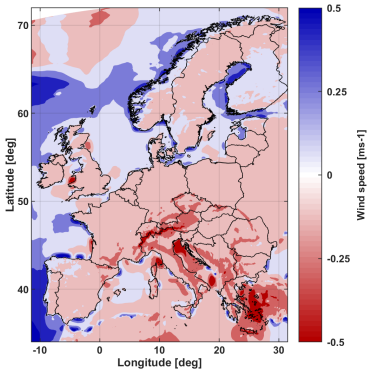

(D) EC-EARTH, mean

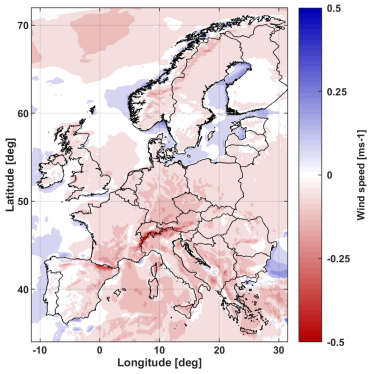

(E) EC-EARTH, stdev

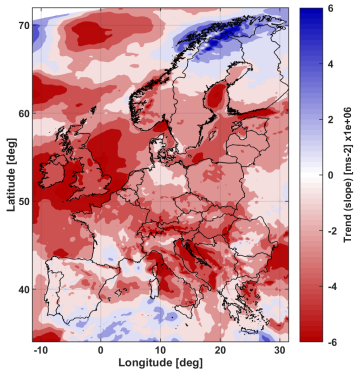

(F) EC-EARTH, trend

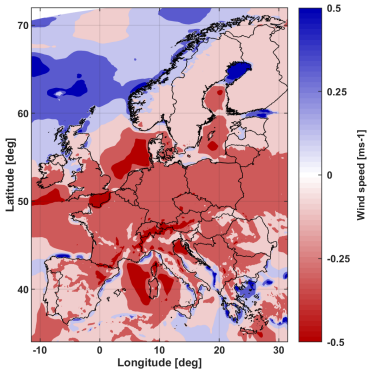

(G) HadGEM2, mean

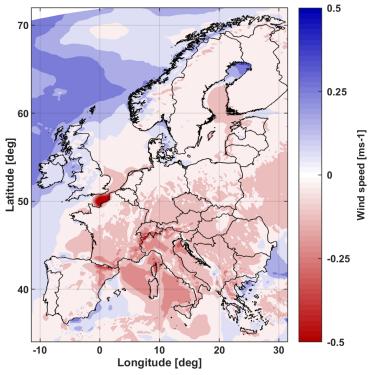

(H) HadGEM2, stdev

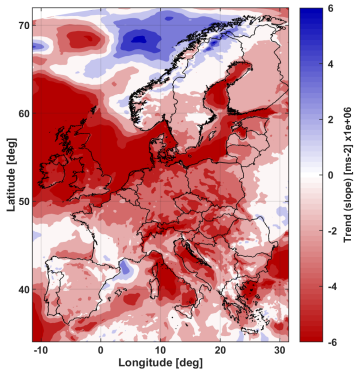

(I) HadGEM2, trend

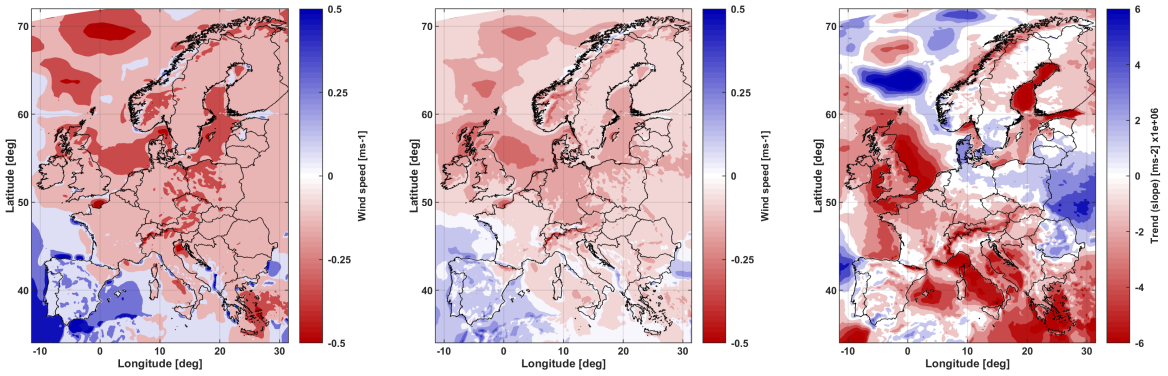

(J) MPI-ESM, mean (K) MPI-ESM, stdev (L) MPI-ESM, trend

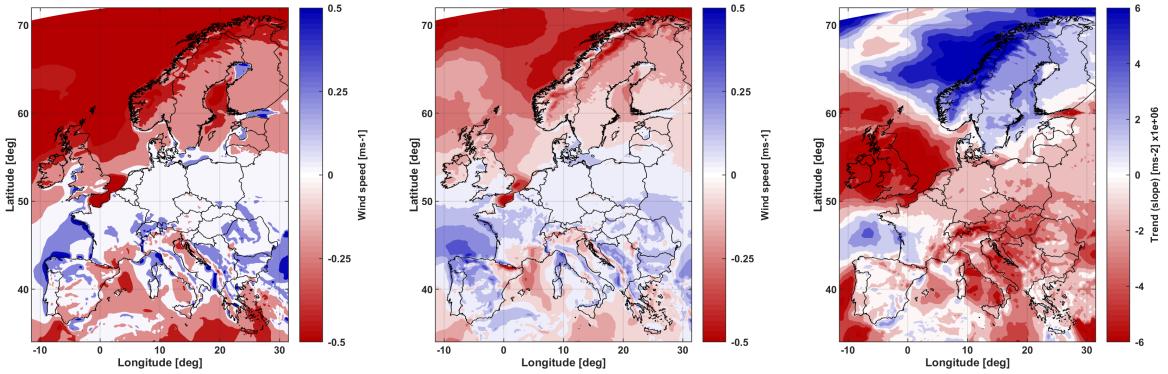

(M) IPSL, mean (N) IPSL, stdev (O) IPSL, trend

FIGURE D.10: Horizontal distribution of residuals between multiple GCM driven and ERA-Interim driven historical simulations with RCA4 (GCM minus ERA-Interim) between 1980 and 2010. Values are given for residuals regarding the mean, standard deviation and trend of 3-hourly surface wind speeds for the respective simulation setup.

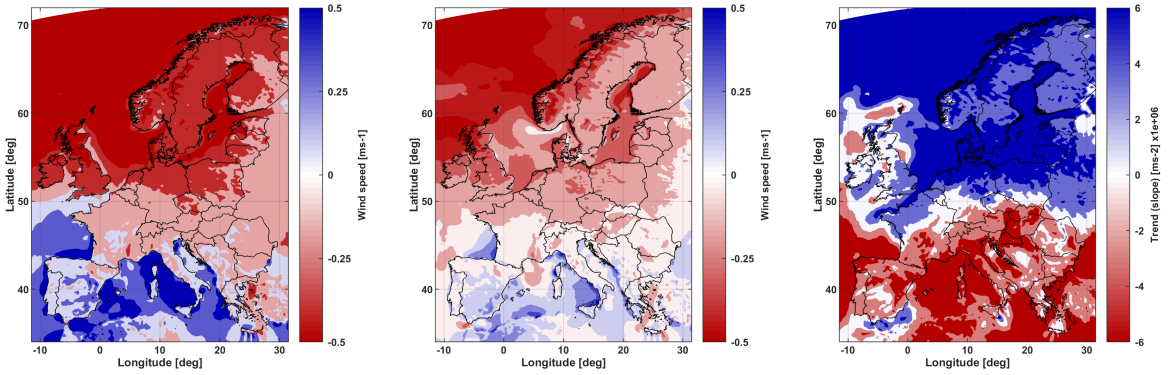

(A) CNRM, mean (B) CNRM, stdev (C) CNRM, trend

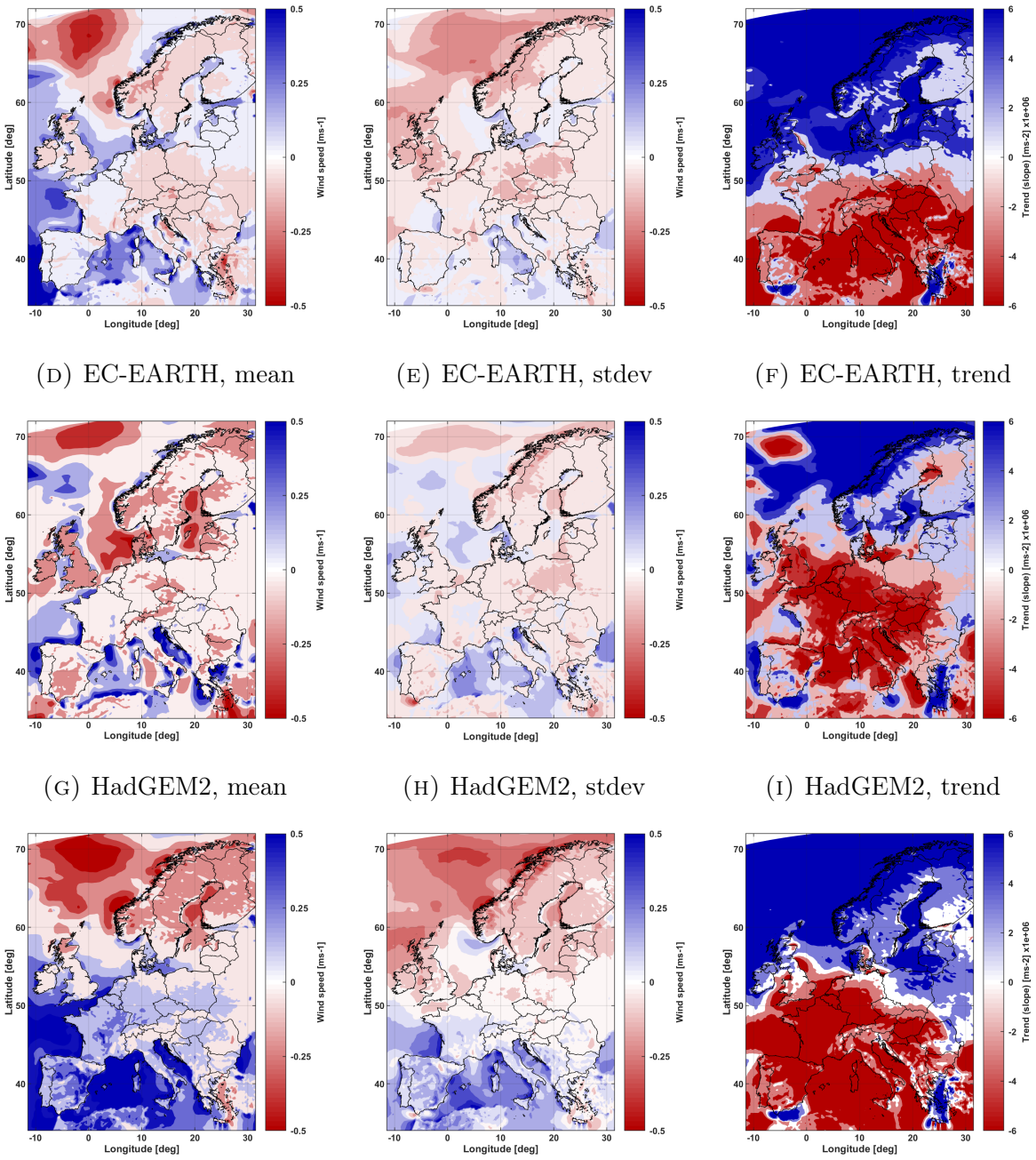

(D) EC-EARTH, mean (E) EC-EARTH, stdev (F) EC-EARTH, trend

(G) HadGEM2, mean (H) HadGEM2, stdev (I) HadGEM2, trend

(J) MPI-ESM, mean (K) MPI-ESM, stdev (L) MPI-ESM, trend

FIGURE D.11: Horizontal distribution of residuals between multiple GCM driven and ERA-Interim driven historical simulations with CCLM4-8-17 (GCM minus ERA-Interim) between 1980 and 2010. Values are given for residuals regarding the mean, standard deviation and trend of 3-hourly surface wind speeds for the respective simulation setup.

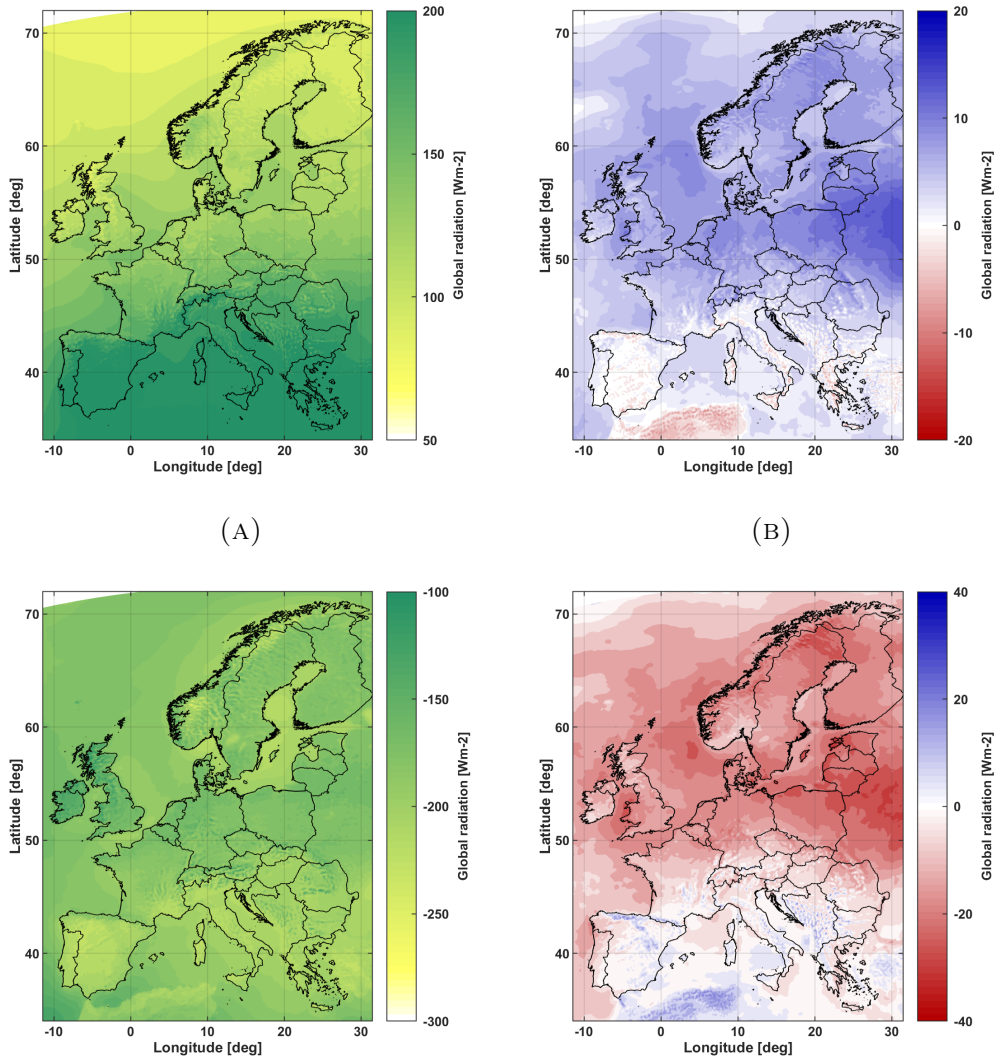

(A) (B)

(C) (D)

FIGURE D.12: Climatology of (A) mean surface downwelling solar radiation for RCA4 with ERA-Interim and (B) the residual to RCA4 with EC-EARTH. The same is presented in (C) and (D) for intra-annual variability (winter minus summer). Residuals are defined as RCP85 minus HIST.

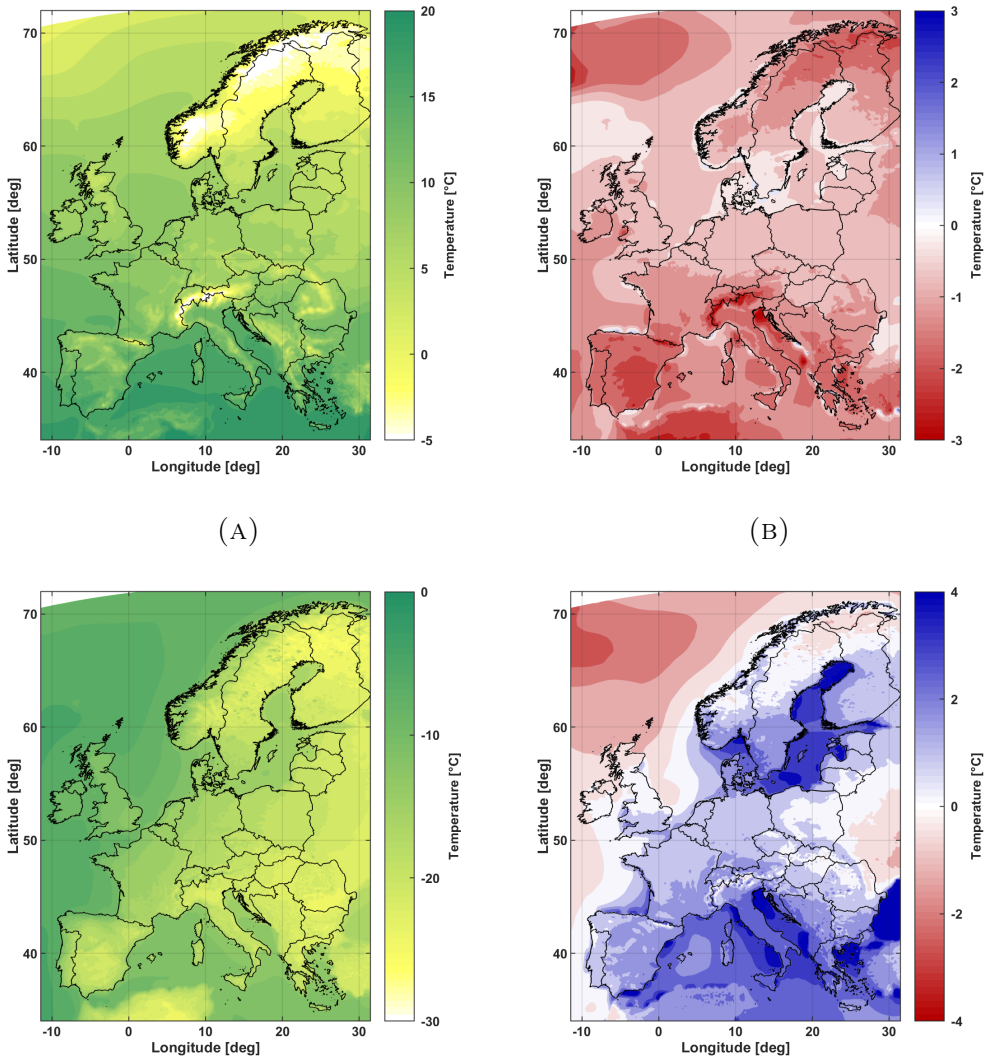

FIGURE D.13: Climatology of (A) mean surface temperature for RCA4 with ERA-Interim and (B) the residual to RCA4 with EC-EARTH. The same is presented in (C) and (D) for intra-annual variability (winter minus summer). Residuals are defined as RCP85 minus HIST.

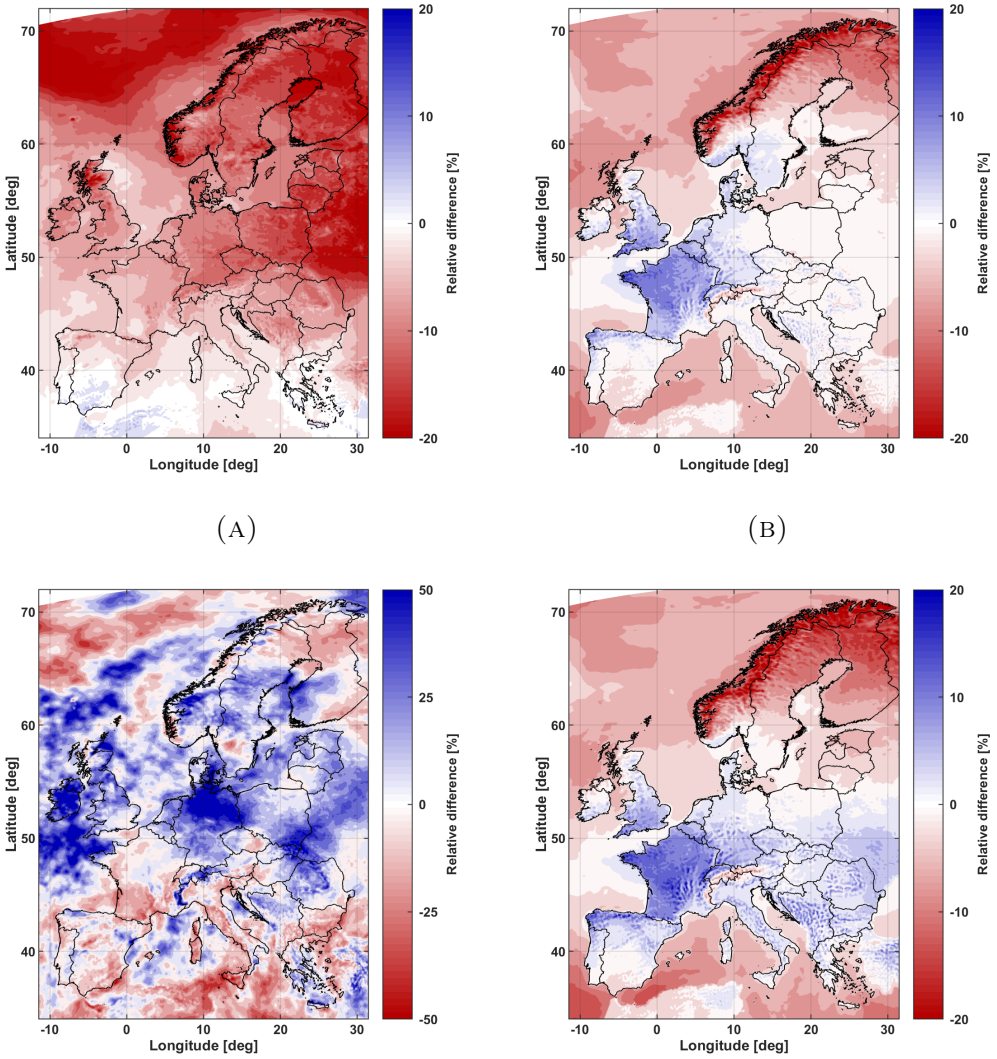

FIGURE D.14: Relative differences of the winter (A) and summer (B) mean as well as the inter-annual (C) and inter-daily (D) variability of surface global solar radiation between the HIST (1970-1999) and RCP85 (2070-2099) simulations. Residuals are defined as RCP85 minus HIST.

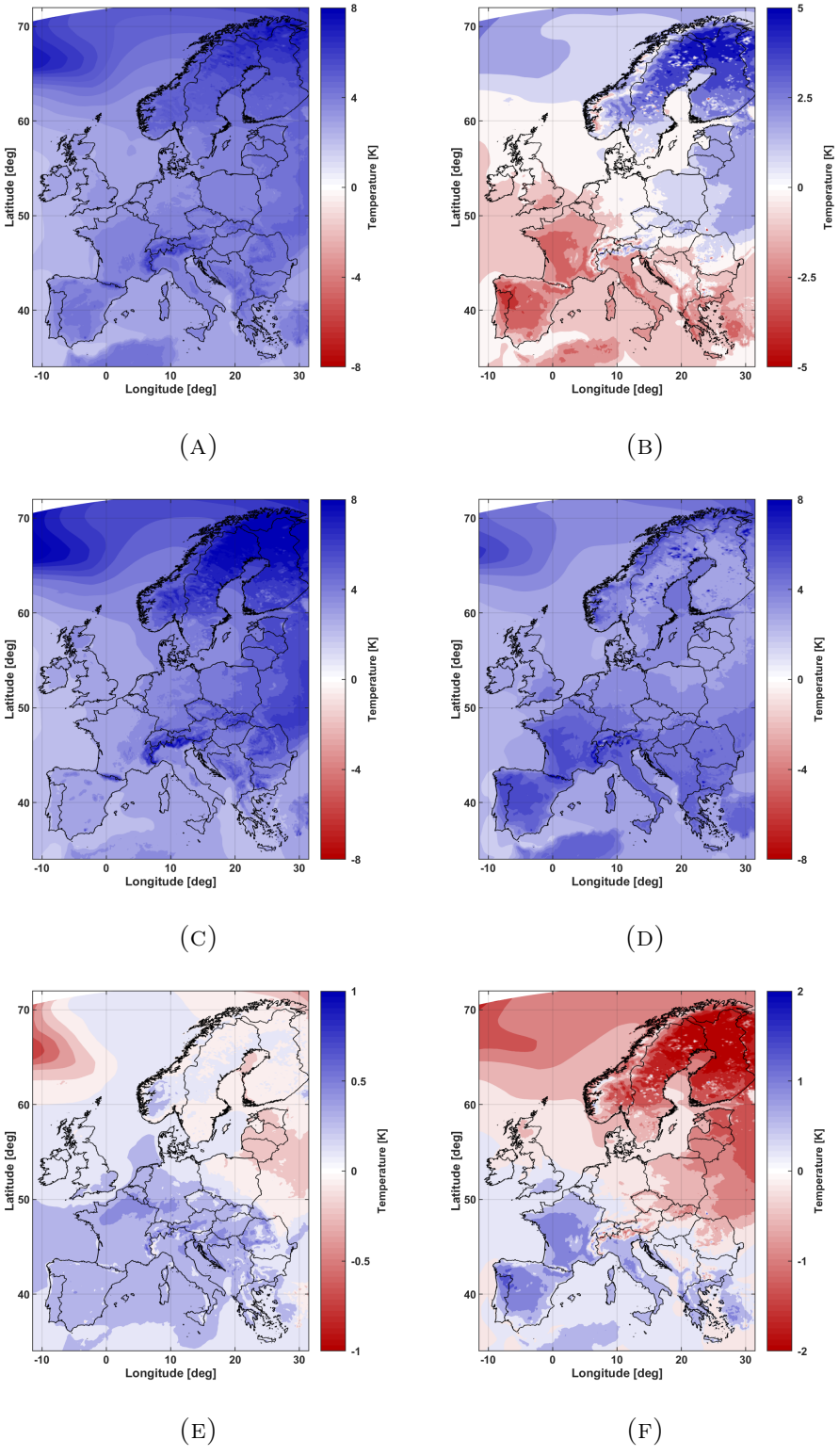

FIGURE D.15: Relative differences of the climatological mean (A), intra-annual variability (B), winter (C) and summer (D) mean as well as the inter-annual (E) and inter-daily (F) variability of surface temperature between the HIST (1970-1999) and RCP85 (2070-2099) simulations. Residuals are defined as RCP85 minus HIST.

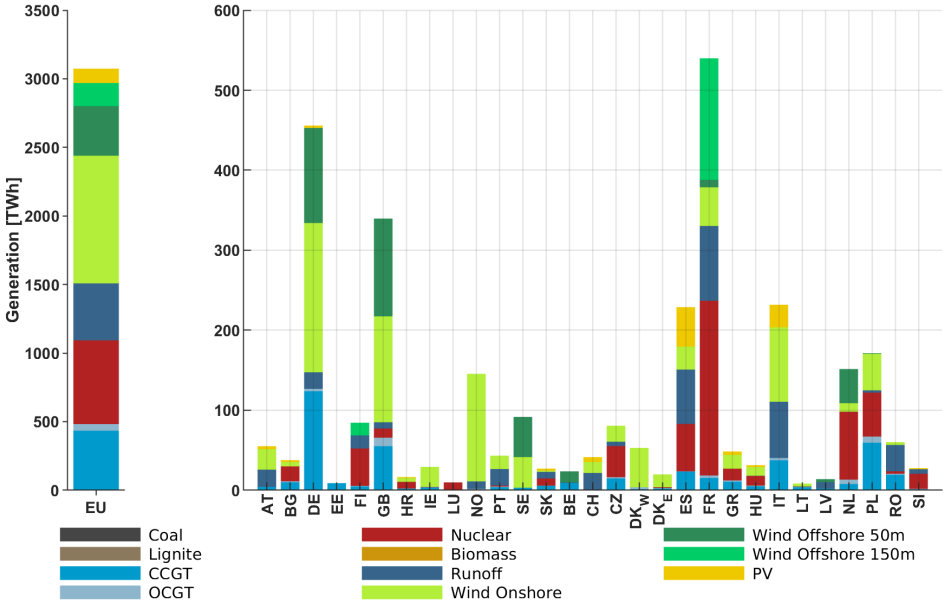

(A)

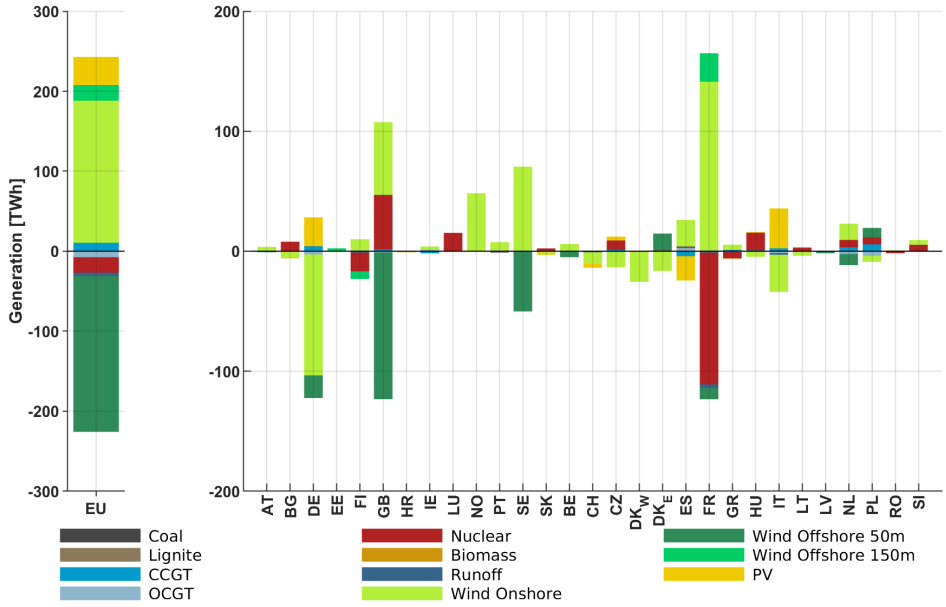

(B)

FIGURE D.16: Electricity generation under historical conditions (A) and its residual to RCP85 future scenario conditions (B). Residuals are defined as RCP85 minus HIST.

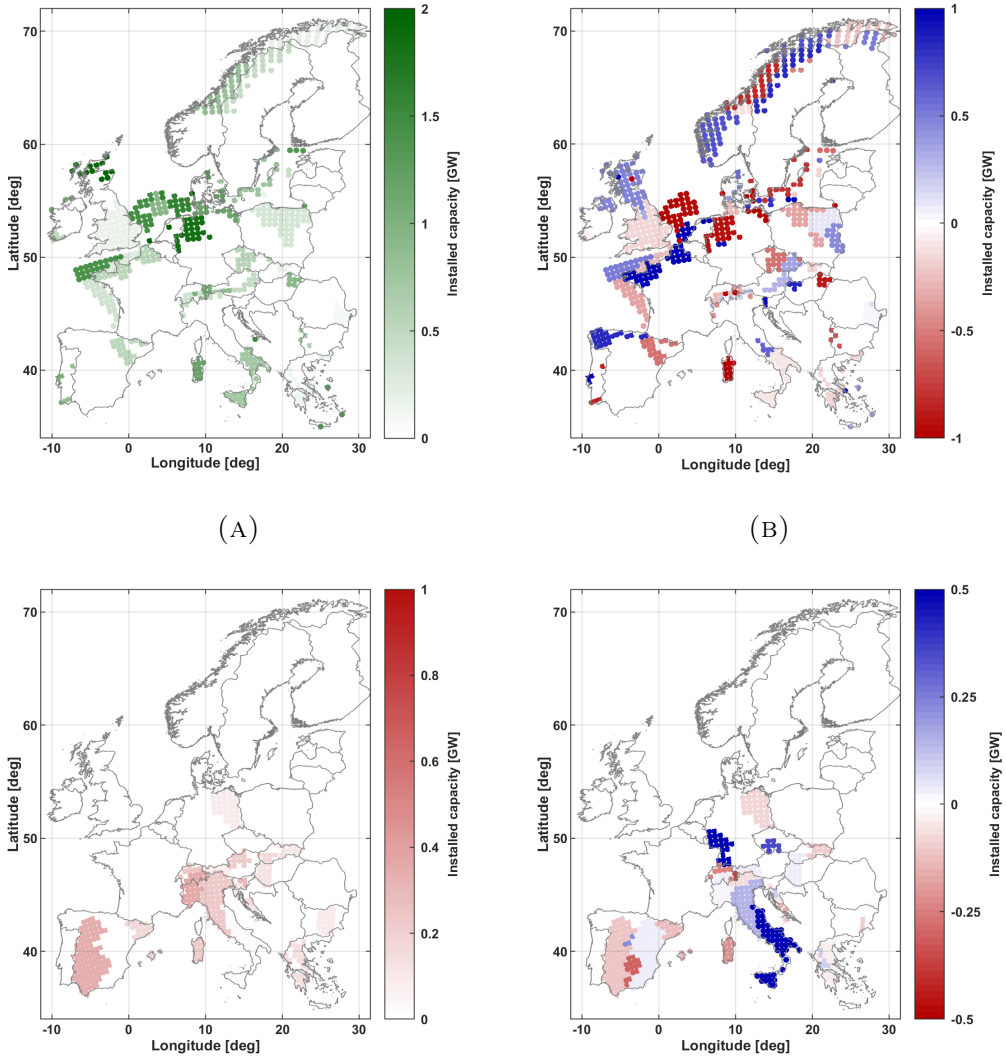

FIGURE D.17: Installed capacity [GW] under historical conditions (A) and its residual to RCP85 future scenario conditions (B) for wind power. Equivalent for PV power in (C) and (D). Residuals are defined as RCP85 minus HIST.

Bibliography

Andresen, G. B., A. A. Søndergaard, and M. Greiner (2015). "Validation of Danish wind time series from a new global renewable energy atlas for energy system analysis". In: *Energy* 93. arXiv: 1409.3353, pp. 1074–1088. ISSN: 03605442. DOI: 10.1016/j.energy.2015.09.071.

Beaudin, Marc et al. (2010). "Energy storage for mitigating the variability of renewable electricity sources: An updated review". In: *Energy for Sustainable Development* 14.4, pp. 302–314. ISSN: 0973-0826. DOI: 10.1016/j.esd.2010.09.007.

Bessa, Ricardo et al. (2014). "Handling renewable energy variability and uncertainty in power systems operation". In: *Wiley Interdisciplinary Reviews: Energy and Environment* 3.2, pp. 156–178. ISSN: 2041-840X. DOI: 10.1002/wene.76.

Bett, Philip E. and Hazel E. Thornton (2016). "The climatological relationships between wind and solar energy supply in Britain". In: *Renewable Energy* 87, Part 1, pp. 96–110. ISSN: 0960-1481. DOI: 10.1016/j.renene.2015.10.006.

Bloomberg (2018). "Fossil Fuels Squeezed by Plunge in Cost of Renewables, BNEF Says". In: *Bloomerg New Energy Finance report*. URL: https://www.bloomberg.com/news/articles/2018-03-28/fossil-fuels-squeezed-by-plunge-in-cost-of-renewables-bnef-says (visited on 03/14/2019).

Bollmeyer, C. et al. (2015). "Towards a high-resolution regional reanalysis for the European CORDEX domain". en. In: *Quarterly Journal of the Royal Meteorological Society* 141.686, pp. 1–15. ISSN: 1477-870X.

Born, Kai, Patrick Ludwig, and Joaquim G. Pinto (2012). "Wind gust estimation for Mid-European winter storms: towards a probabilistic view". In: *Tellus A: Dynamic Meteorology and Oceanography* 64.1, p. 17471. ISSN: null. DOI: 10.3402/tellusa.v64i0.17471.

Boyle, Godfrey (2009). *Renewable Electricity and the Grid: The Challenge of Variability*. Routledge. ISBN: 978-1-84407-789-2.

Cannon, D. J. et al. (2015). "Using reanalysis data to quantify extreme wind power generation statistics: A 33 year case study in Great Britain". In: *Renewable Energy* 75, pp. 767–778. ISSN: 0960-1481. DOI: 10.1016/j.renene.2014.10.024.

Carvalho, D. et al. (2014). "WRF wind simulation and wind energy production estimates forced by different reanalyses: Comparison with observed data for

Portugal". In: *Applied Energy* 117, pp. 116–126. ISSN: 0306-2619. DOI: 10.1016/j.apenergy.2013.12.001.

Cebulla, F., T. Naegler, and M. Pohl (2017). "Electrical energy storage in highly renewable European energy systems: Capacity requirements, spatial distribution, and storage dispatch". In: *Journal of Energy Storage* 14, pp. 211–223. ISSN: 2352-152X. DOI: 10.1016/j.est.2017.10.004.

Connolly, D. and B. V. Mathiesen (2014). "A technical and economic analysis of one potential pathway to a 100% renewable energy system". In: *International Journal of Sustainable Energy Planning and Management* 1, pp. 7–28. ISSN: 2246-2929. DOI: 10.5278/ijsepm.2014.1.2.

Connolly, D., H. Lund, and B. V. Mathiesen (2016). "Smart Energy Europe: The technical and economic impact of one potential 100% renewable energy scenario for the European Union". In: *Renewable and Sustainable Energy Reviews* 60, pp. 1634–1653. ISSN: 1364-0321. DOI: 10.1016/j.rser.2016.02.025.

Cosseron, Alexandra, Udaya Bhaskar Gunturu, and C. A. Schlosser (2013). "Characterization of the Wind Power Resource in Europe and its Intermittency". In: *Energy Procedia*. European Geosciences Union General Assembly 2013, ERE 40, pp. 58–66. ISSN: 1876-6102.

Cradden, Lucy C. et al. (2017). "A 34-year simulation of wind generation potential for Ireland and the impact of large-scale atmospheric pressure patterns". In: *Renewable Energy* 106, pp. 165–176. ISSN: 0960-1481. DOI: 10.1016/j.renene.2016.12.079.

Deng, Yvonne Y., Kornelis Blok, and Kees van der Leun (2012). "Transition to a fully sustainable global energy system". In: *Energy Strategy Reviews*. European Energy System Models 1.2, pp. 109–121. ISSN: 2211-467X. DOI: 10.1016/j.esr.2012.07.003.

Dolter, Brett and Nicholas Rivers (2018). "The cost of decarbonizing the Canadian electricity system". In: *Energy Policy* 113, pp. 135–148. ISSN: 0301-4215. DOI: 10.1016/j.enpol.2017.10.040.

Dominković, D. F. et al. (2016). "Zero carbon energy system of South East Europe in 2050". In: *Applied Energy* 184, pp. 1517–1528. ISSN: 0306-2619. DOI: 10.1016/j.apenergy.2016.03.046.

EEA, European Environmental Agency (2009). *Europe's onshore and offshore wind energy potential*. Publication. URL: https://www.eea.europa.eu/publications/europes-onshore-and-offshore-wind-energy-potential (visited on 01/14/2019).

Emeis, Stefan and Matthias Turk (2007). "Comparison of Logarithmic Wind Profiles and Power Law Wind Profiles and their Applicability for Offshore Wind Profiles". In: *Wind Energy*. Ed. by Joachim Peinke, Peter Schaumann, and Stephan Barth. Springer Berlin Heidelberg, pp. 61–64. ISBN: 978-3-540-33866-6.

Forzieri, Giovanni et al. (2016). "Multi-hazard assessment in Europe under climate change". In: *Climatic Change* 137.1, pp. 105–119. ISSN: 1573-1480. DOI: 10.1007/s10584-016-1661-x.

Fürsch, Michaela et al. (2013). "The role of grid extensions in a cost-efficient transformation of the European electricity system until 2050". In: *Applied Energy* 104, pp. 642–652. ISSN: 0306-2619. DOI: 10.1016/j.apenergy.2012.11.050.

Gils, Hans Christian et al. (2017). "Integrated modelling of variable renewable energy-based power supply in Europe". In: *Energy* 123, pp. 173–188. ISSN: 0360-5442. DOI: 10.1016/j.energy.2017.01.115.

Giorgi, Filippo, Colin Jones, and Ghassem R Asrar (2009). "Addressing climate information needs at the regional level: the CORDEX framework". In: *WMO Bulletin* 58.3, p. 9.

Gonzalez, A. I. et al. (2016). *EMHIRES dataset Part I: Wind power generation. European Meteorological derived High resolution RES generation time series for present and future scenarios*. Publication. URL: https://ec.europa.eu/jrc/en/publication/eur-scientific-and-technical-research-reports/emhires-dataset-part-i-wind-power-generation-european-meteorological-derived-high-resolution (visited on 03/28/2019).

Gunturu, U. B. and C. A. Schlosser (2012). "Characterization of wind power resource in the United States". In: *Atmos. Chem. Phys.* 12.20, pp. 9687–9702. ISSN: 1680-7324.

Haas, R. and J. G. Pinto (2012). "A combined statistical and dynamical approach for downscaling large-scale footprints of European windstorms". In: *Geophysical Research Letters* 39.23. ISSN: 1944-8007. DOI: 10.1029/2012GL054014.

Haas, R., J. G. Pinto, and K. Born (2014). "Can dynamically downscaled windstorm footprints be improved by observations through a probabilistic approach?" In: *Journal of Geophysical Research: Atmospheres* 119.2, pp. 713–725. ISSN: 2169-8996. DOI: 10.1002/2013JD020882. URL: https://agupubs.onlinelibrary.wiley.com/doi/abs/10.1002/2013JD020882 (visited on 02/18/2019).

Hagspiel, Simeon, Andreas Knaut, and Jakob Peter (2017). "Reliability in multi-regional power systems: Capacity adequacy and the role of interconnectors". In: *EWI Working Paper*. URL: https://www.econstor.eu/handle/10419/172837 (visited on 02/12/2019).

Hallgren, Willow, Udaya Bhaskar Gunturu, and Adam Schlosser (2014). "The Potential Wind Power Resource in Australia: A New Perspective". In: *PLOS ONE* 9.7, e99608. ISSN: 1932-6203.

Henckes, Philipp et al. (2018). "The benefit of long-term high resolution wind data for electricity system analysis". In: *Energy* 143.Supplement C, pp. 934–942. ISSN: 0360-5442. DOI: 10.1016/j.energy.2017.10.049.

Henckes, Philipp et al. (2019). "Uncertainty Estimation of Investment Planning Models Under High Shares of Renewables Using Reanalysis Data". In: *Energy, Submitted in July 2019*.

Hirth, Lion, Falko Ueckerdt, and Ottmar Edenhofer (2015). "Integration costs revisited – An economic framework for wind and solar variability". In: *Renewable Energy* 74, pp. 925–939. ISSN: 0960-1481. DOI: 10.1016/j.renene.2014.08.065.

Huber, Matthias, Albert Roger, and Thomas Hamacher (2015). "Optimizing long-term investments for a sustainable development of the ASEAN power system". In: *Energy* 88, pp. 180–193. ISSN: 0360-5442. DOI: 10.1016/j.energy.2015.04.065.

Hueging, Hanna et al. (2012). "Regional Changes in Wind Energy Potential over Europe Using Regional Climate Model Ensemble Projections". In: *Journal of Applied Meteorology and Climatology* 52.4, pp. 903–917. ISSN: 1558-8424. DOI: 10.1175/JAMC-D-12-086.1.

Huld, Thomas and Ana M. Gracia Amillo (2015). "Estimating PV Module Performance over Large Geographical Regions: The Role of Irradiance, Air Temperature, Wind Speed and Solar Spectrum". In: *Energies* 8.6, pp. 5159–5181. DOI: 10.3390/en8065159.

IEA, International Energy Agency, ed. (2011). *World energy outlook 2011*. OCLC: 838801297. Paris: OECD. ISBN: 978-92-64-12413-4.

IPCC (2011). *Summary for Policymakers. In: IPCC Special Report on Renewable Energy Sources and Climate Change Mitigation*. Tech. rep. URL: https://www.ipcc.ch/report/renewable-energy-sources-and-climate-change-mitigation/ (visited on 03/15/2019).

— (2014). *Climate Change 2014: Synthesis Report. Contribution of Working Groups I, II and III to the Fifth Assessment Report of the Intergovernmental Panel on Climate Change*. Tech. rep. Geneva, Switzerland. URL: https://www.ipcc.ch/report/ar5/syr/ (visited on 03/15/2019).

IPCC (2018). *Global Warming of 1.5C. An IPCC Special Report on the impacts of global warming of 1.5C above pre-industrial levels and related global greenhouse gas emission pathways, in the context of strengthening the global response to the threat of climate change, sustainable development, and efforts to eradicate*

poverty. Tech. rep. OCLC: 1056192590. Geneva, Switzerland. URL: http://www.ipcc.ch/report/sr15/ (visited on 03/15/2019).

Jerez, Sonia et al. (2015). "The impact of climate change on photovoltaic power generation in Europe". In: *Nature Communications* 6, p. 10014. ISSN: 2041-1723. DOI: 10.1038/ncomms10014.

Jägemann, Cosima et al. (2013). "Decarbonizing Europe's power sector by 2050 — Analyzing the economic implications of alternative decarbonization pathways". In: *Energy Economics* 40, pp. 622–636. ISSN: 0140-9883. DOI: 10.1016/j.eneco.2013.08.019.

Kaimal, J. C. and John J. Finnigan (1994). *Atmospheric Boundary Layer Flows: Their Structure and Measurement*. en. Oxford University Press. ISBN: 978-0-19-506239-7.

Kaiser-Weiss, A. K. et al. (2015). "Comparison of regional and global reanalysis near-surface winds with station observations over Germany". In: *Adv. Sci. Res.* 12.1, pp. 187–198. ISSN: 1992-0636.

Kjellström, Erik et al. (2005). "A 140-year simulation of European climate with the new version of the Rossby Centre regional atmospheric climate model (RCA3)". eng. In: URL: http://urn.kb.se/resolve?urn=urn:nbn:se:smhi:diva-2309 (visited on 03/14/2019).

Klucher, T.M. (1979). "Evaluation of models to predict insolation on tilted surfaces". In: *Solar Energy* 23.2, pp. 111–114. ISSN: 0038092X. DOI: 10.1016/0038-092X(79)90110-5.

Knaut, Andreas et al. (2016). "The reference forecast of the German energy transition—An outlook on electricity markets". In: *Energy Policy* 92, pp. 477–491. ISSN: 0301-4215. DOI: 10.1016/j.enpol.2016.02.010.

Knutti, Reto and Jan Sedláček (2013). "Robustness and uncertainties in the new CMIP5 climate model projections". In: *Nature Climate Change* 3.4, pp. 369–373. ISSN: 1758-6798. DOI: 10.1038/nclimate1716.

Liléo, Sónia, Vind Ab, and Olga Petrik (2000). "Investigation on the use of NCEP/NCAR, MERRA and NCEP/CFSR reanalysis data in wind resource analysis". In: *Royal Institute of Technology*, p. 11. URL: https://www.researchgate.net/profile/Olga_Petrik/publication/299471167_Investigation_on_the_use_of_NCEPNCAR_MERRA_and_NCEPCFSR_reanalysis_data_in_wind_resource_analysis/links/5982e4e4458515a60df816f9/Investigation-on-the-use-of-NCEP-NCAR-MERRA-and-NCEP-CFSR-reanalysis-data-in-wind-resource-analysis.pdf.

Lund, Peter D. et al. (2015). "Review of energy system flexibility measures to enable high levels of variable renewable electricity". In: *Renewable and Sustainable*

Energy Reviews 45, pp. 785–807. ISSN: 1364-0321. DOI: 10.1016/j.rser.2015.01.057.

Mack, Michael et al. (2013). "Ertragsberechnungen für PV Systeme - Status und künftige Anforderungen". In: *solar-engineering.de*. URL: http://solar-engineering.de/m104v01_upload/Ertragsberechnungen%20f%C3%BCr%20PV-Systeme%20-%20Status%20und%20k%C3%BCnftige%20Anforderungen.pdf (visited on 03/14/2019).

Madsen, H. et al. (2014). "Review of trend analysis and climate change projections of extreme precipitation and floods in Europe". In: *Journal of Hydrology* 519, pp. 3634–3650. ISSN: 0022-1694. DOI: 10.1016/j.jhydrol.2014.11.003.

Manwell, J. F., J. G. McGowan, and Anthony L. Rogers (2009). *Wind energy explained: theory, design and application*. 2nd ed. OCLC: ocn431936159. Chichester, U.K: Wiley. ISBN: 978-0-470-01500-1.

McKenna, R. et al. (2015). "Cost-potentials for large onshore wind turbines in Europe". In: *Energy* 83, pp. 217–229. ISSN: 0360-5442. DOI: 10.1016/j.energy.2015.02.016.

Merrick, James H. (2016). "On representation of temporal variability in electricity capacity planning models". In: *Energy Economics* 59, pp. 261–274. ISSN: 0140-9883. DOI: 10.1016/j.eneco.2016.08.001.

Michelangeli, P.-A., M. Vrac, and H. Loukos (2009). "Probabilistic downscaling approaches: Application to wind cumulative distribution functions". In: *Geophysical Research Letters* 36.11. ISSN: 1944-8007. DOI: 10.1029/2009GL038401.

Mideksa, Torben K. and Steffen Kallbekken (2010). "The impact of climate change on the electricity market: A review". In: *Energy Policy*. Large-scale wind power in electricity markets with Regular Papers 38.7, pp. 3579–3585. ISSN: 0301-4215.

Moemken, Julia et al. (2018). "Future Changes of Wind Speed and Wind Energy Potentials in EURO-CORDEX Ensemble Simulations". In: *Journal of Geophysical Research: Atmospheres* 123.12, pp. 6373–6389. ISSN: 2169-8996. DOI: 10.1029/2018JD028473.

Monforti, F., M. Gaetani, and E. Vignati (2016). "How synchronous is wind energy production among European countries?" In: *Renewable and Sustainable Energy Reviews* 59, pp. 1622–1638. ISSN: 1364-0321. DOI: 10.1016/j.rser.2015.12.318.

Motta, M., R. J. Barthelmie, and P. Vølund (2005). "The influence of non-logarithmic wind speed profiles on potential power output at Danish offshore sites". In: *Wind Energy* 8.2, pp. 219–236. ISSN: 1099-1824.

Najac, Julien (2014). "Predicting future wind power generation and power demand in France using statistical downscaling methods developed for hydropower applications". In: *EGU General Assembly Conference Abstracts*. Vol. 16, p. 6616. URL: http://adsabs.harvard.edu/abs/2014EGUGA..16.6616N (visited on 03/20/2019).

Neumann, Barbara et al. (2015). "Future Coastal Population Growth and Exposure to Sea-Level Rise and Coastal Flooding - A Global Assessment". en. In: *PLOS ONE* 10.3, e0118571. ISSN: 1932-6203. DOI: 10.1371/journal.pone.0118571.

Nolan, Paul et al. (2012). "Simulating climate change and its effects on the wind energy resource of Ireland". In: *Wind Energy* 15.4, pp. 593–608. ISSN: 1099-1824. DOI: 10.1002/we.489.

Obermüller, Frank (2017). *Build wind capacities at windy locations? Assessment of system optimal wind locations*. Working Paper 17/09. EWI Working Paper.

Ong, S. et al. (2013). *Land-Use Requirements for Solar Power Plants in the United States*. Tech. rep. NREL/TP-6A20-56290, 1086349. DOI: 10.2172/1086349.

Pacifici, M. et al. (2015). "Assessing species vulnerability to climate change". In: *Nature Climate Change* 5.3, pp. 215–224. ISSN: 1758-6798. DOI: 10.1038/nclimate2448.

Pan, Z. et al. (2001). "Evaluation of uncertainties in regional climate change simulations". In: *Journal of Geophysical Research: Atmospheres* 106.D16, pp. 17735–17751. ISSN: 2156-2202. DOI: 10.1029/2001JD900193.

Papaefthymiou, G. and Ken Dragoon (2016). "Towards 100% renewable energy systems: Uncapping power system flexibility". In: *Energy Policy* 92, pp. 69–82. ISSN: 0301-4215. DOI: 10.1016/j.enpol.2016.01.025.

Pecl, Gretta T. et al. (2017). "Biodiversity redistribution under climate change: Impacts on ecosystems and human well-being". In: *Science* 355.6332, eaai9214. ISSN: 0036-8075, 1095-9203. DOI: 10.1126/science.aai9214.

Perez, R. et al. (1986). "An anisotropic hourly diffuse radiation model for sloping surfaces: Description, performance validation, site dependency evaluation". In: *Solar Energy* 36.6, pp. 481–497. ISSN: 0038-092X. DOI: 10.1016/0038-092X(86)90013-7.

Perez, Richard et al. (2016). "Spatial and Temporal Variability of Solar Energy". In: *Foundations and Trends in Renewable Energy* 1.1, pp. 1–44. ISSN: 2328-8892, 2328-8906. DOI: 10.1561/2700000006.

Peter, Jakob (2019). "How Does Climate Change Affect Optimal Allocation of Variable Renewable Energy?" In: *EWI Working Paper*. URL: https://www.ewi.uni-koeln.de/cms/wp-content/uploads/2019/02/EWI_WP_19-03_How_Does_Climate_Change_Affect_Optimal_Allocation_of_VRE.pdf.

Peter, Jakob and Johannes Wagner (2018). "Optimal Allocation of Variable Renewable Energy Considering Contributions to Security of Supply". In: *EWI Working Paper*. URL: https://www.ewi.research-scenarios.de/cms/wp-content/uploads/2018/10/EWI_WP_18-02_Optimal_allocation_of_variable_renewable_energy_considering_contributions_to_security_of_supply.pdf.

Pleßmann, Guido et al. (2014). "Global Energy Storage Demand for a 100% Renewable Electricity Supply". In: *Energy Procedia*. 8th International Renewable Energy Storage Conference and Exhibition (IRES 2013) 46, pp. 22–31. ISSN: 1876-6102. DOI: 10.1016/j.egypro.2014.01.154.

Quaschning, Volker (2011). *Regenerative Energiesysteme: Technologie – Berechnung – Simulation*. de. 7th ed. München: Carl Hanser Verlag GmbH & Co. KG. ISBN: 978-3-446-42732-7 978-3-446-42944-4. DOI: 10.3139/9783446429444.

Reyers, Mark, Julia Moemken, and Joaquim G. Pinto (2016). "Future changes of wind energy potentials over Europe in a large CMIP5 multi-model ensemble". In: *International Journal of Climatology* 36.2, pp. 783–796. ISSN: 1097-0088. DOI: 10.1002/joc.4382.

Ritter, Matthias and Lars Deckert (2017). "Site assessment, turbine selection, and local feed-in tariffs through the wind energy index". In: *Applied Energy*. Clean, Efficient and Affordable Energy for a Sustainable Future 185, Part 2, pp. 1087–1099. ISSN: 0306-2619.

Rose, Stephen and Jay Apt (2015). "What can reanalysis data tell us about wind power?" In: *Renewable Energy* 83, pp. 963–969. ISSN: 0960-1481. DOI: 10.1016/j.renene.2015.05.027.

Sanford, Todd et al. (2014). "The climate policy narrative for a dangerously warming world". In: *Nature Climate Change* 4, pp. 164–166. ISSN: 1758-6798. DOI: 10.1038/nclimate2148.

Schlott, Markus et al. (2018). "The impact of climate change on a cost-optimal highly renewable European electricity network". In: *Applied Energy* 230, pp. 1645–1659. ISSN: 0306-2619. DOI: 10.1016/j.apenergy.2018.09.084.

Schmidt, Patrick R et al. (2016). "Empowering a sustainable mobility future with zero emission fuels from renewable electricity - Europe and Germany". In: *16. Internationales Stuttgarter Symposium, Springer*, pp. 185–199.

Schär, Christoph (2016). "Climate extremes: The worst heat waves to come". In: *Nature Climate Change* 6.2, pp. 128–129. ISSN: 1758-6798. DOI: 10.1038/nclimate2864.

Semenov, Mikhail A. and Pierre Stratonovitch (2010). "Use of multi-model ensembles from global climate models for assessment of climate change impacts". In:

Climate Research 41.1, pp. 1–14. ISSN: 0936-577X, 1616-1572. DOI: 10.3354/cr00836.

Staffell, Iain and Stefan Pfenninger (2016). "Using bias-corrected reanalysis to simulate current and future wind power output". In: *Energy* 114, pp. 1224–1239. ISSN: 0360-5442.

Strandberg, Gustav et al. (2015). *CORDEX scenarios for Europe from the Rossby Centre regional climate model RCA4*. SMHI. URL: http://urn.kb.se/resolve?urn=urn:nbn:se:smhi:diva-2839 (visited on 03/14/2019).

Stull, Roland B., ed. (1988). *An Introduction to Boundary Layer Meteorology*. Dordrecht: Springer Netherlands. ISBN: 978-90-277-2769-5 978-94-009-3027-8.

Tebaldi, C. and R. Knutti (2007). "The use of the multi-model ensemble in probabilistic climate projections". In: *Philosophical Transactions of the Royal Society A: Mathematical, Physical and Engineering Sciences* 365.1857, pp. 2053–2075. DOI: 10.1098/rsta.2007.2076.

Teuling, Adriaan J. (2018). "A hot future for European droughts". In: *Nature Climate Change* 8.5, p. 364. ISSN: 1758-6798. DOI: 10.1038/s41558-018-0154-5.

The Wind Power (2016). *Europe wind farms database*. URL: http://www.thewindpower.net/.

Tobin, I. et al. (2016). "Climate change impacts on the power generation potential of a European mid-century wind farms scenario". In: *Environmental Research Letters* 11.3, p. 034013. ISSN: 1748-9326. DOI: 10.1088/1748-9326/11/3/034013.

Tobin, I. et al. (2018). "Vulnerabilities and resilience of European power generation to 1.5C, 2C and 3C warming". In: *Environmental Research Letters* 13.4, p. 044024. ISSN: 1748-9326. DOI: 10.1088/1748-9326/aab211.

Tobin, Isabelle et al. (2014). "Assessing climate change impacts on European wind energy from ENSEMBLES high-resolution climate projections". In: *Climatic Change* 128.1-2, pp. 99–112. ISSN: 0165-0009, 1573-1480. DOI: 10.1007/s10584-014-1291-0.

Ueckerdt, Falko, Robert Brecha, and Gunnar Luderer (2015). "Analyzing major challenges of wind and solar variability in power systems". In: *Renewable Energy* 81, pp. 1–10. ISSN: 0960-1481. DOI: 10.1016/j.renene.2015.03.002. URL: http://www.sciencedirect.com/science/article/pii/S0960148115001846 (visited on 03/15/2019).

Viner, David (2002). "A qualitative assessment of the sources of uncertainty in climate change impacts assessment studies". In: *Climatic Change: Implications for the Hydrological Cycle and for Water Management*. Ed. by Martin Beniston.

Advances in Global Change Research. Dordrecht: Springer Netherlands, pp. 139–149. ISBN: 978-0-306-47983-0. DOI: 10.1007/0-306-47983-4_8.

Watts, Nick et al. (2015). "Health and climate change: policy responses to protect public health". In: *The Lancet* 386.10006, pp. 1861–1914. ISSN: 0140-6736, 1474-547X. DOI: 10.1016/S0140-6736(15)60854-6.

Weisse, R. and F. Feser (2003). "Evaluation of a method to reduce uncertainty in wind hindcasts performed with regional atmosphere models". In: *Coastal Engineering* 48.4, pp. 211–225. ISSN: 0378-3839. DOI: 10.1016/S0378-3839(03)00027-9. URL: http://www.sciencedirect.com/science/article/pii/S0378383903000279 (visited on 03/14/2019).

Wenz, Leonie, Anders Levermann, and Maximilian Auffhammer (2017). "North–south polarization of European electricity consumption under future warming". In: *Proceedings of the National Academy of Sciences* 114.38, E7910–E7918. ISSN: 0027-8424, 1091-6490. DOI: 10.1073/pnas.1704339114.

WindEurope (2017). *Unleashing Europe's offshore wind potential*. Tech. rep. URL: https://windeurope.org/about-wind/reports/unleashing-europes-offshore-wind-potential/ (visited on 01/14/2019).

WindEurope (2017). *Wind in power: 2016 European statistics*. Tech. rep. URL: https://windeurope.org/about-wind/statistics/european/wind-in-power-2016/ (visited on 04/12/2017).

World Meteorological Organization (2008). *Guide to meteorological instruments and methods of observation*. OCLC: 928941505. Geneva: World Meteorological Organization. ISBN: 978-92-63-10008-5.

Wu, H. et al. (2015). "Thermal Generation Flexibility With Ramping Costs and Hourly Demand Response in Stochastic Security-Constrained Scheduling of Variable Energy Sources". In: *IEEE Transactions on Power Systems* 30.6, pp. 2955–2964. ISSN: 0885-8950. DOI: 10.1109/TPWRS.2014.2369473.

List of Tables

List of Figures

List of Abbreviations

AR5	Fifth Assessment Report by the IPCC
BMU	German Federal Ministry of Environment, Nature Conservation & Nuclear Safety
Bn	Billion
CCGT	Combined cycle gas turbine
CDDA	Nationally designated areas
CF	Capacity factor
CLC2000	Corine Land Cover 2000 Version 16
CMIP5	Coupled Model Intercomparison Project Phase 5
CO_2	Carbon dioxide
CON	Unperturbed control simulation in Study II
CORDEX	Coordinated Downscaling Experiment
COSMO	Consortium for Small-scale Modeling
COSMO-REA6	COSMO reanalysis with 6 km resolution
DJF	December, January, February (winter)
DWD	German Weather Service
ECMWF	European Centre for Medium-Range Weather Forecasts
EEA	European Environmental Agency
EEG	Renewable Energy Sources Act
EEX	European Energy Exchange platform
ENTSO-E	European Network of Transmission System Operators for Electricity
ERA-20C	ECMWF reanalysis, 20 century version
ERA-Interim	ECMWF reanalysis, Interim version
ET-CC	Energy Transition & Climate Change
EU	European Union
EWI	Institute of Energy Economics
FLH	Full load hours
FOM	Fixed operation and maintenance costs
GCM	Global Climate Model
GHG	Green house gas
HerZ	Hans-Ertel-Zentrum for Weather Research
HIST	historical simulation in Study III
IDW	Inverse distance weighting
IEK	Institute for Energy and Climate Research
IGM	Institute for Geophysics & Meteorology
IPCC	Intergovernmental Panel on Climate Change
JJA	June, July, August (summer)
KM	Diffuse radiation model following Klucher (1979)
LCOE	Levelized costs of electricity
MAE	Mean Absolute Error
MAM	March, April, May (spring)
MARE	Mean Absolute Relative Error
MERRA	Modern-Era Retrospective analysis for Research and Applications, Version 1

MERRA-2	Modern-Era Retrospective analysis for Research and Applications, Version 2
NASA	National Aeronautics and Space Administration
NEG	Negative perturbed simulation in Study II
NTC	Net transfer capacity
OCGT	Open cycle gas turbine
PM	Diffuse radiation model following Perez et al. (1986)
POS	Positive perturbed simulation in Study II
PV	Photovoltaics
RCM	Regional Climate Model
RCP	Representative Concentration Pathway
REOM	Renewable Energy Output Model
RMSD	Root Mean Square Deviation
RMSE	Root Mean Square Error
RPSM	Renewable Power System Model
SON	September, October, November (autumn)
SRTM	Shuttle Radar Topography Mission
STC	Standard Test Conditions
SYNOP	Surface Synoptic Observations
TSO	Transmission system operators
VRE	Variable Renewable Energies
WCRP	World Climate Research Program
WMO	World Meteorological Organisation

List of Symbols

A_{mod}	PV module's area	m^2
A	Available area	km^2
a	parameter for Perez model	
b	parameter for Perez model	
C	accumulated total system costs	EUR
C^{inv}	total investment costs	EUR
C^{fix}	total fixed FOM costs	EUR
C^{var}	total variable costs (fuel)	EUR
C_{plant}	plant capacity	MW
CF	capacity factor	
c_p	wind power conversion efficiency	
c_T	proportionality factor	
c^{inv}	investment costs	EUR/MW
c^{fix}	FOM costs	EUR/MW/a
c^{var}	variable production costs (fuel)	EUR/MWh_{el}
cv	capacity values	
D	set of model typedays	
d	model typeday	
dt	RPSM simulation time step	a
E	total CO_2 emissions	t
E_0	solar constant	W/m^2
E^{cap}	CO_2 emission cap/target	t
$F_{i,j}$	constants for Perez model, $i = 1, 2$; $j = 1, 2$	
$F_{r,r'}$	energy transmission from region r to region r'	MWh
f	cluster scaling factor	
f_d	occurrence frequencies of typedays	
G	power generation	MWh
G^{hor}_{dif}	diffuse solar radiation on the horizontal plane	W/m^2
G^{hor}_{dir}	direct solar radiation on the horizontal plane	W/m^2
G^{hor}_{ref}	reflected solar radiation on the horizontal plane	W/m^2
G^{hor}_{tot}	global solar radiation on the horizontal plane	W/m^2
G^{tilt}_{dif}	diffuse solar radiation on the tilted plane	W/m^2
G^{tilt}_{dir}	direct solar radiation on the tilted plane	W/m^2
G^{tilt}_{ref}	reflected solar radiation on the tilted plane	W/m^2
G^{tilt}_{STC}	global solar radiation on the tilted plane at STC	W/m^2
G^{tilt}_{tot}	global solar radiation on the tilted plane	W/m^2
g	generation profile (CF)	
H	set of model hours	
h	model hour	
k_T	factor for diffuse solar radiation on horizontal plane	
L	total demand	MWh_{el}
L^{YP}	yearly peak demand	MWh_{el}
$LCOE$	levelized costs of energy	EUR/MWh

M	cluster member	
N_{days}	spatial dimension	
$N_{locations}$	spatial dimension	
N_{hours}	spatial dimension	
NP	number of grid points in country	
P_t	power output at time step t	MWh
$P_{out,ideal}$	ideal PV power output	MWh
$P_{out,real}$	real PV power output	MWh
P_r	performance ratio	
P^{add}	total capacity expansions	MW
P^{inv}	invested capacities	MW
P^{sub}	subtracted capacities	MW
P^{poss}	VRE area potentials	MW
$P^{exi,exo}$	exogenous, initially installed capacities	MW
$P^{inv,exo}$	exogenous investment capacities	MW
$P^{sub,exo}$	exogenous subtracted capacities	MW
$P^{add,bnd}$	total expansion bounds	MW
P^{ntc}	net transfer capacity	MW
p	interpolation point	
p_r	scaling precision range	
R	rotor diameter	m
R_c	cluster representative	
R_{EU}	Set of European countries	
r_d	discount rate	
r	region/country	
T_{2m}	temperature at 2 m height	K
T_{mod}	module's temperature	°C
T_{STC}	module's temperature at STC	°C
T	set of plant technologies	
t	plant technology	
v_{hub}	wind speed at hub height	m/s
v_{in}	cut-in wind speed	m/s
v_{out}	cut-out wind speed	m/s
v_r	rated wind speed	m/s
v_{ref}	wind speed at reference height	m/s
vx	x-component of wind speed	m/s
vy	y-component of wind speed	m/s
w	weight	
y	model year	
Y	set of model years	
z_{hub}	hub height	m
z_{ref}	reference height	m
α	Hellmann exponent	
α_{sfc}	surface albedo	
α^{wbl}	Weibull scale parameter	
α_{bias}	bias correction factor	
α_m	module's azimuth angle	deg
α_s	sun's azimuth angle	deg
β	temperature coefficient	1/°C
β^{wbl}	Weibull shape parameter	
β_{bias}	bias correction offset	
Δ	lightness index	
Δt	tme period	h

ε	CO_2 emission factor	t/MWh_{el}
ϵ	clear-sky index	
ϵ_{bias}	bias error	
η	PV module efficiency	
η_{STC}	module's efficiency at STC	
η^{ntc}	efficiency of net transfer capacity	
η_t	net generation efficiency	MWh_{el}/MWh_{th}
γ_m	module's tilt angle	deg
γ_s	sun's zenith angle	deg
κ	constant for clear-sky index	
λ	technology lifetime	a
μ_c	cluster mean	
ρ	area power density	MW/km^2
ρ_{hub}	air density at hub height	kg/m^3
τ	RPSM inner daily time step	h
Θ_{hor}	solar incident angle on the horizontal plane	deg
Θ_{tilt}	solar incident angle on the tilted plane	deg
ζ	power parameter	

Acknowledgements

Zuallererst möchte ich mich bei Yaping bedanken. Du hast mir die Möglichkeit gegeben, in diesem überaus spannenden und interdsiziplinären Projekt zu arbeiten und hast mir damit den Weg für meine weitere berufliche Zukunft geebnet. Ganz besonders hab ich dabei immer die Freiheiten, die du mir gelassen hast, genossen. Gleichzeitig kann man sich immer auf deine Unterstützung und wissenschaftliche Expertise verlassen.
Daneben geht ein ganz besonderer Dank an Susanne. Durch deinen spontanen Einsatz, Betreuung und Feedback, hast du meinen Abschluss dieser Arbeit, in einer doch eher schwierigen Situation, überhaupt erst ermöglicht. Mit dem Wissen um deinen sehr vollen Terminkalender, ist deine Hilfe umso bewundernswerter.
Danke auch an Felix Höffler, für die immer sehr hilfreichen Korrekturen und Anmerkungen.
Danke an Dagmar und Karin, für die Unterstützung bei sämtlichen bürokratischen und organisatorischen Hürden über die ganze Zeit.
In diesem Zusammenhang, auch ein besonderer Dank an Karin Gotzmann für die große Unterstützung in der Studiensekretariat-Datenschutzverordnung-Bescheinigungs-Angelegenheit.
Christopher und Nils, danke für die Zeit mit euch, die vielen Diskussionen und gegenseitige Hilfe während meiner gesamten Zeit und die immer entspannte Atmosphäre.
Andreas und Frank, danke für die gute und erfolgreiche Zusammenarbeit, die Diskussionen und vielen Treffen. Ihr habt mir den Einstieg in die Welt der Energiewirtschaft wirklich erleichtert und hattet dabei immer Geduld mit mir.
Simeon, danke fürs Einspringen in meinem Committee, auch wenns leider nicht allzu lang war, hast du mir, in einer für mich sehr schwierigen Phase, Orientierung und Unterstützung gegeben.
Johannes und Jakob, danke für die mehr als gelungene Wachablösung im ET-CC Projekt. Danke für vielen Gespräche, Treffen und gelegentlichen Feierabendbiere.
Philipp, danke für die Zuarbeit und fruchtbaren Diskussionen.
Jochen, danke für die unglaublich präzisen und detailierten Korrekturen.

Danke Cedric für diese wiedergefundene intensive Freundschaft, für die ganzen kurzweiligen und doch so langen Abende und Nächte mit Gesprächen über Gott und die Welt.
Danke an meine Familie, mit euch konnte ich mich immer entspannen und so viele Momente des Glücks genießen.
Elena, danke einfach für Alles, dafür dass du bist wie du bist – du bringst mein Herz zum leuchten.
Und danke an alle, deren Namen hier nicht aufgeführt sind, aber aufgeführt sein sollten.

Erklärung

Ich versichere, dass ich die von mir vorgelegte Dissertation selbständig angefertigt, die benutzten Quellen und Hilfsmittel vollständig angegeben und die Stellen der Arbeit - einschließlich Tabellen, Karten und Abbildungen -, die anderen Werken im Wortlaut oder dem Sinn nach entnommen sind, in jedem Einzelfall als Entlehnung kenntlich gemacht habe; dass diese Dissertation noch keiner anderen Fakultät oder Universität zur Prüfung vorgelegen hat; dass sie - abgesehen von unten angegebenen Teilpublikationen - noch nicht veröffentlicht worden ist sowie, dass ich eine solche Veröffentlichung vor Abschluss des Promotionsverfahrens nicht vornehmen werde. Die Bestimmungen der Promotionsordnung sind mir bekannt. Die von mir vorgelegte Dissertation ist von Prof. Dr. Susanne Crewell betreut worden.

Köln, 26. August 2019

Philipp Henckes

Teilpublikationen

Philipp Henckes, Frank Obermüller, Andreas Knaut, Christopher Frank (2018). "The benefit of long-term high resolution wind data for electricity system analysis". In: *Energy* 143. Supplement C, pp. 934–942. ISSN: 0360-5442. DOI: 10.1016/j.energy.2017.10.049

Philipp Henckes, Christopher Frank, Nils Küchler, Jakob Peter, Johannes Wagner (2019). "Uncertainty Estimation of Investment Planning Models Under High Shares of Renewables Using Reanalysis Data". In: *Energy, Submitted in July 2019*